TRACING THE EVOLUTION OF TWO ENERGY GAPS IN MgB_2 WITH INCREASING DISORDER

by

Mauricio José Escobar Medina

A thesis submitted in partial fulfillment of the requirements for the degree of

MASTER OF SCIENCE

in

PHYSICS

UNIVERSITY OF PUERTO RICO

MAYAGÜEZ CAMPUS

2008

Approved by:

_____	_____
Yong-Jihn Kim, Ph.D. President of the Graduate Commitee	Date
_____	_____
Henri A. Radovan, Ph.D Member of the Graduate Commitee	Date
_____	_____
Maharaj S. Tomar, Ph.D. Member of the Graduate Commitee	Date
_____	_____
Hector Jiménez, Ph.D. Chairperson of Physics Department	Date
_____	_____
Silvestre Colón R., M.A., M.S. Representative of the Office of Graduate Studies	Date

ABSTRACT

Magnesium Diboride (MgB_2) is a material recently discovered to exhibit superconducting properties. A trace in the behavior of the energy gaps of this material is performed via numerical calculations by the establishment of a theoretical model based in the BCS theory. Bogoliubov/Valatin transformations are applied to treat the compound in its pure form; later on, when impurities are included, Anderson's theory of dirty superconductors and Kim/Overhauser's observations are implemented to describe the behavior of the energy gaps within the dirty limit. Finally, a weak localization correction, also worked out by Kim, is introduced when the concentration of impurities is increased. A comparison with experimental data is made. It is observed that inter-band scattering is predominant within the dirty limit while when the weak localization correction is adopted, intra-band scattering turns predominant.

RESUMEN

El Diboruro de Magnesio (MgB_2) es un material recientemente descubierto que exhibe propiedades superconductoras. Una descripción del comportamiento de las brechas de energía de este material es llevada a cabo usando cálculos numéricos por medio del planteo de un modelo teórico basado en la teoría BCS. Se aplican las transformaciones canónicas de Bogoluibov/Valatin para tratar el compuesto en su forma pura; luego, cuando se incluyen impurezas, la teoría de Anderson para superconductores "sucios" y observaciones de Kim/Overhauser son implementadas para la descripción del comportamiento de las brechas de energía dentro del límite sucio. Finalmente, se introduce una corrección por localización débil, también elaborada por Kim, cuando la concentración de impurezas se incrementa. Se hace una comparación con datos experimentales. Se observa que la dispersión inter-bandas predomina en el límite sucio mientras que cuando la corrección por localización débil es adoptada, la dispersión intra-bandas se torna predominante.

ACKNOWLEDGEMENTS

I want to devote this space to express my sincere gratitude to that group of people without whom the completion of this document would have been impossible:

First of all, I want to thank God, the most important in this list.

Second of all, I want to thank my immediate family, especially my mother María E. Medina, my aunts Yolanda Martin and Angela Urriaga; all of them offered the spiritual support and inspiration necessary for completing this document as well as my master studies.

Thirdly, I want to thank my advisor, Dr. Yong-Jihn Kim, a wonderful scientist and marvelous person, from who I had a fantastic learning experience and who was always willing to guide me along the entire process.

Also, I want to acknowledge my gratitude to my colleagues Ramón Diaz M. and Joel Martínez for the help and guidance offered in the writing of the `MATLAB` codes required to perform the calculations.

Finally, I want to dedicate a long and sincere "thank you" to all my immediate colleagues and friends from UPRM's Physics Department, which directly or indirectly, consciously or unconsciously, selflessly always offered motivation and support during these two and a half years of my journey throughout the completion of my master studies in Puerto Rico.

TABLE OF CONTENTS

TABLE LIST

TABLES **PAGE**

FIGURE LIST

FIGURES **PAGE**

PLOT LIST

PLOTS **PAGE**

I. INTRODUCTION

Superconductivity is the phenomenon in which the temperature of a metal or alloy is lowered below a specific number bringing as consequence that the system loses its capability of resisting an electrical current when a voltage is applied and its capacity of expelling all magnetic flux except in a thin region near the surface when a weak magnetic field is applied. The first effect, the absence of electrical resistance for which superconductivity is usually known, was discovered in 1911 by Kamerlingh Onnes and his assistant Gilles Holst [1] when the first one discovered that electrical resistance of mercury dropped abruptly to zero at a temperature of 4.2K; the second effect, the so-called Meissner-Ochsenfeld effect, was discovered by Meissner in 1933 [2].

Several approaches in the understanding of the superconducting mechanism were developed over the years after this discovery, most of them unsuccessful [4]. Finally, the ultimate enlightenment was provided by the BCS theory proposed by J. Bardeen, L. Cooper and J. Schrieffer (referred as BCS hereafter) in 1957 [4]. The theory establishes the background for the comprehension of the electron-phonon interaction mechanism responsible of superconductivity in the so-called *conventional superconductors* (see **S.S. 1.3**). This is the mechanism believed to govern superconductivity in the very atypical compound known as MgB_2 or Magnesium Diboride [21] [24]-[30] [65]-[70]. This recently discovered compound (2001), with an extraordinarily simple lattice structure [27], exhibits an unusually high transition temperature of 39K approximately, which makes it scientifically very attractive.

The purpose of this thesis work is the application of the BCS theory [4] and its generalizations [17] [37] [41] [48] to provide a method to outline the theoretical behavior of MgB_2's *energy gaps*, the parameters that dictate the intensity of the binding of the electron pairs participating in superconductivity; by consideration and inclusion of a set of parameters [41] [43], the numerical results derived from such model can be contrasted with real experimental data [64]-[77] and therefore conclusions can be drawn.

This thesis is arranged in the following manner: **Chapters** (**Ch. I**, **II**, …), which are divided in **Sections (S. 1**, **2**, …), which are as well divided in **Sub-sections** (**S.S. 1.1.**, …, **S.S. 2.1.**, …). **Ch. I** corresponds to this Introduction (**S. 1**), Motivation (**S. 2**) and Literature Review (**S. 3**). **Ch. II** is devoted to the Theoretical Background. Here, mathematical and physical tools and concepts are introduced to develop the numerical model to trace the behavior of MgB_2's energy gaps. **S. 1** is rather introductory and, in general, it concentrates conceptually and without mathematical formalities in the main features of the mechanism of conventional superconductivity and their most important representatives (**S.S. 1.1** to **1.4**); as well, the characteristics of the MgB_2 compound are explored (**S.S. 1.5**). All the rigorous mathematical formalism is treated along **S. 2**, where a brief development of the aspects of the BCS theory relevant to the objective of this document is carried out in **S.S. 2.1**; later on, the systematic establishment of a mathematical model allowing the study of the behavior of the energy gaps takes place from **S.S. 2.2** to **S.S. 2.5** using the aspects discussed in **S.S. 2.1**. Numerical results and calculations are finally shown in **Ch. III**, where the model is applied in several regimes

(clean and dirty) and results are compared with experimental data. Finally, **Ch. IV** is devoted to the Conclusions and Future Work. **Ch. V** corresponds to References.

In this document key terms and important Chapters, Sections or Sub-sections are intentionally bolded. As well, bolded mathematical quantities represent vector quantities and non-bolded ones represent scalar quantities.

1. MOTIVATION

The progress of science in present times is undeniable and also is the possible technological applications of that progress. One of the branches of Physics, among a huge number of them which could supply the most useful applications is that related with Material Sciences. Particularly, the superconducting phenomena, whose discovery and application date back to almost a century ago, offer an almost infinite spectrum of technological development for the world as we know it. The discovery or manufacture of superconducting materials with critical temperature each time higher witnessed in the present offer a high incentive to the embracement of this reality, but in order to reach such goal, we have undoubtedly to consider the elaboration of theoretical models capable to draw the structure of such materials and their behavior. The articulation of such models imply a great knowledge of the Physics of the superconducting materials as well as the appropriate mathematical and computational techniques necessary for modeling the governing parameters to be contrasted with the experimental results.

2. LITERATURE REVIEW

The scientific literature available on the MgB_2 compound is abundant and wide-ranging especially after its discovery by Nagamatsu *et al.* [21] in January 2001. As pointed out by Buzea and Yamashita at the Introduction of [22], the number of papers related to this topic spiked that very same year, showing the great interest that MgB_2 generated in the scientific community. An extensive description of this compound and its properties, like crystal structure, band structure, Fermi surface, energy gaps, phonon spectrum and modes, doping effects, defects, isotope effect, specific heat, electron-phonon interaction, density of states, etc., can be found in the studies and experiments performed by Vinod *et al.*, Liu *et al.*, Kong *et al.*, Kortus *et al.*, Mazin and Antropov and Choi *et al.* [24]-[30] respectively, among a huge number of other scientific studies found in the Reference section of these papers [63]-[77]. Y. Wang *et al.* [65], as well as M. Putti *et al.* [67] and Kortus *et al.* [73] supply the most relevant experimental data based on specific-heat measurements on neutron-irradiated MgB_2; such will be used for the contrasting of the numerical results. It is noteworthy the empirical two band model developed by Wang [65], based in the work of Bouquet *et al.* [66], to show the presence of two energy gaps in this compound and to perform a phenomenological trace of these [66]. Putti *et al.* also performs this outline and contrasts it with that of Yang's [67].

A theoretical approach to the MgB_2 system in its pure form is available via the conventional BCS theory [3] [4] [12] [14] [34] [35]. Important formalisms are those suggested by Bogoliubov [17] and Valatin [37] (BV) which make use of the mean-field approach; these

formalisms are extendedly used for theoretical foundation of the model implemented here. As well, Suhl *et al.* [41] introduce an important treatment for the multiple gap case based in the results derived via BV's approach. It is worthy of mention the theoretical Eliashberg formalism implemented by H. J. Choi *et al.* [27] to follow the numerical trace of MgB_2's energy gaps using the formalism proposed by Marsiglio *et al.* [64], closely related to this work.

As well, important and well-founded theoretical models for the understanding of the role of impurities in superconducting systems can be drawn mainly from the theory of Abrikosov and Gor'kov (AG, hereafter) [46] on the subject and Anderson's theory of impure superconductors [47] (or "dirty" superconductors). Essential contributions to these theories concerning both the influence of the impurity concentration in the magnitude of the critical temperature and the range of applicability of Anderson's theorem have been offered by Kim and Overhauser [42] [43] [52] [53] [57] [58] [71] (KO, hereafter) as well as by AG.

II. THEORETICAL BACKGROUND

1. GENERALITIES ON THE SUPERCONDUCTING STATE AND MgB_2

The major concern along **S. 1** will be pointing out the properties and give a general overview, rather conceptual than mathematical, of the mechanism responsible of the loss of resistivity in superconductors. In addition, an outline of the characteristics of the superconducting compound MgB_2, to which the concepts and the theoretical models described in **S. 2** are applicable, will be offered. A detailed mathematical treatment of most of the stated in the following can be found through **S. 2** to **S. 3**.

1.1. PROPERTIES OF THE SUPERCONDUCTING STATE

When a piece of, for example, Tin is cooled down below about 4K it exhibits a series of new thermodynamic behaviors which include the almost total absence of electrical resistance and a perfect diamagnetism [1] [2]. From a purely mathematical point of view, the mechanism hidden behind the superconducting state is due to the abnormal behavior of a fraction of electrons conveniently located in **k**-space [3].

The fraction of the electrons which interact effectively in superconductivity is around 10^{-4} of the total at $T = 0$, which corresponds to a number of nearly 10^6 electrons [3] [4]. The superconducting behavior, hence, can be interpreted as a collective phenomenon. Such collective conduct is very common in Physics, as discovered particularly in the last decades; perhaps, the

best example is the Laser, in which photons play their collective, cooperative role by all oscillating at the same rate, all with the same energy; another exciting example is the Bose-Einstein condensate, in which bosonic atoms, e.g. ^{87}Rb, sit in the ground state until all atoms can be represented by a single wavefunction [5]. Actually, Bose-Einstein condensation and superconductivity exhibit a good number of common similarities [6]. Condensation is an important quantum-mechanical consequence of the collective conduct. Other examples of this phenomenon can be drawn out from the superfluidity experiments, principally those related with liquid Helium and even from Astronomy where a condensed behavior in neutrons is known to be responsible of the differences in the measurements of radiation absorption and moments of inertia in neutron stars when compared with predictions based in individual non-interacting particle models [3].

1.2. THE MECHANISM OF CONVENTIONAL SUPERCONDUCTIVITY

The "anti-social" reputation of electrons is widely known in Quantum Mechanics due to Pauli's Exclusion Principle (PEP, henceforth), which dictates the procedure of arranging a given number of electrons when a certain number of states is available; electrons are thus said to be slightly tolerant to be placed next to a partner, only if this partner has an opposite spin. Such unfriendly conduct is not reserved for electrons only but belongs to all particles with half-integer spin or **fermions**, for example, electrons, neutrons, protons, the components inside them and ^{3}He among others; in such cases, PEP applies. In contrast, **bosons** are particles with integer spin. This imprints a forthcoming personality on them because not only bosons won't "exclude" each other but the probability for a boson to fill a level will be increased if that level is already occupied by

another boson [8]. Photons and phonons along with a large proportion of atoms are examples of bosons; but obviously, any substance made up of an even number of fermions behaves like boson. This is the case for electrons, which under certain restrictions can be considered as bosons when paired together.

Fermions obey the so-called **Fermi-Dirac statistical distribution**, dictated by

$$f_{F-D}(\varepsilon) = \frac{1}{\exp\left[\left(\varepsilon - \mu / k_B T\right)\right] + 1} \tag{1.1}$$

and bosons obey the so-called **Bose-Einstein statistical distribution**, dictated by

$$f_{B-E}(\varepsilon) = \frac{1}{\exp\left[\left(\varepsilon - \mu / k_B T\right)\right] - 1}, \tag{1.2}$$

where in both cases *f* stands for the probability for a given particle at a given temperature *T* to lie in a particular energy state with energy ε and chemical potential μ. Considerations bringing $f_{F-D} \to 0$ while $f_{B-E} \to 1$ as $T \to 0$ are commonly discussed in textbooks, highlighting that something out of the ordinary occurs when temperature approaches to zero [8].

Electron pairing and superconductivity behavior seen as a condensation of bosons was not an idea attained by snap. A microscopic theory of superconductivity based in this initiative implied several failed attempts, some of them referenced at the Introduction of [4]. Evidently, the major inconvenient in electron pairing lies in the impossibility of attraction between electrons imposed by its mutual Coulombian repulsion. It was not until Fröhlich's suggestion of the role of the interaction between electrons and lattice vibrations in superconductivity [9] that a major

advance in the understanding of this phenomenon showed to be successful. Fröhlich's theory received a dramatic confirmation when in 1950 the isotope effect was discovered [10] [11],

$$T_c \sqrt{M} = const \qquad \textbf{(1.3)}$$

demonstrating a dependence of the superconducting transition temperature (T_c) with the ionic mass (M) of the material, and thus the lattice. Fröhlich's theory, however, failed in other aspects, the most important being the order of difference in energy between the normal and superconducting state [6]. The correct approach was offered by BCS with the BCS theory [4].

The aspects of BCS theory relevant to this document will be fully discussed in the next Section; only a rather conceptual insight of the electron-phonon interaction mechanism will be offered in the following lines. To this aim, consider **Fig. 1.1**: if as a very rough approximation electrons are treated as free, the journey of a given electron through the ion matrix can temporarily polarize a particular zone in the lattice; any neighboring electron might therefore perceive the polarization and become attracted to that temporary wrench in the lattice. In this manner, both electrons interact attractively by exchange of a virtual phonon [6]; we refer to this pair of electrons as the **Cooper pair**.

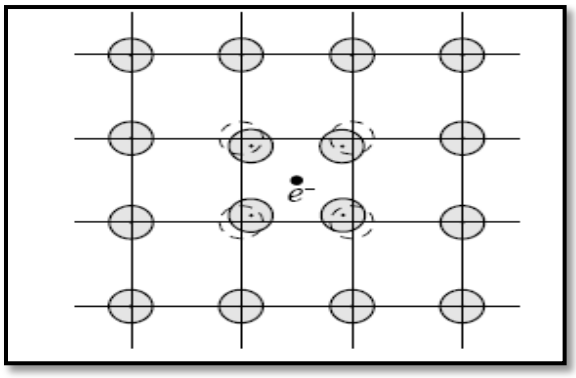

Figure 1.1. Polarization of the lattice by a traveling electron [3]

The process that leads to the formation of Cooper pairs in low-T_c superconductors is understood as follows:

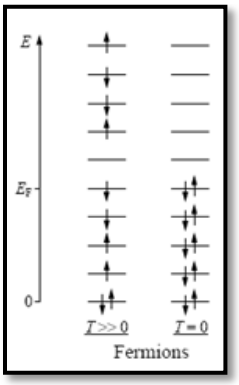

Figure 1.2. Arrangement of fermions at different temperatures [3]

It's commonly known that a system of fermions at a given temperature T will settle in different energy states according to their energies and in concordance with PEP, as in **Fig. 1.2** above. When $T \gg 0$, a lot of empty energy states are available and given the selfish character of fermions, each one will settle singly in some energy level if possible. However, when

temperature is lowered (ideally) to zero, empty spots stop being accessible and fermions are forced to share levels with a partner with opposite spin up to a maximum level, the **Fermi level**; it has to be remembered that no electron in any of the filled levels will tolerate a third partner, thus, if an electron, say, in the ground state level interacts with a phonon, the probability of that electron to accept the phonon will be small since the latter would kick the former just a few levels up where it will find no spot to settle. This is a situation similar to trying to convince one of the spectators in the first row of a filled theater whose assistants are, say, recently divorced couples to move to the rear seats with the promise of a ticket for an entire row for his (or her) own; in this analogy, PEP establishes that no spectator will accept the offer but, even more, he or she will tolerate his (or her) annoying ex-partner on behalf of not giving up his (or her) V.I.P. seat. In consequence, technically, phonons cannot interact with the electrons in the first levels. However, and carrying on with our analogy, for couples sitting in the last filled rows the situation is different because they *can* move to the empty rows behind them, they just don't have a ticket; in consequence, they *will* accept the offer. In other words, just like shown in **Fig. 1.3**, phonons are more likely to interact with the electrons lying in the last filled levels or near the Fermi surface because these electrons can be promoted to further empty levels.

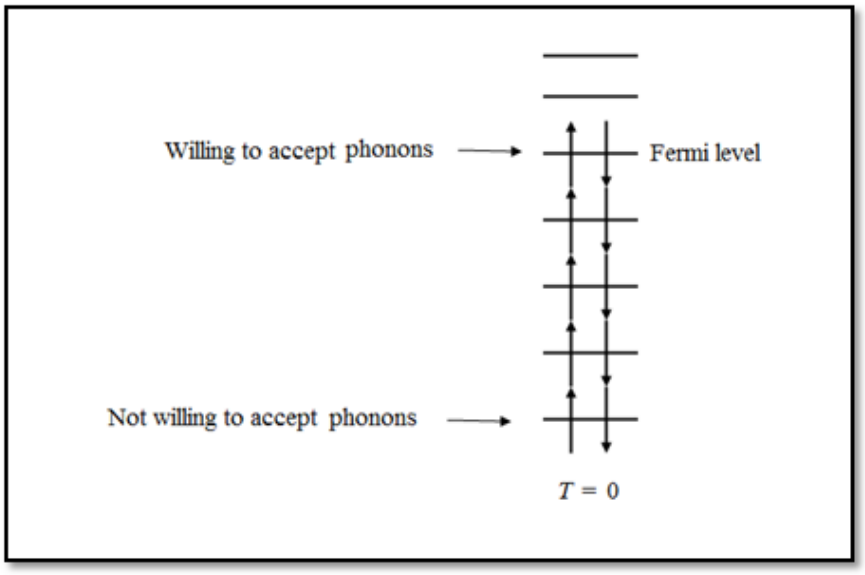

Figure 1.3. Acceptation of phonons by fermions arranged in energy levels.

As suggested by Fröhlich [9] and demonstrated by L. N. Cooper [12], are the electrons within a thin layer around the Fermi surface (see **page 30**) the ones responsible of the instability of the system and subsequently responsible of the superconducting state. It has to be mentioned that the basis of Cooper's result lies in the convenient approximation of the attractive interaction matrix element by the constant $-V < 0$ (See **S.S. 2.2**), but no link between the form of this attractive interaction and the electron-phonon interaction is made. This suggests that the nature of the attractive interaction is not limited to the exchange of phonons; apparently the mechanism of such mediation is very different for other systems such as high-T_c superconductors and others [13]. A formal calculation of the above-mentioned electron-lattice interaction matrix element is performed by Bardeen himself [14] and others via a Hartree approach, being the main feature in this calculation the inclusion of the dynamics of the lattice and the electrons. This differed with

the standard calculations of Bloch type (See **S.S. 2.2**) done to that time which considered the motion of the electron through a static lattice as independent of its vibrations, leading to the well known band structure theory. The mathematical proof offered by Cooper won't be showed in this document, neither Bardeen's, but these are standard calculations in most of the literature in superconductivity [4] [6] [12].

After electrons become attracted by mediation of phonons, these pairs behave like bosons and migrate to a state of lower energy which differs from the normal state ground state energy by an exponential factor [4]; this is, actually, the benefit of becoming paired if one is electron. In the context of our previous analogy, the situation resembles one in which the spectators of the hypothetical theater at the "Fermi row" were proposed to have to pay half the price for their ticket if they joined with a partner and, in addition to this, were allowed to see the show not from the first row but from the set itself. In this way, money charges would split and both electrons would enjoy the benefits. However, due to the bosonic behavior associated to Cooper pairs, once the first couple accepts the ticket and moves, other couples will want to join them in the set, so to speak; no set will sustain such situation and in consequence will collapse. The same instability can be transferred to the interpretation of the instability of the Fermi sea [15], which will collapse at $T = 0$. This is precisely Cooper's result [12]. Notice that the presence of the electrons below the layer only provides a "floor" for those electrons involved in the Cooper pairing in the sense of not allowing the occupancy of **k**-states below $\mathbf{k}_F$ in virtue of PEP.

Although some of the similarities between the Bose-Einstein (BE) condensation and the superconducting behavior are marked, certain care should be taken when subscribing to such interpretation. The approach of superconductivity from the BE condensation point of view was taken for several years as a theoretical oddity, except probably for the case of Schafroth *et al.* [6], who developed a serious formalism based on this perspective inspired in the observations of Ogg on very dilute solutions of alkali metals in liquid ammonia [16]. Bogoliubov [17] also became aware of this idea when developing his formalism, to be described in **S. 2**. The major difficulty in seeing the Cooper pair as a composite boson lies in the location of the pairing taking place in the momentum space rather than real space. Differences are also marked when normal states above T_c are compared in both BE and BCS cases; one probably should speak of a BCS condensation instead of a BE condensation of Cooper pairs. Abundant discussions are pertaining to a crossover between BCS theory and BE condensation can extensively be found in scientific literature and journals [18]. Despite the differences, this author will subscribe to the condensation of Cooper pairs perspective of one of the BE-type.

Because of Cooper pairing, the existence of a difference in energy between normal and superconducting state suggests the appearance of an **energy gap** (Δ) as the parameter giving account for the binding energy of the Cooper pair at the ground state [3]. The energy gap is the most important term along this document. A detailed discussion and calculations will be left on hold until the upcoming Sections.

Subscribing oneself to the assumptions of the range of the electron-phonon interaction at $T = 0$ adopted by Cooper [14] and Fröhlich [9] the energy gap would be located at the edge of the Fermi sphere, pretty much in the way schematized in **Fig. 1.4**. The minimum excitation energy would be 2Δ [4] on the account of the excitation of both of the paired electrons; it has to be in this way given the restrictions of the PEP and the conservation of momentum. Within rough approximations, $2\Delta(0) \sim 3.52 k_B T_c$ for a given superconductor [13] (See **Eq. (2.42)** on page 47).

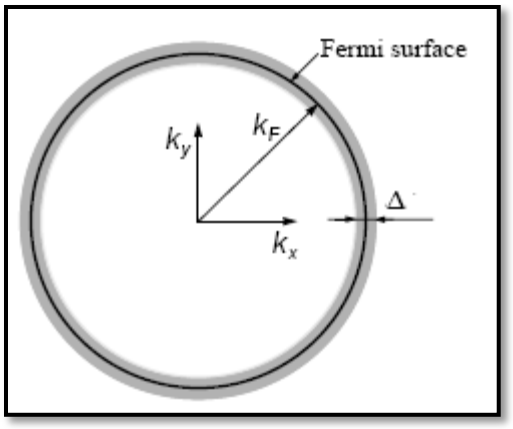

Figure 1.4. Energy gap in the **k**-space [3]

For excited states ($T \neq 0$), Δ exhibits a dependence of the temperature described in **Fig. 1.5**. A complete mathematical approach for the computation of Δ within different regimes and superconducting systems await in **S. 2**. A numerical calculation in which **Fig. 1.5** is reproduced will be performed in **Ch. III**. Discussions about the behavior sketched below will be postponed until **S. 2**, where the proper mathematics is introduced.

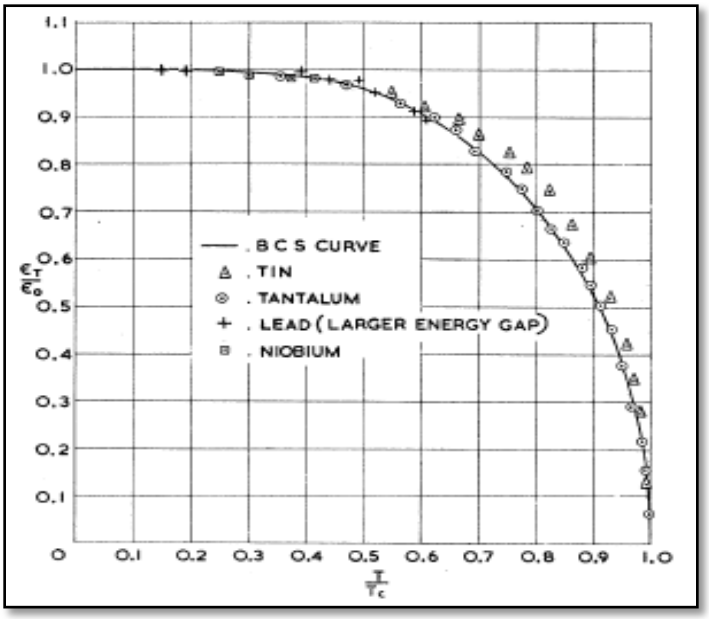

Figure 1.5. Temperature dependence of the energy gap [7]

1.3. THE SUPERCONDUCTING MATERIALS

A glimpse to **Fig. 1.6** picked from Internet [19] tells us the wide variety with which the superconducting phenomenon is found in the elements found in nature. **Table 1.1** excerpted from [20] is even more complete.

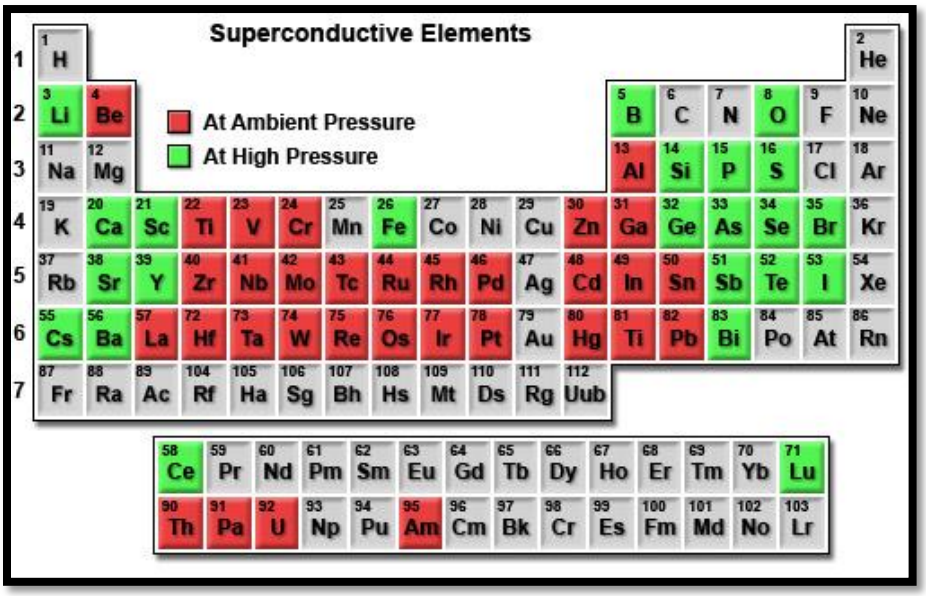

Figure 1.6. Periodic Table of Superconductivity [19]

Element[b]	N_e	Crystal Structure[c]	T_c (K)	Θ_D (K)	B_c (mT)	$2B_c/T_c$ (mT/K)	γ $\left(\frac{\text{mJ}}{\text{mole K}^2}\right)$	$\chi \times 10^6$ (cm³/mole)	λ	μ_c^*	dT_c/dP (K/GPa)	P (GPa)	α	WF (eV)	$E_g = 2\Delta$ (meV)	E_g/kT_c	$D(E_F)$ (states, atom eV)	Z
Be	2	hcp	0.026	940			0.21							5.0				4
Al	3	fcc	1.18	420	10.5	18	1.4							4.3	0.35	3.4		13
Sc	3	hcc	0.01	470			10.9							5.9				21
Ti	4	hcp	0.40	415	5.6	28	3.3	155	0.38	0.17	0.6	0–1.4		4.33			≈ 1.4	22
V	5	bcc	5.40	383	141.0	52	9.82	300	0.60	0.17	6.3	0–2.5		4.3	1.6	3.4	≈ 2.1	23
Zn	12	hcp	0.85	316	5.4	12	0.66						0.45	4.3	0.23	3.2		30
Ga	3	orthr	1.08	325	5.83	11	0.60								0.33	3.5		31
Zr	4	hcp	0.61	290	4.7	15	2.77	129	0.41	0.15	15.0	0–2.0	0	4.05			≈ 0.8	40
Nb	5	bcc	9.25	276	206.0	45	7.80	212	0.82	0.15	−2.0	0–2.5		4.3	3.0	3.8	≈ 2.1	41
Mo	6	bcc	0.92	460	9.6	21	1.83	89	0.41	0.10	−1.4	0–2.5	0.37	4.6	0.26	3.4	0.65	42
Tc	7	hcp	7.8	411	141.0	36	6.28	270			−12.5	0–1.5		5.0	2.4	3.6		43
Ru	8	hcp	0.49	580	6.9	28	2.8	39	0.38	0.14	−2.3	0–1.8	0	4.7	0.15	3.5	0.91	44
Cd	12	hcp	0.517	210	2.8	11	0.69						0.5	4.2	0.14	3.2		48
In	3	tetrg	3.41	108	28.2	17	1.67							3.8	1.05	3.6		49
Sn(w)	4	tetrg	3.72	195	30.5	16	1.78						0.47	4.38	1.4	4.4		50
La(α)	3	hcp	4.88	152	80.0	33	9.8				190	0–2.3			1.5	3.5		57
La(β)	3	fcc	6.3	140	110.0	37	11.3				110							57
Lu	3	hcp	0.1		< 40.0										0.028	3.3		71
Hf	4	hcp	0.13	252	1.27	20	2.2	70	0.14		−2.6	0–1.0			0.044	3.9	0.83	72
Ta	5	bcc	4.47	258	82.9	37	6.15	162	0.75		−2.6				≈ 1.7	≈ 3.5	≈ 1.7	73
W	6	bcc	0.015	383	0.12	16	0.90	53	0.25					4.5	≈ 0.006	≈ 4.5	≈ 0.5	74
Re	7	hcp	1.70	415	20.0	24	2.35	68	0.37	0.10	−2.3	0–1.8	0.23		0.78	3.4	0.76	75
Os	8	hcp	0.66	500	7.0	21	2.35	13	0.44	0.12	−1.8		0.20		0.29	4.8	0.70	76
Ir	9	fcc	0.11	425	1.6	29	3.2	24	0.35						0.048	5.6		77
Hg(α)	12	trig	4.15	88	41.1	20	1.81						0.50	4.52	1.7	4.6		80
Hg(β)	12	tetrg	3.9	93	33.9	17	1.37											80
Tl	3	hcp	2.38	79	17.8	15	1.47		0.80				0.50	3.7	0.79	3.8		81
Pb	4	fcc	7.20	96	80.3	22	3.1		1.55				0.48	4.3	2.7	4.3		82
Th	4	fcc	1.38	165	16.0	23	4.32								0.41	3.4		90
Pa	5		1.4															91
Am	9	fcc	1.0															95

Table 1. Properties of the superconducting elements [20]

Up to date there are around 7000 known superconducting materials [3]. Very roughly speaking such a wide collection can be classified in two groups:

I. **Metals and Alloys**. In this group we will find non-magnetic elemental superconductors and some of their alloys. This is the group of superconductors referred as **conventional superconductors**. As a general feature of this group, critical temperatures do not exceed 10 K (MgB_2 can possibly be considered an exception of this rule) and members of this group enjoy of highly symmetrical crystallographic structures [19]. Some of the conventional superconducting elements become superconductors only under high pressure, because of the dramatic influence of this procedure in the density of states, or when prepared into thin films, which raises the critical temperature [3]. The mechanism governing the superconductivity in these materials is the classical, BCS-type described in **S.S. 1.2**. As said before, it's very likely that MgB_2 can be categorized into this family but its uncommonly high T_c provides for it a very particular spot if one wants to consider it strictly conventional. A summary of the characteristics of this compound will be discussed in **S.S. 1.4**.

II. **Unconventional superconductors**. In this group we will mainly find magnetic low-dimensional compounds. In these materials the superconductivity is of "unconventional" type, in the sense that the electron-phonon interaction is strong and non-linear [3] as well as other more exotic mechanisms of superconductivity seem to be in play. The strong correlation between electrons sheds a shadow in the understanding of the mechanism of superconductivity in these systems, of which

there is not yet a complete theory. As examples of members of this group one can find the so-called Chevrel phases (which are molybdenum sulfides with high transition temperatures and critical fields) along with Copper oxides or **cuprates** (which are the also called high-T_c superconductors and represented a revolutionary discovery, back in 1986); several cuprates, from [3], are listed in **Table 1.2**. As seen, critical temperatures range over 100 K. Cuprates represent a good example of superconductivity of the unconventional type in which neither BCS nor mean-field theory are applicable. Other members of this group are also the charge-transfer organics [19] (which are organic compounds and polymers who exhibit superconductivity), heavy-fermion systems (superconductors whose electrons exhibit huge effective mass, ~100 times the electron mass), nickel borocarbides, strontium ruthenates, ruthenocuprates (hybrids from cuprates and strontium ruthenate), along with a good number of recently found high-T_c superconductors.

Cuprate	*CuO_2 planes*	*T_c (K)*	*abbreviation*
$La_{2-x}Sr_xCuO_4$	1	38	LSCO
$Nd_{2-x}Ce_xCuO_4$	1	24	NCCO
$YBa_2Cu_3O_{6+x}$	2	93	YBCO
$Bi_2Sr_2CuO_6$	1	~12	Bi2201
$Bi_2Sr_2CaCu_2O_8$	2	95	Bi2212
$Bi_2Sr_2Ca_2Cu_3O_{10}$	3	110	Bi2223
$Tl_2Ba_2CuO_6$	1	95	Tl2201
$Tl_2Ba_2CaCu_2O_8$	2	105	Tl2212
$Tl_2Ba_2Ca_2Cu_3O_{10}$	3	125	Tl2223
$TlBa_2Ca_2Cu_4O_{11}$	3	128	Tl1224
$HgBa_2CuO_4$	1	98	Hg1201
$HgBa_2CaCu_2O_8$	2	128	Hg1212
$HgBa_2Ca_2Cu_3O_{10}$	3	135	Hg1223

Table 2. Some examples of cuprates [3]

1.4. MgB_2 : FEATURES AND SUPERCONDUCTING PROPERTIES

Magnesium Diboride, or MgB_2, is an atypical superconductor discovered very recently (2001) [21] with a considerable high transition temperature of about 39 K, at ambient pressure. MgB_2 appears to fall in the category of a very exceptional conventional superconductor with uncommon high T_c when compared with other more known conventional superconducting materials. The family of borocarbides RE-TM_2B_2C, with RE = Y, Lu, Er, Dy or other rare earths and TM = Ni or Pd, share this feature along with an anisotropic layered structure [22].

The task of pushing up the critical temperature of conventional BCS-like superconductors was a labor undertaken since back in the 1960s, way before the discovery of high-T_c superconductivity, with the suggestion of metallic Hydrogen as possible candidate for a high-T_c superconductivity [23]. Roughly speaking, such initiative was based in the belief that Hydrogen's light mass would imply high phonon frequencies and subsequently a low coupling constant [24]. As shown with detail in **Eq. (2.41)** in **S. 2**, this would reflect in a higher T_c; for example, MgB_2's T_c requires a coupling constant of ≈ 1 [25]. Yet being metallic Hydrogen scarce, the idea was transferred to compounds made of light elements, like carbides and nitrides. It is believed that the high transition temperature (among conventional superconductors) in MgB_2 is the confirmation of this suggestion and the interest in superconductivity of light mass superconductors has been found reinvigorated since its discovery in 2001 [22]. It also represents a hope for high-T_c superconductivity with simple compounds. Such discovery inspired

experiments with other diborides, whose transition temperatures range from 0.5 K to 15.6 K, placing MgB_2 at the top; for an extensively detailed list of these diborides, refer to [22].

The structure of MgB_2 is shown in **Fig. 1.7**, while a comparison between structures is shown in **Fig. 1.8** [26]. MgB_2's structure corresponds to a simple hexagonal AlB_2-type structure [22], very usual among diborides; boron atoms form graphite-type honeycombed flat layers and magnesium atoms are located above the centre of the hexagons in-between the boron planes [27] as part of a parallel also flat triangular lattice approximately halfway between the boron layers [22] [25]. The distance between the boron planes being appreciably longer than the boron-boron distance corresponds to an evidence of strong anisotropy along the boron-boron lengths [22] similar to that exhibited by graphite.

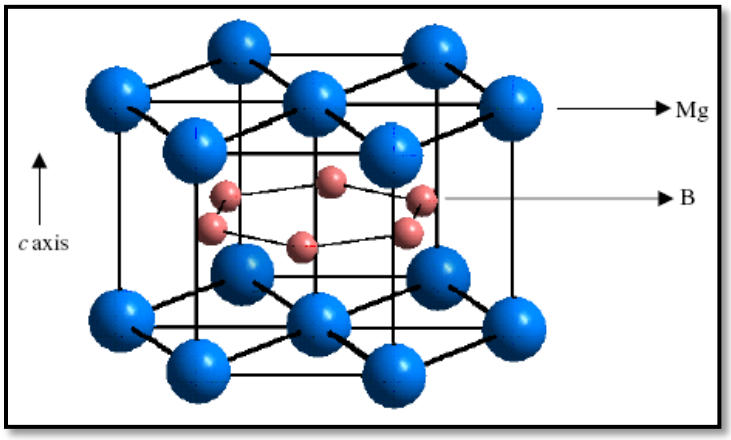

Figure 1.7. Structure of MgB_2 [22].

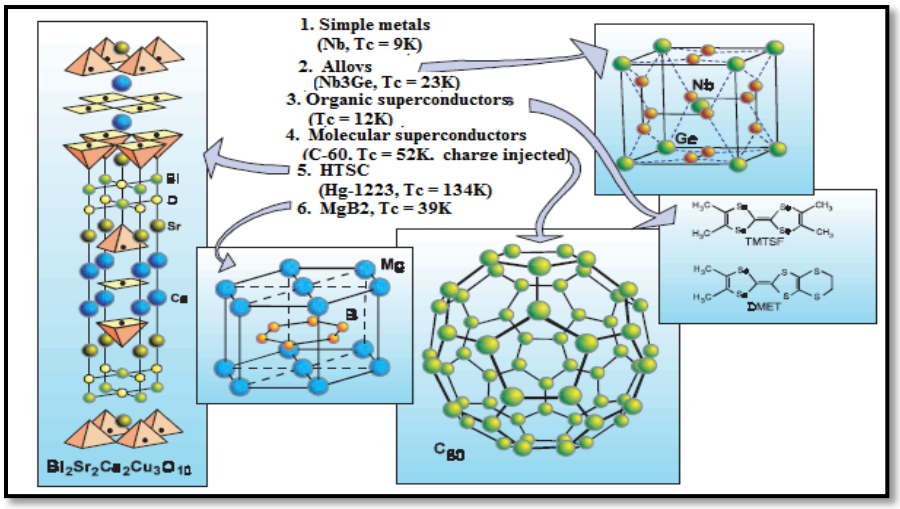

Figure 1.8. Structure of MgB_2 compared to other superconducting materials [22]**.**

Band-structure calculations show that MgB_2 exhibits two types of bands at the Fermi surface: one narrow band made up of boron π-orbitals and a broader one made up of boron σ-orbitals. At the Fermi level the electronic states are either σ-boron orbitals or π-boron orbitals [27]. Magnesium atoms donate their valence electrons to the boron planes forming an ionic bond with the boron atoms; the in-plane Boron atoms are supported together by 2D-covalent bonds while there are 3D-metallic bonds between the layers [26]. The peculiarity of MgB_2 lies in the incomplete filling of the two σ-bands associated with strongly covalent, sp^2-hybrid bonding within the graphite-like boron layers; holes at the top of this band are the ones exhibiting two-dimension properties and are located within the boron sheets; three-dimensional electrons and holes in the π-bands are delocalized over the crystal [28] like n graphite. A band-structure diagram is shown below along with the symmetry lines of the Brilloin zone.

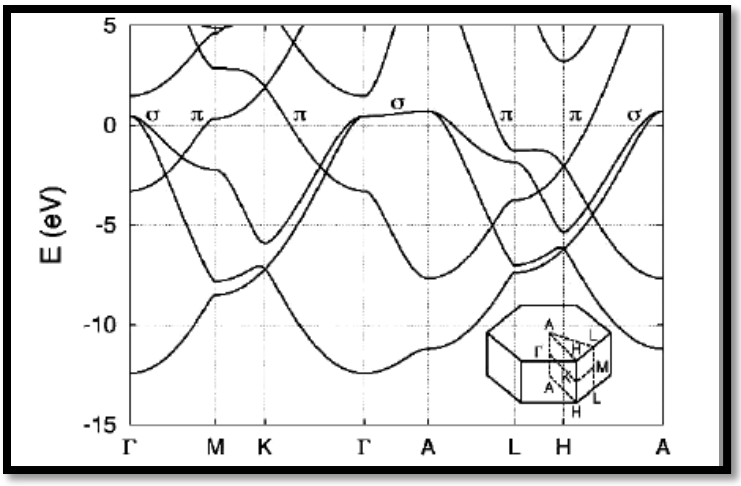

Figure 1.9. Band structure diagram of MgB_2 [29]

The Fermi surface of MgB_2 consists of four sheets where σ-bands form two hole-like coaxial cylinders along the $\Gamma \rightarrow A$ line and π-bands form a hole-like tubular net near *K* and *M*, and an electron-like tubular net near *H* and *L* [28] [29]. The diagram of MgB_2's Fermi surface is exhibited below. More details can be found in [27]-[30].

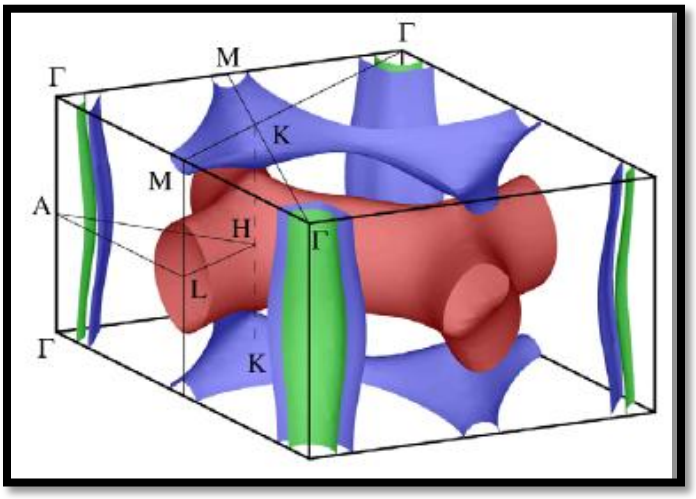

Figure 1.10. Fermi surface of MgB_2 [28]

The electronic states in MgB_2 in the boron plane couple strongly to specific phonon modes, which results favorable for Cooper pairing. The calculated phonon spectrum of MgB_2 is well determined. Six non-acoustic modes have been classified as phonon modes at the center Γ: The so-called A_{2u} and B_{1g}, which are singly degenerate modes involving vibrations along the *c* axis; in the latter, boron atoms are moving in opposite directions with the magnesium atom stationary and in the former with both Mg and B atoms are moving along *c*. Next one is the so-called E_{1u} mode in which Mg and B planes vibrate in opposite directions along the *x* or *y* directions with the Mg ions staying stationary [26]. Finally, there is the so-called E_{2g} mode, which is highly anharmonic. Is this mode the one proved to be responsible of the boron σ-bands strong coupling and subsequent superconductivity in MgB_2 [30]. The intensity of this coupling, and consequently the intensity of the energy gap associated to this type of electron pairing (Δ_σ, henceforth), is calculated as 6.8 meV [27]. This corresponds to the 2D strongly coupled gap.

A schematization of this mode is offered below:

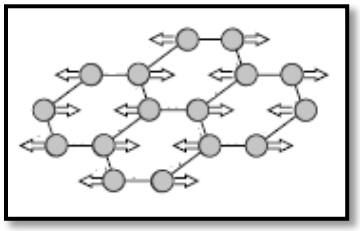

Figure 1.11. A vibration mode in Boron planes in MgB_2 [27].

The charge distribution of the σ- bonds is not symmetrical with respect of the in-plane positions of boron atoms which brings σ-bond states to couple very strongly with the in-plane vibration of boron atoms [27]. As boron layers oscillate, for example in the manner shown

above, some bonds are shortened while others are elongated; shortened bonds become attractive to electrons whereas the elongated ones turn repulsive. The σ-bonds are shown schematically in **Fig. 1.12**.

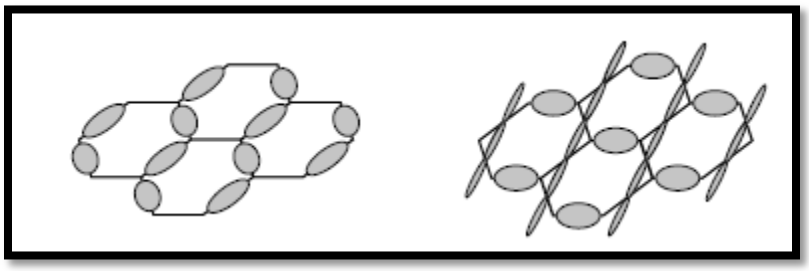

Figure 1.12. σ-bondings in MgB_2 coupling strongly with the vibrational E_{2g} phonon mode [27]

On the other hand, π-bonding states also couple with the mentioned mode but forming a much weaker electron pair bounded by a smaller energy gap (Δ_π, henceforth) calculated as 1.8 meV [30]. This corresponds to the 3D weakly coupled gap [22]. Observe that both energy gaps seem to have risen from the anharmonicity of the E_{2g} mode. Although evidence in favor of the existence of two separated energy gaps appears to be yet inconclusive [22], this document will subscribe to a doubly-gapped MgB_2 model. Experimental results and behavior of these energy gaps are shown in **Fig. 1.13**. Notice the experimental data offering evidence of a single anisotropic energy gap. Compare the shape of curves in **Fig. 1.13** with that of **Fig. 1.5** in **page 16**.

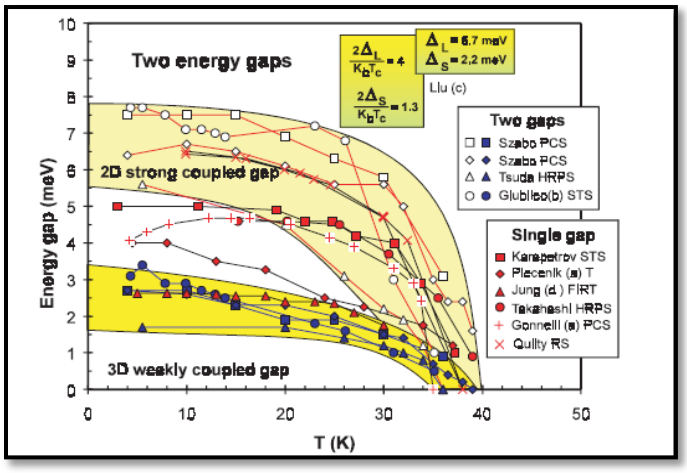

Figure 1.13. Temperature dependence experimentally observed of the energy gaps in MgB2 [22]

The size of the energy gaps is proven to change in different sections of the Fermi surface [27], ranging form 1.2 to 3.7 meV for the π sheets (Δ_π) and from 6.4 to 7.2 meV for the σ sheets (Δ_σ). Such differences can be attributed to surface impurities or non-uniformity [22]. A minute treatment of MgB_2 in the BCS framework and one particularly related with its energy gaps will be postponed until **S. 2**.

The main characteristics of MgB_2 as far as this document is concerned have been mentioned. Abundant literature and journals are available being [22] probably the most illuminating. Magnesium Diboride holds its spot at the top of the list as probably one of the most uncommon conventional superconductors, not only because of its exceptional high T_c but also because of its structure whose seeming simplicity (compared with cuprates') makes this compound scientifically interesting, in addition with the considerably low costs of manufacture

implied due to the abundance of its components in nature, its high critical currents and its high critical temperature. Practical applications above 20 K (boiling temperature of Hydrogen) are in order.

2. BCS THEORY FOR TRACING THE BANDS OF MgB_2

2.1. GENERALITIES: HAMILTONIAN AND GROUND STATE WAVEFUNCTION

An adequate microscopic theory of superconductivity has to be able to account for the infinite conductivity, the Meissner effect and the isotope effect exhibited by conventional superconductors. Bloch's one-particle model for the normal metal turns out to fail dramatically on this purpose. Following BCS, we can conceive a trial wavefunction as a product of Bloch wavefunctions of each Cooper pair in the system,

$$\psi_N(\mathbf{r}_1,...,\mathbf{r}_N) = \sum_{\mathbf{k}_1,...,\mathbf{k}_{N/2}} g(\mathbf{k}_1,...,\mathbf{k}_{N/2}) \exp\left[i\mathbf{k}_1\cdot(\mathbf{r}_1-\mathbf{r}_2)\right]\cdots\exp\left[i\mathbf{k}_{N/2}\cdot(\mathbf{r}_{N-1}-\mathbf{r}_N)\right], \quad \textbf{(2.1)}$$

where g weighs the probability of a certain pair to be placed at a given **k**-state, and then find that this function is incalculable; however, since the wave number will have to run over all the **k** values in the band, and being $N \sim 10^{23}$, the number of factors in the sum above and the number of g's to be determined will range up to the frantic quantity of $\sim 10^{10^{23}}$ [13]. The inadequacy of Bloch's theory to explain superconductivity, despite of its successful description of the band structure in normal metals, is evident. In Bloch's treatment, it is assumed that the movement of

the electron through the lattice occurs independently and in the presence of a rather self-consistent field produced by the other electrons and ions [4] therefore neglecting the dynamical effects of the lattice vibrations due to the electrons as well as the correlation between electrons by Coulomb forces.

Upon Fröhlich's suggestion of an attraction mechanism between electrons provided by the electron-phonon interaction [9], briefly described in **S. 1**, an insight on the interaction energies in the superconducting system becomes necessary. This is tackled by calculating the interaction between an electron and a polarized medium, via

$$H_{el-ph} = e\int d\mathbf{r}'\,\mathbf{P}(\mathbf{r}')\bullet\nabla_{\mathbf{r}'}\tfrac{1}{|\mathbf{R}-\mathbf{r}'|},$$

which yields [31]

$$H_{el-ph} = \sum_{\mathbf{q}''\mathbf{k},\sigma}\left(M_{\mathbf{q}}^{*}c_{\mathbf{q}''-\mathbf{k},\sigma}^{\dagger}c_{\mathbf{q}'',\sigma}a_{\mathbf{k}}^{\dagger} + M_{\mathbf{q}}c_{\mathbf{q}''+\mathbf{k},\sigma}^{\dagger}c_{\mathbf{q}'',\sigma}a_{\mathbf{k}}\right), \qquad \textbf{(2.2)}$$

with $\mathbf{q}=\mathbf{k}-\mathbf{k}'$ and $M_{\mathbf{q}}$ the interacting matrix element [32]. This calculation is carried by the second quantization (SQ) framework of the annihilation/creation fermionic operators (c and $c^{\dagger}$) and the annihilation/creation bosonic phonon operators (a and $a^{\dagger}$). Since we'll be more interested in the first ones rather than the second ones, we enunciate their anti-commutation properties, to be extensively used in the following:

$$\left\{c_{\mathbf{k},\sigma},\, c^{\dagger}_{\mathbf{k}',\sigma}\right\} = \delta_{\mathbf{k}\mathbf{k}',\sigma\sigma'}$$
$$\left\{c^{\dagger}_{\mathbf{k},\sigma}, c^{\dagger}_{\mathbf{k}',\sigma}\right\} = \left\{c_{\mathbf{k},\sigma}, c_{\mathbf{k}',\sigma}\right\} = 0. \qquad \textbf{(2.3)}$$

Here σ denotes the electron spin. In the same context, from considerations of the effects of electrons and ions on the conductivity, an expression for the electron-electron interaction will read as [31]-[34]

$$H_{el-el} = \sum_{\mathbf{q}\mathbf{k}\mathbf{k}',\sigma\sigma'} \tfrac{1}{2} \tfrac{4\pi e^2}{q^2+\kappa_c^2} c^{\dagger}_{\mathbf{k}'-\mathbf{q},\sigma} c^{\dagger}_{\mathbf{k}'+\mathbf{q},\sigma'} c_{\mathbf{k},\sigma} c_{\mathbf{k}',\sigma'} \ , \qquad \textbf{(2.4)}$$

with κ_c standing for the electron-ion screening length. The sum of all these interactions, along with the kinetic energy of the electrons and phonons, results in the so-called **Fröhlich Hamiltonian** [9] [34],

$$H_{Fr} = \sum_{\mathbf{k},\sigma} \varepsilon_{\mathbf{k}} c^{\dagger}_{\mathbf{k},\sigma} c_{\mathbf{k},\sigma} + \sum_{\mathbf{k}} \hbar\omega_{\mathbf{k}} a^{\dagger}_{\mathbf{k}} a_{\mathbf{k}} + \sum_{\mathbf{q}\mathbf{k}\mathbf{k}',\sigma\sigma'} \tfrac{1}{2} \tfrac{4\pi e^2}{q^2+\kappa_c^2} c^{\dagger}_{\mathbf{k}'-\mathbf{q},\sigma} c^{\dagger}_{\mathbf{k}'+\mathbf{q},\sigma} c_{\mathbf{k},\sigma} c_{\mathbf{k}',\sigma'} + \sum_{\mathbf{q}\mathbf{q}',\sigma} M_{\mathbf{q}} c^{\dagger}_{\mathbf{q}+\mathbf{q}',\sigma} c_{\mathbf{q}',\sigma} \left(a^{\dagger}_{-\mathbf{q}} + a_{\mathbf{q}}\right), \qquad \textbf{(2.5)}$$

with $\varepsilon_{\mathbf{k}}$ representing the Bloch energies. In order to integrate the effect of the phonons into a single total effective interaction with electrons, a canonical transformation is carried out [31] [32] [34],

$$H' = e^{-S} H_{Fr} e^{S} \ ,$$

with the result of diagonalizing the Hamiltonian by the appropriate selection of *S*, this yielding

$$H' = \sum_{\mathbf{k}\mathbf{k}'\mathbf{q},\sigma\sigma'} \left\{ \frac{2\hbar\omega_{\mathbf{q}} |M_{\mathbf{q}}|^2}{\left(\varepsilon_{\mathbf{k}} - \varepsilon_{\mathbf{k}+\mathbf{q}}\right)^2 - \left(\hbar\omega_{\mathbf{q}}\right)^2} + \frac{4\pi e^2}{q^2+\kappa_c^2} \right\} c^{\dagger}_{\mathbf{k}'-\mathbf{q},\sigma'} c_{\mathbf{k}',\sigma'} c^{\dagger}_{\mathbf{k}+\mathbf{q},\sigma} c_{\mathbf{k},\sigma} . \qquad \textbf{(2.6)}$$

For the interested reader, details of this diagonalization procedure are offered in Refs. [31] and [32], among other standard textbooks [6] [15].

It is noteworthy that the main feature of the Hamiltonian of **Eq. (2.6)** is the fact that the term in brackets becomes negative for $\left|\varepsilon_{\mathbf{k}}-\varepsilon_{\mathbf{k}+\mathbf{q}}\right|\ll\hbar\omega_{\mathbf{q}}$ when the electron-phonon interaction term dominates over the screened Coulomb interaction. BCS postulate that $\left|\varepsilon_{\mathbf{k}}-\varepsilon_{\mathbf{k}+\mathbf{q}}\right|\ll\hbar\omega_{\mathbf{q}}$ is the order of the energy difference for the important superconducting transitions to occur [33] [34]. In addition, they narrow the interval of the attractive interaction down to $E_F-\hbar\omega_D\le\varepsilon_{\mathbf{k}}\le E_F+\hbar\omega_D$, leaving only those electron states with **k**'s sufficiently close to the Fermi surface because these play the most significant role in the process; finally, BCS introduce the form of the interacting matrix elements for these electrons as the averaged quantity [4]

$$-V=\left\langle -\frac{2\left|M_{\mathbf{q}}\right|^2}{\hbar\omega_{\mathbf{q}}}+\frac{4\pi e^2}{\kappa_c^2}\right\rangle_{Av}<0. \qquad \textbf{(2.7)}$$

These approximations relax **Eq. (2.6)** down to

$$H'=-V\sum_{\mathbf{k}\mathbf{k}'\mathbf{q},\sigma\sigma'}c^{\dagger}_{\mathbf{k}'-\mathbf{q},\sigma'}c_{\mathbf{k}',\sigma}c^{\dagger}_{\mathbf{k}+\mathbf{q},\sigma'}c_{\mathbf{k},\sigma}, \qquad \textbf{(2.8)}$$

leading to the complete Hamiltonian (kinetic plus potential energy), to be written as

$$H=\sum_{\mathbf{k},\sigma}\varepsilon_{\mathbf{k}\sigma}c^{\dagger}_{\mathbf{k}\sigma}c_{\mathbf{k}\sigma}-V\sum_{\mathbf{k}\mathbf{k}'\mathbf{q},\sigma\sigma'}c^{\dagger}_{\mathbf{k}'-\mathbf{q},\sigma'}c_{\mathbf{k}',\sigma'}c^{\dagger}_{\mathbf{k}+\mathbf{q},\sigma}c_{\mathbf{k},\sigma}. \qquad \textbf{(2.9)}$$

A further simplification on **Eq. (2.9)** is still on the way when BCS exclude out all the interacting pairs within the energy interval of interest except those with opposite wave numbers [4]. The footing of this decision is closely related to the requisition of an adequate wavefunction for the ground state [32] [35]. For further simplicity, $\mathbf{q} = 0$ is chosen. Furthermore, since the exchange energy between electrons is minimum for electrons with anti-parallel spins, such assumption is also adopted. In **Eq. (2.9)** we replace them by $\uparrow$ or $\downarrow$; because wave numbers are also opposite, we decide to compile this observation into the single notation, $\mathbf{k}\uparrow$ or $-\mathbf{k}\downarrow$. However, we will prefer the use of the spin index whenever a simplification in the notation is gained.

With all these truncations considered, **Eq. (2.9)** can be finally rewritten in the more condensed form, known as **reduced Hamiltonian** [4]:

$$H_{red} = \sum_{\mathbf{k}} \varepsilon_{\mathbf{k}} \left(c^{\dagger}_{\mathbf{k}\uparrow} c_{\mathbf{k}\uparrow} + c^{\dagger}_{-\mathbf{k}\downarrow} c_{-\mathbf{k}\downarrow} \right) - \sum_{\mathbf{k}\mathbf{k}'} V_{\mathbf{k}\mathbf{k}'} c^{\dagger}_{\mathbf{k}\uparrow} c^{\dagger}_{-\mathbf{k}\downarrow} c_{\mathbf{k}\uparrow} c_{-\mathbf{k}\downarrow}. \qquad \textbf{(2.10)}$$

Finally, it has to be observed that c and $c^{\dagger}$ still satisfy **Eq. (2.3)** but cc and $c^{\dagger}c^{\dagger}$ satisfy a completely different set of commutation rules [4].

The enunciation of a ground state wavefunction for Hamiltonian **(2.10)** is in close link to its structure. In detail, BCS first propose and reduce the Hamiltonian in the manner described above and then use all the negative terms from **Eq. (2.6)** to enter them with equal phases into a

constructed wavefunction [4]; later, they demonstrate that with the proper selection of the coefficients of the argument this wavefunction is an eigenstate of **Eq. (2.10)** [6].

The construction of this wavefunction is not hard to see within the SQ notation. If one returns to **Eq. (2.1)** and brings the expression into the SQ scheme, considering the simplifications discussed before and introducing the proper normalization constant, one is left with [31]

$$\left|\psi_N\right\rangle = \tfrac{1}{N!}\left(\sum_{\mathbf{k}} g_{\mathbf{k}} c^{\dagger}_{\mathbf{k}\uparrow} c^{\dagger}_{-\mathbf{k}\downarrow}\right)^N \left|0\right\rangle, \qquad \textbf{(2.11)}$$

where **Eq. (2.11)** remains yet incalculable because of the size of N; for matters of convenience it was supposed that the number of pairs is $2N$ instead of N. The correct course in deriving the weight coefficients $g_{\mathbf{k}}$ would be to submit the reduced Hamiltonian to a variational minimization procedure in which mean values, with **Eq. (2.11)** as basis, would have to be estimated [6]. This is an evidently tiresome task, again because of N; consequently, BCS decide to work with the function

$$\left|\psi\right\rangle = \sum_N \lambda_N \left|\psi_N\right\rangle, \qquad \textbf{(2.12)}$$

where λ_N is a weight factor. By direct substitution of **Eq. (2.11)** into **Eq. (2.12)** it becomes easy to realize that $\left|\psi\right\rangle$ can be rewritten as

$$|\psi\rangle = N \exp\left(\sum_{\mathbf{k}} g_{\mathbf{k}} c^{\dagger}_{\mathbf{k}\uparrow} c^{\dagger}_{-\mathbf{k}\downarrow} \right) |0\rangle .$$

Expanding out,

$$\begin{aligned} |\psi\rangle &= N \left(1 + g_{\mathbf{k}} c^{\dagger}_{\mathbf{k}\uparrow} c^{\dagger}_{-\mathbf{k}\downarrow} + \tfrac{1}{2!}\left(g_{\mathbf{k}} c^{\dagger}_{\mathbf{k}\uparrow} c^{\dagger}_{-\mathbf{k}\downarrow}\right)^2 + \cdots\right)\left(1 + g_{\mathbf{k}'} c^{\dagger}_{\mathbf{k}'\uparrow} c^{\dagger}_{-\mathbf{k}'\downarrow} + \tfrac{1}{2!}\left(g_{\mathbf{k}'} c^{\dagger}_{\mathbf{k}'\uparrow} c^{\dagger}_{-\mathbf{k}'\downarrow}\right)^2 + \cdots\right)\cdots|0\rangle \\ &= \prod_{\mathbf{k}} \left(1 + g_{\mathbf{k}} c^{\dagger}_{\mathbf{k}\uparrow} c^{\dagger}_{-\mathbf{k}\downarrow} + \tfrac{1}{2!}\left(g_{\mathbf{k}} c^{\dagger}_{\mathbf{k}\uparrow} c^{\dagger}_{-\mathbf{k}\downarrow}\right)^2 + \cdots\right)|0\rangle = N \prod_{\mathbf{k}} \left(1 + g_{\mathbf{k}} c^{\dagger}_{\mathbf{k}\uparrow} c^{\dagger}_{-\mathbf{k}\downarrow}\right)|0\rangle, \end{aligned}$$

where the last equality is the result of the properties enunciated in **Eq. (2.3)**. The Hartee-like function derived above is proposed by BCS in their fundamental paper [4], showing the probabilities of finding a given **k** level occupied in pairs or empty. The normalization leads to [13],

$$|\psi_{BCS}\rangle = \prod_{\mathbf{k}} \left(u_{\mathbf{k}} + v_{\mathbf{k}} c^{\dagger}_{\mathbf{k}\uparrow} c^{\dagger}_{-\mathbf{k}\downarrow}\right)|0\rangle , \qquad \textbf{(2.13)}$$

where

$$u^2_{\mathbf{k}} + v^2_{\mathbf{k}} = 1 \ . \qquad \textbf{(2.14)}$$

A formal interpretation of **Eq. (2.14)** will be offered in **S.S. 2.2**.

The success of BCS' approach in using **Eq. (2.13)** as the correct ground-state wavefunction lies in the easiness of the computation in the grand-canonical ensemble rather than in the canonical ensemble [13] [31] (See **S.S. 2.3**). The simplicity of **Eq. (2.13)** when compared with **Eq. (2.1)** or **Eq. (2.12)** is straightforward. However, working with **Eq. (2.13)** implies a cost;

in this case, the fact that the average particle number $\langle N \rangle$ is not uniquely defined when calculated using **Eq. (2.13)** as basis [6]. Nonetheless, BCS show that $\sqrt{\langle N^2 \rangle - \langle N \rangle^2}$ is in the order of $N^{-\frac{1}{2}}$ and thereby the quantity is neglectible with increasing number of particles. With a manageable wavefunction in hand, the path to a minimization procedure is clear and direct.

2.2. BCS THEORY FOR A PURE SINGLE ENERGY GAP SUPERCONDUCTOR AT $T = 0$.

The simplest superconducting system corresponds to a pure superconductor at zero temperature where the treatment discussed above plainly applies. The quest for the coefficients *u* and *v* in **Eq. (2.13)** and its determination via minimization of the mean value of the reduced Hamiltonian will become the main task in this Sub-section. To do so, we mathematically shift the ground-state energy by defining

$$\xi_{\mathbf{k}} = \varepsilon_{\mathbf{k}} - E_F \qquad \textbf{(2.15)}$$

and substitute this into **Eq. (2.10)**, which results transformed into

$$H = H_{red} - E_F N \ , \qquad \textbf{(2.16)}$$

where *N* stands for the **number operator**, given by

$$N = \sum_{\mathbf{k}\sigma} c^{\dagger}_{\mathbf{k}\sigma} c_{\mathbf{k}\sigma} \ , \qquad \textbf{(2.17)}$$

$\sigma = \{\uparrow, \downarrow\}$. The second addend at the right of **Eq. (2.16)** is a direct consequence of keeping $\langle N \rangle$ fixed [13]. The effect of minimization results in

$$0 = \delta \left\langle \Psi_G^{BCS} \left| \left(H_{red} - E_F N \right) \right| \Psi_G^{BCS} \right\rangle = \delta \left[2 \sum_{\mathbf{k}\sigma} \xi_{\mathbf{k}\sigma} \left| v_{\mathbf{k}}^2 \right| + \sum_{\mathbf{kl}} V_{\mathbf{kl}} u_{\mathbf{k}} v_{\mathbf{k}} u_{\mathbf{l}} v_{\mathbf{l}} \right] , \qquad \textbf{(2.18)}$$

where the constraint **Eq. (2.14)** is imposed by introducing

$$\begin{aligned} u_{\mathbf{k}} &= \cos\theta_{\mathbf{k}} \\ v_{\mathbf{k}} &= \sin\theta_{\mathbf{k}} \ . \end{aligned} \qquad \textbf{(2.19)}$$

Substitution in **Eq. (2.18)** and explicit differentiation with respect $\theta_{\mathbf{k}}$ yields

$$-2\xi_{\mathbf{k}\sigma} \sin 2\theta_{\mathbf{k}} + \cos 2\theta_{\mathbf{k}} \sum_{\mathbf{l}} V_{\mathbf{kl}} \sin 2\theta_{\mathbf{l}} = 0.$$

When some algebra is performed in this expression [13], the equation above can be manipulated into

$$\tan 2\theta_{\mathbf{k}} = \frac{\sum_{\mathbf{l}} V_{\mathbf{kl}} \sin 2\theta_{\mathbf{l}}}{2\xi_{\mathbf{k}}} = -\frac{\Delta_{\mathbf{k}}}{\xi_{\mathbf{k}}} , \qquad \textbf{(2.20)}$$

where

$$\Delta_{\mathbf{k}} = -\tfrac{1}{2} \sum_{\mathbf{l}} V_{\mathbf{kl}} \sin 2\theta_{\mathbf{k}} \ . \qquad \textbf{(2.21)}$$

The term of **Eq. (2.21)** represents the most important physical quantity along this document; it corresponds to a preliminary version of the **energy gap** (henceforth referred as Δ- **term**). A simple geometric construction shown in **Fig. 2.1** allows one to interpret its meaning.

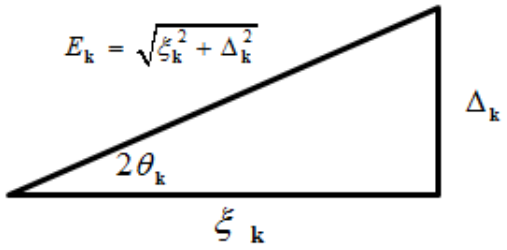

Figure 2.1. Geometric meaning of θ_{k} [13]

Since $E_{\mathbf{k}} = \Delta_{\mathbf{k}}$ if $\xi_{\mathbf{k}} = 0$ (Fermi level), it stands clear that $\Delta_{\mathbf{k}}$ is evidently the **minimum excitation energy**, hence

$$E_{\mathbf{k}} = \sqrt{\xi_{\mathbf{k}}^2 + \Delta_{\mathbf{k}}^2} \ . \tag{2.22}$$

is the **excitation energy** over the Fermi level. BCS demonstrate the existence of the energy gap by computing the energy difference between a state where a Cooper pair is broken in uncorrelated electrons and one in which they lay in the ground state, deriving 2Δ as result [4] [6]. It's interesting to contrast this with what was discussed in **S.S. 1.3**.

With the help of **Eq. (2.22)**, **Eq. (2.21)** can be transformed into

$$\Delta_{\mathbf{k}} = -\tfrac{1}{2} \sum_{\mathbf{l}} V_{\mathbf{kl}} \frac{\Delta_{\mathbf{l}}}{\sqrt{\xi_{\mathbf{l}}^2 + \Delta_{\mathbf{l}}^2}} \ , \tag{2.23}$$

which will be referred henceforth as the **self-consistency equation**. In the following Sub-sections it'll be seen how this condition changes with the introduction of excitations and the

increase of the number of energy gaps. The self-consistency equation is important because it directly hands a procedure for computing the Δ- term(s).

A little algebraic game with **Eq. (2.19)**, **Eq. (2.20)**, **Eq. (2.21)** and the geometrics of **Fig. 2.1** lead to the result

$$\begin{aligned} u_{\mathbf{k}}^2 &= \tfrac{1}{2}\left(1+\tfrac{\xi_{\mathbf{k}}}{E_{\mathbf{k}}}\right) \\ v_{\mathbf{k}}^2 &= \tfrac{1}{2}\left(1-\tfrac{\xi_{\mathbf{k}}}{E_{\mathbf{k}}}\right). \end{aligned} \qquad \textbf{(2.24)}$$

Attention should be paid to the behavior of these quantities; for example, it's seen that when $\xi_{\mathbf{k}} \to -\infty$, then $v_{\mathbf{k}}^2 \to 1$ and $u_{\mathbf{k}}^2 \to 0$; when $\xi_{\mathbf{k}} \to +\infty$, then $v_{\mathbf{k}}^2 \to 0$ and $u_{\mathbf{k}}^2 \to 1$. Thus, these coefficients account for the probability of occupation of states below and above the Fermi level in the superconducting state. On the other hand, when $\Delta_{\mathbf{k}} = 0$ (normal state) then $u_{\mathbf{k}}^2 = 0$ and $v_{\mathbf{k}}^2 = 1$. A description of this behavior can be drawn out from **Fig. 2.2**. Observe the resemblance with the Fermi-Dirac distribution, although they're slightly different [13].

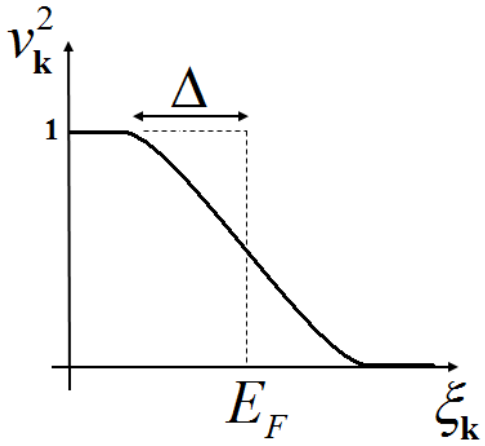

Figure 2.2. Plot of $v_{\mathbf{k}}^2$ vs. $\xi_{\mathbf{k}}$

Important information can be derived from **Eq. (2.23)** when the condition **(2.7)** is introduced in the following manner:

$$V_{\mathbf{kl}} = \begin{cases} -V, |\xi_{\mathbf{k}}| \le \hbar\omega_D \\ 0, |\xi_{\mathbf{k}}| > \hbar\omega_D \end{cases} . \qquad \textbf{(2.25)}$$

Then, substituting into **Eq. (2.23)**, it is found that the self-consistency equation is satisfied only if $\Delta_{\mathbf{k}}$ fulfills [13] [36]

$$\Delta_{\mathbf{k}} = \begin{cases} \Delta, |\xi_{\mathbf{k}}| \le \hbar\omega_D \\ 0, |\xi_{\mathbf{k}}| > \hbar\omega_D \end{cases}, \qquad \textbf{(2.26)}$$

which upon the cancelation of Δ at both sides leaves **Eq. (2.23)** reading as

$$1 = \tfrac{V}{2} \sum_{\mathbf{k}} \left(\xi_{\mathbf{k}}^2 + \Delta^2 \right)^{-\frac{1}{2}}.$$

By transformation of the sum into an integral, the sum becomes

$$1 = \frac{V}{2}\int N(\xi)\frac{1}{\sqrt{\xi^2+\Delta^2}}\,d\xi,$$

where the weight function N is the density of states within the energy layer $-\hbar\omega_D \le \xi \le \hbar\omega_D$; here, for the sake of simplicity in the calculation, we will choose it to be constant and equal to $N(\xi = 0) = N^0$ allowing us to factor it out of the integral. Finally, given that V is different from zero only within the mentioned region and using the symmetry of ξ, one draws

$$\frac{1}{N^0 V} = \int_0^{\hbar\omega_D}\frac{d\xi}{\sqrt{\xi^2+\Delta^2}} = \sinh^{-1}\left(\frac{\hbar\omega_D}{\Delta^0}\right).$$

When Δ is cleared up from the equation, the specific form of $\sinh^{-1}$ is used and the approximation $\lambda = N^0 V \ll 1$ (known in literature as **weak-coupling limit**) is applied, a simple expression for the Δ- term is finally derived as

$$\Delta^0 \approx 2\hbar\omega_D \exp\left(-\frac{1}{\lambda}\right), \qquad \textbf{(2.27)}$$

where λ denotes the **coupling constant**. Typically $\lambda \le 0.3$ in the weak-coupling limit; this approximation makes the former estimation accurate enough up to a 1% [13] which is surprisingly small considering that the possible influence of the electron-phonon interaction with electrons outside energy interval $-\hbar\omega_D \le \xi \le \hbar\omega_D$, as well as other assumptions already mentioned, were totally neglected. Substitution of typical values in **Eq. (2.27)** place Δ^0 around 0.8 meV for a Debye temperature of about 300K.

Result of **Eq. (2.27)** is a demonstrative estimation of the Δ- term under the simple conditions inherent to the superconducting system at $T = 0$. The logical next step will be to consider such estimation when $T \neq 0$.

2.3. BCS THEORY FOR A PURE SINGLE ENERGY GAP SUPERCONDUCTOR AT $T \neq 0$.

An immediate generalization of the previous results is in order for the treatment of our system when excited states are allowed; however, an approach based in a variational-like minimization of the energy will prove to be rather tiresome and complicated. A more sophisticated, modern, simplifying and elegant procedure is that suggested by N. Bogoliubov and J. Valatin [17] [37]; we will refer it henceforth as **BV formalism**. BCS theory and BV formalism are proved to be equivalent, as showed by Yoshida [38], however, the BV approach will prove to be more convenient when applied in the treatment of excitations in the superconducting system.

The BCS procedure for dealing with excitations is done exactly in the same way of **S.S. 2.2**. and such is adopted by BCS in their fundamental paper [4]. Bogoliubov, however, chooses a different path. Briefly describing, he rewrites the Fröhlich's Hamiltonian of **Eq. (2.5)**, ignoring the Coulomb contribution of the third sum at the right as a very crude approximation, and integrates the remaining terms in a new Hamiltonian [6]:

$$H'_{Fr} = \sum_{\mathbf{kq}} M_{\mathbf{q}} \left(\frac{\hbar\omega_{\mathbf{q}}}{2\Omega}\right)^{\frac{1}{2}} \left(a^{\dagger}_{\mathbf{q}} + a_{-\mathbf{q}}\right)\left(c^{\dagger}_{\mathbf{k}\uparrow} c_{\mathbf{k}+\mathbf{q},\uparrow} + c^{\dagger}_{-\mathbf{k}-\mathbf{q},\downarrow} c_{-\mathbf{k}\downarrow}\right), \qquad \textbf{(2.28)}$$

where the matrix element $M_{\mathbf{q}}$, the $a / a^{\dagger}$- and $c / c^{\dagger}$- operators have the same interpretation and properties as in **Eq. (2.5)**. A set of elementary excitations with respect to the normal state, including the creation/annihilation of electrons and holes, is defined by the author; however, he concludes that the normal Fermi sea is not the adequate starting point, due to its instability because of the presence of the interaction **(2.28)**, hence the correct set of excitations has to be made more general. As observed independently by Valatin [37], the correct description of such excitations can be done by introducing a canonical transformation on the *c*-operators in **Eq. (2.28)** defined by

$$\begin{aligned} \gamma^{\dagger}_{\mathbf{k}\uparrow} &= u_{\mathbf{k}} c^{\dagger}_{\mathbf{k}\uparrow} - v_{\mathbf{k}} c_{-\mathbf{k}\downarrow} \\ \gamma_{-\mathbf{k}\downarrow} &= u_{\mathbf{k}} c_{-\mathbf{k}\downarrow} + v_{\mathbf{k}} c^{\dagger}_{\mathbf{k}\uparrow}, \end{aligned} \qquad \textbf{(2.29)}$$

where *u* and *v* still satisfy condition **(2.14)** and again they have to be determined. The $\gamma / \gamma^{\dagger}$- operators are named **quasi-particles annihilation/creation operators**. It is demonstrated that $\gamma / \gamma^{\dagger}$- operators satisfy the same anticommutation rules **(2.3)**,

$$\begin{aligned} \left\{\gamma_{\mathbf{k},\sigma},\, \gamma^{\dagger}_{\mathbf{k}',\sigma}\right\} &= \delta_{\mathbf{k}\mathbf{k}',\sigma\sigma'} \\ \left\{\gamma^{\dagger}_{\mathbf{k},\sigma}, \gamma^{\dagger}_{\mathbf{k}',\sigma}\right\} &= \left\{\gamma_{\mathbf{k},\sigma}, \gamma_{\mathbf{k}',\sigma}\right\} = 0. \end{aligned} \qquad \textbf{(2.30)}$$

When **Eq. (2.29)** is inverted and substituted into **Eq. (2.28)** and by applying the condition that $\langle N \rangle$ is kept fixed, Hamiltonian **(2.28)** is transformed into

$$H'_{Fr} - E_F N =$$
$$2\sum_{\mathbf{k}}\left(\varepsilon_{\mathbf{k}} - E_F\right)v_{\mathbf{k}}^2 + \sum_{\mathbf{k}}\left(\varepsilon_{\mathbf{k}} - E_F\right)\left(u_{\mathbf{k}}^2 - v_{\mathbf{k}}^2\right)\left(\gamma_{\mathbf{k}\uparrow}^{\dagger}\gamma_{\mathbf{k}\uparrow} + \gamma_{-\mathbf{k}\downarrow}^{\dagger}\gamma_{-\mathbf{k}\downarrow}\right) + \sum_{\mathbf{q}}\hbar\omega_{\mathbf{q}}a_{\mathbf{q}}^{\dagger}a_{\mathbf{q}} + \qquad \textbf{(2.31)}$$
$$H' + H'',$$

where the mathematical structure of the Hamiltonians H' and H'' is not shown but both are so complicated that it is not obvious to consider them as small perturbations. Bogoliubov demonstrates that the condition of $H' + H''$ seen as a small perturbation is precisely the condition that enables the determination of the coefficients *u* and *v* [6] [17]. Such is accomplished by the realization that the perturbations induced by H' and H'' exactly cancel each other's "dangerous terms" out [6] [17] simplifying singularities and leading to a compensation condition that carries **Eq. (2.31)** into a nicer form which ultimately delivers the values of *u* and *v*.

Nonetheless, Valatin carries out an equivalent procedure [37] which uses less complicated expressions. Using a rather relaxed notation compared with that used by the author, Valatin introduces the transformations **(2.29)** by considering that due to the large number of particles involved and for low order excitations, the occupation of Bloch states with Cooper pairs, given by the particle number $c_{\mathbf{k},\sigma}c_{\mathbf{k},\sigma}^{\dagger}$, should not vary considerably around its mean value [13]; here the mean value is computed with respect to the ground state [36]. This allows us to write, in **Eq. (2.10)**,

$$c_{\mathbf{k},\sigma}c_{\mathbf{k},\sigma}^{\dagger} = \left(c_{\mathbf{k},\sigma}c_{\mathbf{k},\sigma}^{\dagger} - \left\langle c_{\mathbf{k},\sigma}c_{\mathbf{k},\sigma}^{\dagger}\right\rangle\right) + \left\langle c_{\mathbf{k},\sigma}c_{\mathbf{k},\sigma}^{\dagger}\right\rangle. \qquad \textbf{(2.32)}$$

By making the spin direction explicit and introducing

$$b_{\mathbf{k}}^{*} = \left\langle c_{\mathbf{k}\uparrow}^{\dagger} c_{-\mathbf{k}\downarrow}^{\dagger} \right\rangle$$
$$b_{\mathbf{l}} = \left\langle c_{-\mathbf{l}\downarrow} c_{\mathbf{l}\uparrow} \right\rangle, \tag{2.33}$$

the quartic term in the second sum of **Eq. (2.10)** can be rewritten as

$$c_{\mathbf{k}\uparrow}^{\dagger} c_{-\mathbf{k}\downarrow}^{\dagger} c_{-\mathbf{l}\downarrow} c_{\mathbf{l}\uparrow} = b_{\mathbf{l}} c_{\mathbf{k}\uparrow}^{\dagger} c_{-\mathbf{k}\downarrow}^{\dagger} + b_{\mathbf{k}}^{*} c_{-\mathbf{l}\downarrow} c_{\mathbf{l}\uparrow} - b_{\mathbf{k}}^{*} b_{\mathbf{l}},$$

where bilinear terms of higher order were neglected. This substitution yields

$$\begin{aligned} H_M^{\mathrm{I}} &= \sum_{\mathbf{k}\sigma} \xi_{\mathbf{k}} c_{\mathbf{k}\sigma}^{\dagger} c_{\mathbf{k}\sigma} + \sum_{\mathbf{kl}} V_{\mathbf{kl}} \left(b_{\mathbf{l}} c_{\mathbf{k}\uparrow}^{\dagger} c_{-\mathbf{k}\downarrow}^{\dagger} + b_{\mathbf{k}}^{*} c_{-\mathbf{l}\downarrow} c_{\mathbf{l}\uparrow} - b_{\mathbf{k}}^{*} b_{\mathbf{l}} \right) \\ &= \sum_{\mathbf{k}\sigma} \xi_{\mathbf{k}} c_{\mathbf{k}\sigma}^{\dagger} c_{\mathbf{k}\sigma} - \sum_{\mathbf{k}} \left(\Delta_{\mathbf{k}} c_{\mathbf{k}\uparrow}^{\dagger} c_{-\mathbf{k}\downarrow}^{\dagger} + \Delta_{\mathbf{k}}^{*} c_{-\mathbf{k}\downarrow} c_{\mathbf{k}\uparrow} - \Delta_{\mathbf{k}} b_{\mathbf{k}}^{*} \right), \end{aligned} \tag{2.34}$$

where dummy indices were conveniently exchanged in the second summation. Notice in this expression, known henceforth as **model Hamiltonian** for the single energy gap superconductor (hence the superscript), that the Δ- term was introduced as

$$\Delta_{\mathbf{k}} = -\sum_{\mathbf{l}} V_{\mathbf{kl}} b_{\mathbf{l}} = -\sum_{\mathbf{l}} V_{\mathbf{kl}} \left\langle c_{-\mathbf{l}\downarrow} c_{\mathbf{l}\uparrow} \right\rangle, \tag{2.35}$$

which corresponds to **Eq. (2.23)**. Also, because of the disappearance of quartic terms in the *c*-operators in **Eq. (2.34)**, the calculation of the grand canonical partition function, and thus the thermodynamics of the system, is clear-cut [31]. The substitution of **Eq. (2.29)** into Hamiltonian **(2.34)** yields

$$H_M^1 =$$
$$\sum_{\mathbf{k}} \xi_{\mathbf{k}} \left\{ \left(u_{\mathbf{k}}^2 - v_{\mathbf{k}}^2 \right) \left(\gamma_{\mathbf{k}\uparrow}^{\dagger} \gamma_{\mathbf{k}\uparrow} + \gamma_{-\mathbf{k}\downarrow}^{\dagger} \gamma_{-\mathbf{k}\downarrow} \right) + 2v_{\mathbf{k}}^2 + 2u_{\mathbf{k}} v_{\mathbf{k}} \gamma_{\mathbf{k}\uparrow}^{\dagger} \gamma_{-\mathbf{k}\downarrow}^{\dagger} + 2u_{\mathbf{k}} v_{\mathbf{k}} \gamma_{\mathbf{k}\uparrow} \gamma_{-\mathbf{k}\downarrow} \right\} +$$
$$\sum_{\mathbf{k}} \left\{ u_{\mathbf{k}} v_{\mathbf{k}} \left(\Delta_{\mathbf{k}} + \Delta_{\mathbf{k}}^{*} \right) \left(\gamma_{\mathbf{k}\uparrow}^{\dagger} \gamma_{\mathbf{k}\uparrow} + \gamma_{-\mathbf{k}\downarrow}^{\dagger} \gamma_{-\mathbf{k}\downarrow} - 1 \right) - \left(\Delta_{\mathbf{k}} u_{\mathbf{k}}^2 - \Delta_{\mathbf{k}} v_{\mathbf{k}}^2 \right) \gamma_{\mathbf{k}\uparrow}^{\dagger} \gamma_{-\mathbf{k}\downarrow}^{\dagger} + \left(\Delta_{\mathbf{k}} u_{\mathbf{k}}^2 - \Delta_{\mathbf{k}}^{*} v_{\mathbf{k}}^2 \right) \gamma_{\mathbf{k}\uparrow} \gamma_{-\mathbf{k}\downarrow} + \Delta_{\mathbf{k}} b_{\mathbf{k}} \right\},$$

and if a convenient rearrangement of the terms above is done via the condition **(2.30)**, one derives

$$H_M^1 =$$
$$\sum_{\mathbf{k}} \xi_{\mathbf{k}} \left\{ \left(u_{\mathbf{k}}^2 - v_{\mathbf{k}}^2 \right) + u_{\mathbf{k}} v_{\mathbf{k}} \left(\Delta_{\mathbf{k}} + \Delta_{\mathbf{k}}^{*} \right) \right\} \left(\gamma_{\mathbf{k}\uparrow}^{\dagger} \gamma_{\mathbf{k}\uparrow} + \gamma_{-\mathbf{k}\downarrow}^{\dagger} \gamma_{-\mathbf{k}\downarrow} \right) + \sum_{\mathbf{k}} \left(\Delta_{\mathbf{k}}^{*} v_{\mathbf{k}}^2 + 2\xi_{\mathbf{k}} u_{\mathbf{k}} v_{\mathbf{k}} - \Delta_{\mathbf{k}} u_{\mathbf{k}}^2 \right) \gamma_{\mathbf{k}\uparrow}^{\dagger} \gamma_{-\mathbf{k}\downarrow}^{\dagger}$$
$$+ \sum_{\mathbf{k}} \left(\Delta_{\mathbf{k}} v_{\mathbf{k}}^2 + 2\xi_{\mathbf{k}} u_{\mathbf{k}} v_{\mathbf{k}} - \Delta_{\mathbf{k}}^{*} u_{\mathbf{k}}^2 \right) \gamma_{-\mathbf{k}\downarrow} \gamma_{\mathbf{k}\uparrow} + \sum_{\mathbf{k}} \left(2\xi_{\mathbf{k}} v_{\mathbf{k}}^2 - u_{\mathbf{k}} v_{\mathbf{k}} \left(\Delta_{\mathbf{k}} + \Delta_{\mathbf{k}}^{*} \right) + \Delta_{\mathbf{k}}^{*} b_{\mathbf{k}} \right).$$

(2.36)

Notice the resemblance of **Eq. (2.36)** with Hamiltonian **(2.31)**. Operators $\gamma^{\dagger}\gamma^{\dagger}$ and $\gamma\gamma$ stand for second order excitations and by assuming that our formalism is valid up to excitations of first order we can conveniently choose *u* and *v* to make these terms to vanish and complete the diagonalization. By noticing that the coefficients of the second and third sums in Hamiltonian **(2.36)** are complex conjugate of each other and treating $\Delta_{\mathbf{k}}$ as real, the neglecting condition lightens up to

$$\Delta_{\mathbf{k}} v_{\mathbf{k}}^2 + 2\xi_{\mathbf{k}} u_{\mathbf{k}} v_{\mathbf{k}} - \Delta_{\mathbf{k}} u_{\mathbf{k}}^2 = 0, \qquad \textbf{(2.37)}$$

which allows the straightforward solution

$$\frac{v_{\mathbf{k}}}{u_{\mathbf{k}}} \Delta_{\mathbf{k}} = E_{\mathbf{k}} - \xi_{\mathbf{k}}.$$

Here the choice of the positive square root as the correct one corresponds with the minimum energy criteria [13]. Implementation of the result above, together with the condition **(2.14)**, yields

$$u_{\mathbf{k}}^2 = \tfrac{1}{2}\left(1+\tfrac{\xi_{\mathbf{k}}}{E_{\mathbf{k}}}\right)$$
$$v_{\mathbf{k}}^2 = \tfrac{1}{2}\left(1-\tfrac{\xi_{\mathbf{k}}}{E_{\mathbf{k}}}\right),$$

which is the exact same result of **Eq. (2.24)** derived by the variational principle.

The effect of the BV formalism and the set of transformations **(2.29)** on our cherished Δ-term prove its suitability. Just inserting the transformation **(2.29)** inverted into **Eq. (2.35)** leaves

$$\Delta_{\mathbf{k}} = \sum_{\mathbf{l}} V_{\mathbf{kl}} \left\langle c_{-\mathbf{l}\downarrow} c_{\mathbf{l}\uparrow} \right\rangle = \sum_{\mathbf{l}} V_{\mathbf{kl}} \left\langle \left(-v_{\mathbf{l}}\gamma_{\mathbf{l}\uparrow}^{\dagger} + u_{\mathbf{l}}\gamma_{-\mathbf{l}\downarrow}\right)\left(u_{\mathbf{l}}\gamma_{\mathbf{l}\uparrow} + v_{\mathbf{l}}\gamma_{-\mathbf{l}\downarrow}^{\dagger}\right)\right\rangle$$
$$= \sum_{\mathbf{l}} V_{\mathbf{kl}} u_{\mathbf{l}} v_{\mathbf{l}} \left\langle 1 - \gamma_{-\mathbf{l}\downarrow}^{\dagger}\gamma_{-\mathbf{l}\downarrow} - \gamma_{\mathbf{l}\uparrow}^{\dagger}\gamma_{\mathbf{l}\uparrow} \right\rangle,$$

where the terms implying second order excitations, as $\left\langle \gamma_{\mathbf{l}\uparrow}^{\dagger}\gamma_{-\mathbf{l}\downarrow}^{\dagger} \right\rangle$ and $\left\langle \gamma_{-\mathbf{l}\downarrow}\gamma_{\mathbf{l}\uparrow} \right\rangle$, are neglected. The quantum statistical mechanical average computes [6] [36]

$$\left\langle 1 - \gamma_{-\mathbf{l}\downarrow}^{\dagger}\gamma_{-\mathbf{l}\downarrow} - \gamma_{\mathbf{l}\uparrow}^{\dagger}\gamma_{\mathbf{l}\uparrow} \right\rangle = \frac{\mathrm{tr}\left[e^{-\beta H_M}\left(1-\gamma_{-\mathbf{l}\downarrow}^{\dagger}\gamma_{-\mathbf{l}\downarrow} - \gamma_{\mathbf{l}\uparrow}^{\dagger}\gamma_{\mathbf{l}\uparrow}\right)\right]}{\mathrm{tr}\left(e^{-\beta H_M}\right)} = 1 - 2f^{F}\left(E_{\mathbf{l}}\right), \qquad \textbf{(2.38)}$$

where

$$f^{F}\left(E\right) = \frac{1}{1+\exp(\beta E)} \qquad \textbf{(2.39)}$$

stands for the **Fermi function**, $\beta = \left(k_B T\right)^{-1}$. Upon these results the Δ- term can now be written as

$$\Delta_{\mathbf{k}} = -\sum_{\mathbf{l}} V_{\mathbf{kl}} u_{\mathbf{l}} v_{\mathbf{l}} \left(1 - 2 f^{F}\left(E_{\mathbf{l}}\right)\right) = -\tfrac{1}{2} \sum_{\mathbf{l}} V_{\mathbf{kl}} \frac{\Delta_{\mathbf{l}}}{\sqrt{\xi_{\mathbf{l}}^2 + \Delta_{\mathbf{l}}^2}} \tanh\left(\tfrac{1}{2} \beta \sqrt{\xi_{\mathbf{l}}^2 + \Delta_{\mathbf{l}}^2}\right), \qquad \textbf{(2.40)}$$

where **Eq. (2.22)**, **Eq. (2.24)** and **Eq. (2.39)** were used. **Eq. (2.40)** corresponds to the generalized equivalent self-consistency equation **(2.23)** for the superconducting system when excitations are allowed; just note that **Eq. (2.40)** turns into **Eq. (2.23)** by taking $T = 0$ in the first, indicating that **(2.40)** is indeed a more generalized expression.

The inclusion of the condition **(2.25)** will lead again to condition **(2.26)** but will transform **Eq. (2.40)** into

$$1 = \tfrac{V}{2} \sum_{\mathbf{k}} \left(\xi_{\mathbf{k}}^2 + \Delta_{\mathbf{k}}^2\right)^{-\frac{1}{2}} \tanh\left[\tfrac{1}{2} \beta \left(\xi_{\mathbf{k}}^2 + \Delta_{\mathbf{k}}^2\right)^{\frac{1}{2}}\right],$$

and the transformation of the sum into an integral with the density of states as weight function, as done before, will yield

$$\frac{1}{N^0 V} = \int_0^{\hbar\omega_D} \frac{\tanh\frac{1}{2}\beta\sqrt{\xi^2 + \Delta^2}}{\sqrt{\xi^2 + \Delta^2}} d\xi,$$

where the symmetry of ξ around the Fermi level (or the parity of the integrand) again was used. The solution of this expression, however, is rather more complicated than its equivalent in **S.S. 2.2** and demands numerical work when $0 < T < T_c$. The behavior of the solution of this integral

equation is illustrated in **Fig. 1.5**. Such numerical procedure will be outlined and implemented in **Ch. III**.

In spite of the complications inherent to it, estimations can still be performed on this integral expression. By the observation that the Cooper pairing kicks in once $T = T_c$ and therefore $\Delta(T \to T_c) \to 0$ with Δ growing from zero as $T \to 0$, our expression softens up to

$$\frac{1}{N^0 V} = \int_0^{\hbar\omega_D} \frac{\tanh\frac{1}{2}\beta_c\xi}{\xi} d\xi ,$$

with $\beta_c = (k_B T_c)^{-1}$. Upon the mathematical substitution $x = \beta\xi$, the use of the explicit form of tanh [39] and the weak-coupling approximation (or $\beta_c\hbar\omega_D \approx \infty$), we compute [13] [31] [36]

$$\frac{1}{N^0 V} \approx \ln A(\beta_c\hbar\omega_D),$$

where $A = \frac{2\gamma_E}{\pi} \approx 1.14$, γ_E standing for Euler's constant. Solving for T_c

$$k_B T_c \approx 1.14\hbar\omega_D \exp\left(-\frac{1}{\lambda}\right). \qquad \textbf{(2.41)}$$

From **Eq. (2.41)** a comparison with **Eq. (2.27)** is immediate, with an estimate of the size of $\Delta(0) \equiv \Delta^0$ as result,

$$\Delta^0 = 1.764 k_B T_c \ . \qquad \textbf{(2.42)}$$

Compare this with the said about the size of the energy gap in **S.S. 1.3**.

2.4. BCS THEORY FOR A PURE DOUBLE ENERGY GAP SUPERCONDUCTOR AT $T \neq 0$.

With the most difficult part of the BV formalism being discussed, a generalization of BCS theory for the multiple energy gap case is immediate. The direct consequence of this extension consists in the addition of extra terms in the reduced Hamiltonian **(2.10)**, where now the notation will have to account for the different scattering possibilities for electrons lying in the two bands under study. Inspired by the theory of resistivity in transition metals, where electronic bands are labeled *s* and *d* [41], the corresponding emission and absorption of phonons can occur in four different manners in the vicinity of the Fermi level: via a *s*-*d* process (meaning the exchange of a phonon between an electron in *s*-band and an electron in *d*-band), a *d*-*s* process (meaning the exchange of a phonon between an electron in *d*-band and an electron in *s*-band), a *s*-*s* process (meaning the exchange occurs between electrons in *s*-band) or a *d*-*d* process (meaning the exchange occurs in the *d*-band); in consequence, three matrix elements $V_{sd} = V_{ds}$, V_{ss} and V_{dd} will be necessary leaving the reduced Hamiltonian reading as [41]

$$
\begin{aligned}
&H_{red} = \\
&\sum_{\mathbf{k}\sigma} \xi^{s}_{\mathbf{k}} c^{\dagger}_{\mathbf{k}\sigma} c_{\mathbf{k}\sigma} + \sum_{\mathbf{q}\sigma} \xi^{d}_{\mathbf{q}} d^{\dagger}_{\mathbf{q}\sigma} d_{\mathbf{q}\sigma} \\
&-V_{ss} \sum_{\mathbf{k}\mathbf{k}'} c^{\dagger}_{\mathbf{k}\uparrow} c^{\dagger}_{-\mathbf{k}\downarrow} c_{-\mathbf{k}'\downarrow} c_{\mathbf{k}'\uparrow} - V_{dd} \sum_{\mathbf{q}\mathbf{q}'} d^{\dagger}_{\mathbf{q}\uparrow} d^{\dagger}_{-\mathbf{q}\downarrow} d_{-\mathbf{q}'\downarrow} d_{\mathbf{q}'\uparrow} - V_{sd} \sum_{\mathbf{k}\mathbf{q}} \left(c^{\dagger}_{\mathbf{k}\uparrow} c^{\dagger}_{-\mathbf{k}\downarrow} d_{-\mathbf{q}\downarrow} d_{\mathbf{q}\uparrow} + d^{\dagger}_{\mathbf{k}\uparrow} d^{\dagger}_{-\mathbf{k}\downarrow} c_{-\mathbf{q}\downarrow} c_{\mathbf{q}\uparrow} \right),
\end{aligned}
\qquad \textbf{(2.43)}
$$

where the letter ξ stands for the kinetic energy and the $c/c^{\dagger}$- and $d/d^{\dagger}$- operators and their respective adjoints stand for the annihilation/creation operators, all in the respective bands. As seen, condition **(2.25)** has been made explicit respectively for each band and the cutoff restrictions were included in the summations. Hereafter, we will refer to the inter/intra band scattering matrix elements V_{ss}, V_{sd} and V_{dd} as the ***V*- terms**.

Following the BV formalism, the same argument that led to **(2.32)** applies for each band and operator and the use of definition **(2.33)** transforms our sums containing quartic terms in the Hamiltonian **(2.43)** into our double energy gap, model Hamiltonian version dictated by

$$
\begin{aligned}
&H_M^d = \\
&\sum_{\mathbf{k}\sigma}\xi_{\mathbf{k}}^s c_{\mathbf{k}\sigma}^{\dagger}c_{\mathbf{k}\sigma} + \sum_{\mathbf{q}\sigma}\xi_{\mathbf{q}}^d d_{\mathbf{q}\sigma}^{\dagger}d_{\mathbf{q}\sigma} \\
&-V_{ss}\left(S\sum_{\mathbf{k}} c_{\mathbf{k}\uparrow}^{\dagger}c_{-\mathbf{k}\downarrow}^{\dagger} + SV_{ss}\sum_{\mathbf{k}} c_{-\mathbf{k}\downarrow}c_{\mathbf{k}\uparrow} - S^2\right) - V_{dd}\left(D\sum_{\mathbf{q}} d_{\mathbf{q}\uparrow}^{\dagger}d_{-\mathbf{q}\downarrow}^{\dagger} + D\sum_{\mathbf{q}} d_{-\mathbf{q}\downarrow}d_{\mathbf{q}\uparrow} - D^2\right) - \\
&\qquad V_{sd}\left(D\sum_{\mathbf{k}} c_{\mathbf{k}\uparrow}^{\dagger}c_{-\mathbf{k}\downarrow}^{\dagger} + S\sum_{\mathbf{q}} d_{-\mathbf{q}\downarrow}d_{\mathbf{q}\uparrow} + D\sum_{\mathbf{k}} c_{-\mathbf{k}\downarrow}c_{\mathbf{k}\uparrow} + S\sum_{\mathbf{q}} d_{\mathbf{q}\uparrow}^{\dagger}d_{-\mathbf{q}\downarrow}^{\dagger} - 2SD\right),
\end{aligned}
\tag{2.44}
$$

where the superscript in the Hamiltonian accounts for the number of bands and were it became necessary to introduce

$$
S = \sum_{\mathbf{k}}\left\langle c_{\mathbf{k}\uparrow}^{\dagger}c_{-\mathbf{k}\downarrow}^{\dagger}\right\rangle \tag{2.45}
$$

and

$$D = \sum_{\mathbf{q}} \left\langle d_{-\mathbf{q}\downarrow} d_{\mathbf{q}\uparrow} \right\rangle . \tag{2.46}$$

It's important to notice that **Eqs. (2.45-46)** are *not* the Δ- terms equivalent with **Eq. (2.35)** in the single band case as a reader might mistakenly assume. Notice the symmetry between the coefficients of the scattering matrix elements in parentheses in the Hamiltonian **(2.44)**.

Immediately next, the BV canonical transformations of the type **(2.29)** for each operator are introduced in the form of

$$\begin{aligned} c_{\mathbf{k}\uparrow} &= u_{\mathbf{k}} e_{\mathbf{k}\uparrow} + v_{\mathbf{k}} e^{\dagger}_{-\mathbf{k}\downarrow} \\ c_{-\mathbf{k}\downarrow} &= -v_{\mathbf{k}} e^{\dagger}_{\mathbf{k}\uparrow} + u_{\mathbf{k}} e_{-\mathbf{k}\downarrow} \\ d_{\mathbf{q}\uparrow} &= u_{\mathbf{q}} f_{\mathbf{q}\uparrow} + v_{\mathbf{q}} f^{\dagger}_{-\mathbf{q}\downarrow} \\ d_{-\mathbf{q}\downarrow} &= -v_{\mathbf{q}} f^{\dagger}_{\mathbf{q}\uparrow} + u_{\mathbf{q}} f_{-\mathbf{q}\downarrow}, \end{aligned} \tag{2.47}$$

where the transformations are shown here inverted. Operators *e* and *f* obviously satisfy the anticommutation rules **(2.3)**, which are used whenever appropriate in the process of substitution of **Eq. (2.47)** into the Hamiltonian **(2.44)**; such process is tedious and will not be displayed here. The final result holds as

$$
\begin{aligned}
H_M^2 = & \\
&\sum_{\mathbf{k}}\left\{\xi_{\mathbf{k}}^s\left(u_{\mathbf{k}}^2-v_{\mathbf{k}}^2\right)+\left(2SV_{ss}+2DV_{sd}\right)u_{\mathbf{k}}v_{\mathbf{k}}\right\}\left(e_{\mathbf{k}\uparrow}^{\dagger}e_{\mathbf{k}\uparrow}+e_{-\mathbf{k}\downarrow}^{\dagger}e_{-\mathbf{k}\downarrow}\right)+ \\
&\qquad\qquad\sum_{\mathbf{q}}\left\{\xi_{\mathbf{q}}^d\left(u_{\mathbf{q}}^2-v_{\mathbf{q}}^2\right)+\left(2DV_{dd}+2SV_{sd}\right)u_{\mathbf{q}}v_{\mathbf{q}}\right\}\left(f_{\mathbf{q}\uparrow}^{\dagger}f_{\mathbf{q}\uparrow}+f_{-\mathbf{q}\downarrow}^{\dagger}f_{-\mathbf{q}\downarrow}\right)+ \\
&\sum_{\mathbf{k}}\left\{2\xi_{\mathbf{k}}^s u_{\mathbf{k}}v_{\mathbf{k}}-\left(u_{\mathbf{k}}^2-v_{\mathbf{k}}^2\right)\left(SV_{ss}+DV_{sd}\right)\right\}e_{\mathbf{k}\uparrow}^{\dagger}e_{-\mathbf{k}\downarrow}^{\dagger}\ +\ \sum_{\mathbf{q}}\left\{2\xi_{\mathbf{q}}^d u_{\mathbf{q}}v_{\mathbf{q}}-\left(u_{\mathbf{q}}^2-v_{\mathbf{q}}^2\right)\left(DV_{dd}+SV_{sd}\right)\right\}f_{\mathbf{q}\uparrow}^{\dagger}f_{-\mathbf{q}\downarrow}^{\dagger}+ \\
&\sum_{\mathbf{k}}\left\{-2\xi_{\mathbf{k}}^s u_{\mathbf{k}}v_{\mathbf{k}}+\left(u_{\mathbf{k}}^2-v_{\mathbf{k}}^2\right)\left(SV_{ss}+DV_{sd}\right)\right\}e_{\mathbf{k}\uparrow}e_{-\mathbf{k}\downarrow}+\sum_{\mathbf{q}}\left\{-2\xi_{\mathbf{q}}^d u_{\mathbf{q}}v_{\mathbf{q}}+\left(u_{\mathbf{q}}^2-v_{\mathbf{q}}^2\right)\left(DV_{dd}+SV_{sd}\right)\right\}f_{\mathbf{q}\uparrow}f_{-\mathbf{q}\downarrow}+ \\
&\qquad\qquad\sum_{\mathbf{k}}2\xi_{\mathbf{k}}^s v_{\mathbf{k}}^2+\sum_{\mathbf{q}}2\xi_{\mathbf{q}}^d v_{\mathbf{q}}^2-\left(S^2V_{ss}+D^2V_{dd}+2SDV_{sd}\right).
\end{aligned}
\tag{2.48}
$$

Again, notice the symmetries and contrast the looks of this expression with the Hamiltonian **(2.36)**.

Just as before, we neglect the second order excitations allowing the coefficients of the operators ee, $e^{\dagger}e^{\dagger}$, ff and $f^{\dagger}f^{\dagger}$ and the independent term to vanish with the adequate selection of the quantities *u* and *v*, where condition **(2.14)** is satisfied in each band . Naming

$$\Delta_s = SV_{ss}+DV_{sd} \tag{2.49}$$

and

$$\Delta_d = DV_{dd}+SV_{sd} \tag{2.50}$$

as the *actual* Δ- terms equivalent with **Eq. (2.35)**, we easily derive the quadratic equation

$$\Delta_s v_{\mathbf{k}}^2+2\xi_{\mathbf{k}}^s u_{\mathbf{k}}v_{\mathbf{k}}-\Delta_s u_{\mathbf{k}}^2=0\,,$$

with an analogous expression for Δ_d. Solving exactly as done in **Eq. (2.37)** and using condition **(2.14)**, we obtain for the *s*-band

$$u_{\mathbf{k}}^2 = \tfrac{1}{2}\left(1+\tfrac{\xi_{\mathbf{k}}^s}{E_{\mathbf{k}}^s}\right)$$
$$v_{\mathbf{k}}^2 = \tfrac{1}{2}\left(1-\tfrac{\xi_{\mathbf{k}}^s}{E_{\mathbf{k}}^s}\right) \qquad \textbf{(2.51)}$$

and for the *d*-band

$$u_{\mathbf{q}}^2 = \tfrac{1}{2}\left(1+\tfrac{\xi_{\mathbf{q}}^d}{E_{\mathbf{q}}^d}\right)$$
$$v_{\mathbf{q}}^2 = \tfrac{1}{2}\left(1+\tfrac{\xi_{\mathbf{q}}^d}{E_{\mathbf{q}}^d}\right), \qquad \textbf{(2.52)}$$

with

$$E_{\mathbf{k}}^s = \sqrt{\left(\xi_{\mathbf{k}}^s\right)^2 + \Delta_s^2}$$
$$E_{\mathbf{q}}^d = \sqrt{\left(\xi_{\mathbf{q}}^d\right)^2 + \Delta_d^2}, \qquad \textbf{(2.53)}$$

which, once more, matches faithfully the results of **Eq. (2.22)** and **Eq. (2.24)** now extended for our two bands.

With the coefficients *u* and *v* known in both bands, the calculation of the Δ- terms of **Eqs. (2.49-50)** is easy. However, a quick view reveals the need of solving the mean values of **Eqs. (2.45-46)** first; upon the substitution of the transformations **(2.47)** into **Eqs. (2.45-46)** the yielded result is **Eq. (2.38)** extended for the two bands, i.e.,

$$S = \sum_{\mathbf{k}} u_{\mathbf{k}} v_{\mathbf{k}} \left[1 - 2 f^F \left(E_{\mathbf{k}}^s \right) \right]$$
$$D = \sum_{\mathbf{q}} u_{\mathbf{q}} v_{\mathbf{q}} \left[1 - 2 f^F \left(E_{\mathbf{q}}^d \right) \right],$$

where f^F is the Fermi function of **Eq. (2.39)**. Carrying this result back into **Eqs. (2.49-50)** and with the aim of **Eqs. (2.51-52)** and **Eq. (2.53)** one finally draws, for example in the case of Δ_s,

$$\Delta_s = V_{ss} \sum_{\mathbf{k}} \frac{\Delta_s^{\mathbf{k}}}{\sqrt{\left(\xi_{\mathbf{k}}^s\right)^2 + \left(\Delta_s^{\mathbf{k}}\right)^2}} \tanh \tfrac{1}{2} \beta \sqrt{\left(\xi_{\mathbf{k}}^s\right)^2 + \left(\Delta_s^{\mathbf{k}}\right)^2} + V_{sd} \sum_{\mathbf{q}} \frac{\Delta_d^{\mathbf{q}}}{\sqrt{\left(\xi_{\mathbf{q}}^d\right)^2 + \left(\Delta_s^{\mathbf{k}}\right)^2}} \tanh \tfrac{1}{2} \beta \sqrt{\left(\xi_{\mathbf{q}}^d\right)^2 + \left(\Delta_d^{\mathbf{q}}\right)^2}, \qquad \textbf{(2.54)}$$

where an analogous expression holds for Δ_d. As it has probably been noticed, **Eq. (2.54)** is **Eq. (2.40)** generalized. The transformation of sums into integrals in the manner done in **S.S. 2.3** and **S.S. 2.4** goes similar; just noting $N_s(0) \equiv N_s^0$ and $N_d(0) \equiv N_d^0$ as the density of states at the Fermi surface and introducing

$$F(\Delta) = \int_0^{\hbar\omega_D} \frac{\tanh \frac{1}{2} \beta \sqrt{\xi^2 + \Delta^2}}{\sqrt{\xi^2 + \Delta^2}} d\xi, \qquad \textbf{(2.55)}$$

the same kind of approximations done before yield the two simultaneous equations [41]

$$\Delta_s \left[1 - N_s^0 V_{ss} F(\Delta_s) \right] = \Delta_d N_d^0 V_{sd} F(\Delta_d) \qquad \textbf{(2.56)}$$

$$\Delta_d \left[1 - N_d^0 V_{dd} F(\Delta_d) \right] = \Delta_s N_s^0 V_{sd} F(\Delta_s). \qquad \textbf{(2.57)}$$

Numerical work is necessary to solve the behavior of both Δ and such will be done in **Ch. III**.

Likewise in **S.S. 2.3**, an expression for the transition temperature T_c can be derived by observing that $\Delta_{s,d} \to 0$ when $T \to T_c$. Solving **Eqs. (2.56-57)** simultaneously for $F(0)$, we obtain

$$\left[1 - N_d^0 V_{dd} F(0)\right]\left[1 - N_s^0 V_{ss} F(0)\right] = N_d^0 N_s^0 V_{sd}^2 F^2(0).$$

Equating to zero and solving the respective quadratic equation, one winds up with

$$F(0) = -\frac{N_s^0 V_{ss} + N_d^0 V_{dd}}{2N_s^0 N_d^0 \left(V_{sd}^2 - V_{ss} V_{dd}\right)} \pm \frac{\sqrt{\left(N_s^0 V_{ss} + N_d^0 V_{dd}\right)^2 + 4\left(V_{sd}^2 - V_{dd} V_{ss}\right)}}{2N_s^0 N_d^0 \left(V_{sd}^2 - V_{ss} V_{dd}\right)} = -\frac{\frac{1}{2}\left(\frac{V_{ss}}{N_d^0} + \frac{V_{dd}}{N_s^0}\right)}{V_{sd}^2 - V_{ss} V_{dd}} \pm \frac{\sqrt{\frac{V_{sd}^2}{N_s^0 N_d^0} + \frac{1}{4}\left(\frac{V_{ss}}{N_d^0} - \frac{V_{dd}}{N_s^0}\right)^2}}{V_{sd}^2 - V_{ss} V_{dd}}.$$

However, because of definition **(2.55)**, the left hand side is identical to $\approx \ln\left(A\beta_c \hbar\omega_D\right)$, $A \approx 1.14$, as derived before, and solving for T_c we determine [41]:

$$k_B T_c \approx 1.14 \hbar\omega_D \exp\left[-F(0)\right] \qquad \textbf{(2.58)}$$

which stands equivalent with **Eq. (2.41)** for the double-gap case.

As suspected, the BV formalism in the number of energy gaps can be readily extended to a generalized version from the set of formulas **(2.56-57)** to the set [41]

$$\Delta_i = \sum_i V_{ij} \Delta_j F\left(\Delta_j\right) \qquad \textbf{(2.59)}$$

for more complicated systems, where *i* runs over the number of energy gaps.

2.5. BCS THEORY FOR A DOUBLE ENERGY GAP SUPERCONDUCTOR AT $T \neq 0$ IN THE PRESENCE OF NON-MAGNETIC IMPURITIES.

As far as **Eqs. (2.56-57)** are concerned, the *V*- terms are constants faithful to the BCS approximation **(2.25)** for a pure conventional superconductor but, as it'll be seen in the following, such matrix elements are showed to exhibit a behavior markedly influenced by the impurity concentration [42] [43]. Our main task along this Sub-section will consist of demonstrating the way in which such phonon-mediated interaction matrix elements change in the presence of these impurities.

The presence of impurities in the superconducting system implies a series of effects: a change in the number of conduction electrons, an alteration in the density of states, a modification in the Bloch states due to the impurity-electron scattering [42] [44] [45] and a minimum decrease in T_c [42] [46].

As result of our tour on BCS theory in previous Sub-sections, it is clear that the correlations of electrons with opposite momenta and spins hold responsible for the superconducting properties. In literature is commonly said that electrons are formed in pairs with mutually "time-reversed states" [40]. P. W. Anderson suggested a BCS-type theory which employs time-reversed scattered state pairs to treat impurities [47]. In general, this theory is

based on the idea that superconductivity is not sensitive to perturbations that do not destroy time-reversal invariance [48]. In order to follow such formalism, we turn again to Bogoliubov, although this time a rephrase is introduced. We will follow Bogoliubov's effective-field method in the manner done by de Gennes [49] in which a self-consistency field scheme is invoked [48]; in such notation the Hamiltonian for a system in the presence of non-magnetic impurities reads

$$H = \int d\mathbf{r} \sum_{\alpha} \Psi^{\dagger}(\mathbf{r}) \left[\tfrac{\mathbf{p}^2}{2m} + V^{imp}(\mathbf{r}) \right] \Psi(\mathbf{r}) - \tfrac{1}{2} V \int d\mathbf{r} \sum_{\alpha\beta} \Psi^{\dagger}(\mathbf{r}\alpha) \Psi^{\dagger}(\mathbf{r}\beta) \Psi(\mathbf{r}\beta) \Psi(\mathbf{r}\alpha), \quad \textbf{(2.60)}$$

where Ψ and $\Psi^{\dagger}$ are operators defined by

$$\begin{aligned} \Psi(\mathbf{r}\alpha) &= \sum_{\mathbf{k}} e^{i\mathbf{k}\cdot\mathbf{r}} c_{\mathbf{k},\alpha} \\ \Psi^{\dagger}(\mathbf{r}\beta) &= \sum_{\mathbf{k}} e^{-i\mathbf{k}\cdot\mathbf{r}} c^{\dagger}_{\mathbf{k},\beta}. \end{aligned} \qquad \textbf{(2.61)}$$

Their anticommutation properties are enunciated as:

$$\begin{aligned} \left\{ \Psi^{\dagger}(\mathbf{r}\alpha), \Psi(\mathbf{r}'\beta) \right\} &= \delta_{\alpha\beta} \delta(\mathbf{r} - \mathbf{r}') \\ \left\{ \Psi(\mathbf{r}\alpha), \Psi(\mathbf{r}'\beta) \right\} &= \left\{ \Psi^{\dagger}(\mathbf{r}\alpha), \Psi^{\dagger}(\mathbf{r}'\beta) \right\} = 0, \end{aligned} \qquad \textbf{(2.62)}$$

where indices α and β stand for spin. Notice that the $\Psi / \Psi^{\dagger}$- operators are written as linear expansions of the $c / c^{\dagger}$- operators which satisfy rules **(2.3)** as well. In the Hamiltonian **(2.60)**, $V^{imp}(\mathbf{r})$ denotes the impurity potential, which is purposely assumed to be independent of spin indices (in order to concord with the non-magnetic character of impurities) and *V* stands for the phonon-mediated interaction. A consideration of the type **(2.32)** transforms the Hamiltonian

(2.60) into our version of the model Hamiltonian [48], which in literature is found to be called **effective Hamiltonian** [49],

$$H_{eff} = \int d\mathbf{r} \left\{ \sum_{\alpha} \Psi^{\dagger}(\mathbf{r}\alpha) \left[\frac{\mathbf{p}^2}{2m} + V^{imp}(\mathbf{r}) \right] \Psi(\mathbf{r}\alpha) \right. \\ \left. + \Delta(\mathbf{r}) \Psi^{\dagger}(\mathbf{r}\uparrow) \Psi^{\dagger}(\mathbf{r}\downarrow) + \Delta^{*}(\mathbf{r}) \Psi(\mathbf{r}\downarrow) \Psi(\mathbf{r}\uparrow) \right\}, \tag{2.63}$$

with

$$\Delta(\mathbf{r}) = -V \left\langle \Psi(\mathbf{r}\downarrow) \Psi(\mathbf{r}\uparrow) \right\rangle. \tag{2.64}$$

The introduction of the unitary transformation [49]

$$\Psi(\mathbf{r}\uparrow) = \sum_{n} \left(\gamma_{n\uparrow} u_n(\mathbf{r}) - \gamma_{n\downarrow}^{\dagger} v_n^{*}(\mathbf{r}) \right) \\ \Psi(\mathbf{r}\downarrow) = \sum_{n} \left(\gamma_{n\downarrow} u_n(\mathbf{r}) + \gamma_{n\uparrow}^{\dagger} v_n^{*}(\mathbf{r}) \right), \tag{2.65}$$

as a generalization of the transformations **(2.29)**, where $\gamma / \gamma^{\dagger}$- operators are the same quasi-particles annihilation/creation operators introduced in **Eq. (2.29)** satisfying condition **(2.30)**, leads to the so-called **Bogoliubov-de Gennes equations** [50],

$$E \begin{bmatrix} u(\mathbf{r}) \\ v(\mathbf{r}) \end{bmatrix} = \begin{bmatrix} H_E & \Delta(\mathbf{r}) \\ \Delta^{*}(\mathbf{r}) & -H_E^{*} \end{bmatrix} \begin{bmatrix} u(\mathbf{r}) \\ v(\mathbf{r}) \end{bmatrix}, \tag{2.66}$$

where matrix notation was used. In **Eq. (2.66)**, $H_E = \frac{\mathbf{p}^2}{2m} + V^{imp}(\mathbf{r}) - E_F = -\frac{\hbar^2}{2m}\nabla^2 + V^{imp}(\mathbf{r}) - E_F$.

Because of the nature of V^{imp} and V, the set of **Eqs. (2.66)** is still too complicated to be solved. A not too rigorous but acceptable assumption is to suppose $\Delta(\mathbf{r})$ independent of **r** despite of the presence of impurities [49]. By introducing the one-electron wavefunctions satisfying

$$\xi_n \psi_n(\mathbf{r}) = H_E \psi_n(\mathbf{r}) \tag{2.67}$$

and substituting into the set **(2.66)** one easily solves the system to end up with the expressions for u_n and v_n which read exactly identical to **Eq. (2.24)**, where the assumption $\Delta(\mathbf{r}) = \Delta = const.$ was adopted. The subsequent calculations, which unfold in a manner very similar than in latter Sub-sections, demonstrate that the presence of nonmagnetic impurities have no considerable effects in T_c [46]. This is precisely the enunciation of **Anderson's theorem** [47] and the range up which the approximation $\Delta(\mathbf{r}) = const.$ holds is denominated **dirty limit**. Kim and Overhauser (KO) assert that Anderson's theorem holds valid up to the first power in the impurity concentration [42]; such observation will be extremely helpful to truncate our calculations to be implemented later.

In spite of all this, the assumption $\Delta(\mathbf{r}) = const.$ is not entirely accurate [48] [50] and instead one should use

$$\Delta_{n'} = \sum_n V_{nn'} u_n v_n \left(1 - 2 f_n^F\right), \tag{2.68}$$

with f^F again the Fermi function; it is demonstrated that [42] [48] [50]

$$V_{nn'} = -V\int d\mathbf{r}\,\psi^{*}_{n'}(\mathbf{r})\psi^{*}_{\bar{n}'}(\mathbf{r})\psi_{n}(\mathbf{r})\psi_{\bar{n}}(\mathbf{r}), \qquad \textbf{(2.69)}$$

where index $\bar{n}$ denotes the time-reversed scattered state partner of index *n*, i.e., $\bar{n} = -n$. **Eq. (2.67)** is rather formal; in a pure metal, they represent Bloch functions, but in our impure system they have a complicated structure describing the scattering between electrons and impurities [49]. Such scattered-state wavefunctions (exact scattered states) can be sculpted from the time-independent perturbation theory (TIP theory) with the result [51]

$$\psi^{k}_{n}(\mathbf{r}) = N\left\{\phi_{k}(r) + \sum_{k'\neq k}\phi_{k'}(r)\frac{\langle k'|V^{imp}|k\rangle}{E_{k'}-E_{k}} + \cdots\right\}. \qquad \textbf{(2.70)}$$

with $\phi_{k}(r) = e^{ikr}$.

Up to this point, we can start matching our derivations with the corresponding parameters of the MgB_2 compound. For example, because of the existence of the two electronic bands σ and π mentioned in **S.S. 1.4**, our wavefunction **(2.70)** should read, up to a second order of perturbative approximation and respectively for each band, as [52]

$$\psi^{\sigma}_{n}(\mathbf{r}) = N_{n}\left[\phi^{\sigma}_{\mathbf{k}}(\mathbf{r}) + \sum_{\mathbf{k}'}\phi^{\sigma}_{\mathbf{k}'}(\mathbf{r})\frac{\langle \mathbf{k}'|V^{imp}|\mathbf{k}\rangle}{\varepsilon^{\sigma}_{\mathbf{k}}-\varepsilon^{\sigma}_{\mathbf{k}'}} + \sum_{\mathbf{q}'}\phi^{\pi}_{\mathbf{q}'}(\mathbf{r})\frac{\langle \mathbf{q}'|V^{imp}|\mathbf{k}\rangle}{\varepsilon^{\sigma}_{\mathbf{k}}-\varepsilon^{\pi}_{\mathbf{q}'}}\right] \qquad \textbf{(2.71)}$$

$$\psi^{\pi}_{m}(\mathbf{r}) = N_{m}\left[\phi^{\pi}_{\mathbf{q}}(\mathbf{r}) + \sum_{\mathbf{q}'}\phi^{\pi}_{\mathbf{q}'}(\mathbf{r})\frac{\langle \mathbf{q}'|V^{imp}|\mathbf{q}\rangle}{\varepsilon^{\pi}_{\mathbf{q}}-\varepsilon^{\pi}_{\mathbf{q}'}} + \sum_{\mathbf{k}'}\phi^{\sigma}_{\mathbf{k}'}(\mathbf{r})\frac{\langle \mathbf{k}'|V^{imp}|\mathbf{q}\rangle}{\varepsilon^{\pi}_{\mathbf{q}}-\varepsilon^{\sigma}_{\mathbf{k}'}}\right]. \qquad \textbf{(2.72)}$$

On the other hand, our impurity potential will be assumed to be in the form of a point interaction [42],

$$V^{imp} = \sum_i V_o^{imp} \delta\left(\mathbf{r} - \mathbf{R}_i\right), \tag{2.73}$$

where $\{\mathbf{R}_i\}$ correspond to the impurity site position vectors and therefore the index runs up to the number of impurities in the system; if N^{imp} impurities are supposed to settle at $\{\mathbf{R}_j\}$ the "sandwich" products within the summation symbols in **Eqs. (2.71-72)** are nicely calculable as:

$$\langle \mathbf{s} | V^{imp} | \mathbf{s}' \rangle = V_o^{imp} \delta\left(\mathbf{r} - \mathbf{R}_j\right) \sum_j \exp\left[i\left(\mathbf{s}' - \mathbf{s}\right) \cdot \mathbf{R}_j \right] \tag{2.74},$$

with **s** standing for **k** or **q**. In **Eqs. (2.71-72)** constants N_n and N_m stand for the normalization constants and the zeroth approximation functions (ϕ) correspond to the free-electron wavefunctions for each band respectively.

Each of the *V* terms to be inserted in **Eqs. (2.56-57)** can now be estimated via **Eq. (2.69)** with the scattered state wavefunctions given as in **Eqs. (2.71-72)**. As expected, this task is extremely tedious. I will show the calculation of only one of the terms in a very simplified manner, only with demonstrative purposes.

Let us consider $V_{\sigma\sigma}$. Substitutions yield:

$$
\begin{aligned}
V_{\sigma\sigma} &= -V\int d\mathbf{r}\left|\psi_{n'}^{\sigma}(\mathbf{r})\right|^2\left|\psi_{n}^{\sigma}(\mathbf{r})\right|^2 \\
&= -\left|N_n\right|^2\left|N_{n'}\right|^2 V\int d\mathbf{r}\Bigg\{\left|\phi_{\mathbf{k}'}^{\sigma}(\mathbf{r})\right|^2\left|\phi_{\mathbf{k}}^{\sigma}(\mathbf{r})\right|^2 \\
&\quad + N^{imp}V_o^{imp}\Bigg[\left|\phi_{\mathbf{k}}^{\sigma}(\mathbf{r})\right|^2\phi_{\mathbf{k}'}^{\sigma}(\mathbf{r})\sum_{\mathbf{K}'}\frac{\phi_{\mathbf{k}'+\mathbf{K}'}^{\sigma}{}^{*}(\mathbf{r})}{\varepsilon_{\mathbf{k}'}^{\sigma}-\varepsilon_{\mathbf{k}'+\mathbf{K}'}^{\sigma}} + \left|\phi_{\mathbf{k}}^{\sigma}(\mathbf{r})\right|^2\phi_{\mathbf{k}'}^{\sigma}(\mathbf{r})\sum_{\mathbf{q}'}\frac{\phi_{\mathbf{q}'}^{\pi*}(\mathbf{r})}{\varepsilon_{\mathbf{k}'}^{\sigma}-\varepsilon_{\mathbf{q}'}^{\pi}} + \\
&\qquad \left|\phi_{\mathbf{k}}^{\sigma}(\mathbf{r})\right|^2\phi_{\mathbf{k}'}^{\sigma*}(\mathbf{r})\sum_{\mathbf{K}}\frac{\phi_{\mathbf{k}'+\mathbf{K}}^{\sigma}{}^{*}(\mathbf{r})}{\varepsilon_{\mathbf{k}'}^{\sigma}-\varepsilon_{\mathbf{k}'+\mathbf{K}}^{\sigma}} + \left|\phi_{\mathbf{k}}^{\sigma}(\mathbf{r})\right|^2\phi_{\mathbf{k}'}^{\sigma*}(\mathbf{r})\sum_{\mathbf{q}}\frac{\phi_{\mathbf{q}}^{\pi*}(\mathbf{r})}{\varepsilon_{\mathbf{k}'}^{\sigma}-\varepsilon_{\mathbf{q}}^{\pi}} + \\
&\qquad \left|\phi_{\mathbf{k}'}^{\sigma}(\mathbf{r})\right|^2\phi_{\mathbf{k}}^{\sigma}(\mathbf{r})\sum_{\mathbf{K}'''}\frac{\phi_{\mathbf{k}'+\mathbf{K}'''}^{\sigma}{}^{*}(\mathbf{r})}{\varepsilon_{\mathbf{k}'}^{\sigma}-\varepsilon_{\mathbf{k}'+\mathbf{K}'''}^{\sigma}} + \left|\phi_{\mathbf{k}'}^{\sigma}(\mathbf{r})\right|^2\phi_{\mathbf{k}}^{\sigma}(\mathbf{r})\sum_{\mathbf{q}'''}\frac{\phi_{\mathbf{q}'''}^{\pi*}(\mathbf{r})}{\varepsilon_{\mathbf{k}}^{\sigma}-\varepsilon_{\mathbf{q}'''}^{\pi}} + \\
&\qquad \left|\phi_{\mathbf{k}'}^{\sigma}(\mathbf{r})\right|^2\phi_{\mathbf{k}}^{\sigma*}(\mathbf{r})\sum_{\mathbf{K}''}\frac{\phi_{\mathbf{k}+\mathbf{K}''}^{\sigma}{}^{*}(\mathbf{r})}{\varepsilon_{\mathbf{k}}^{\sigma}-\varepsilon_{\mathbf{k}+\mathbf{K}''}^{\sigma}} + \left|\phi_{\mathbf{k}'}^{\sigma}(\mathbf{r})\right|^2\phi_{\mathbf{k}}^{\sigma*}(\mathbf{r})\sum_{\mathbf{q}''}\frac{\phi_{\mathbf{q}''}^{\pi*}(\mathbf{r})}{\varepsilon_{\mathbf{k}}^{\sigma}-\varepsilon_{\mathbf{q}''}^{\pi}}\Bigg] \\
&\quad + N^{imp}\left(V_o^{imp}\right)^2\Bigg[\left|\phi_{\mathbf{k}}^{\sigma}(\mathbf{r})\right|^2\sum_{\mathbf{q}\mathbf{q}'}\frac{\phi_{\mathbf{q}}^{\pi}(\mathbf{r})\phi_{\mathbf{q}'}^{\pi*}(\mathbf{r})}{\left(\varepsilon_{\mathbf{k}'}^{\sigma}-\varepsilon_{\mathbf{q}}^{\pi}\right)\left(\varepsilon_{\mathbf{k}'}^{\sigma}-\varepsilon_{\mathbf{q}'}^{\pi}\right)} + \\
&\qquad \left|\phi_{\mathbf{k}'}^{\sigma}(\mathbf{r})\right|^2\sum_{\mathbf{K}''\mathbf{K}'''}\frac{\phi_{\mathbf{k}+\mathbf{K}''}^{\sigma}(\mathbf{r})\phi_{\mathbf{k}'+\mathbf{K}'''}^{\sigma}{}^{*}(\mathbf{r})}{\left(\varepsilon_{\mathbf{k}}^{\sigma}-\varepsilon_{\mathbf{k}+\mathbf{K}''}^{\sigma}\right)\left(\varepsilon_{\mathbf{k}}^{\sigma}-\varepsilon_{\mathbf{k}+\mathbf{K}'''}^{\sigma}\right)} + \left|\phi_{\mathbf{k}'}^{\sigma}(\mathbf{r})\right|^2\sum_{\mathbf{q}''\mathbf{q}'''}\frac{\phi_{\mathbf{q}''}^{\pi*}(\mathbf{r})\phi_{\mathbf{q}'''}^{\pi*}(\mathbf{r})}{\left(\varepsilon_{\mathbf{k}}^{\sigma}-\varepsilon_{\mathbf{q}''}^{\pi}\right)\left(\varepsilon_{\mathbf{k}}^{\sigma}-\varepsilon_{\mathbf{q}'''}^{\pi}\right)}\Bigg];
\end{aligned}
$$

(2.75)

as it is easily noticed above, the approximation was carried up to the second order in the impurity potential V_o^{imp}, hence terms of higher order were ignored. When "impurity-averaging" is considered, i.e., when one takes $\frac{1}{\Omega}\int d\mathbf{R}_i$ at both sides of **Eq. (2.75)**, all the first order terms vanish; in order to see why, consider a representative term with coefficient $\left(V_o^{imp}\right)^1$, e. g., $\sum_{\mathbf{K}'}\frac{\phi_{\mathbf{k}'+\mathbf{K}'}^{\sigma}{}^{*}(\mathbf{r})}{\varepsilon_{\mathbf{k}'}^{\sigma}-\varepsilon_{\mathbf{k}'+\mathbf{K}'}^{\sigma}}$. When impurity-averaging is carried out,

$$
\int d\mathbf{R}_j\sum_{\mathbf{K}'}\frac{\langle\mathbf{k}'+\mathbf{K}'|V^{imp}|\mathbf{k}'\rangle}{\varepsilon_{\mathbf{k}'}^{\sigma}-\varepsilon_{\mathbf{k}'+\mathbf{K}'}^{\sigma}}\phi_{\mathbf{k}'+\mathbf{K}'}^{\sigma}{}^{*}(\mathbf{r}) = N^{imp}V_o^{imp}\int d\mathbf{R}_j\sum_j\exp\left(-i\mathbf{K}'\cdot\mathbf{R}_j\right)\sum_{\mathbf{K}'}\frac{\exp\left[-i(\mathbf{k}'+\mathbf{K}')\cdot\mathbf{r}\right]}{\varepsilon_{\mathbf{k}'}^{\sigma}-\varepsilon_{\mathbf{k}'+\mathbf{K}'}^{\sigma}} = 0,
$$

because $\int \exp\left(-i\mathbf{K}'\cdot\mathbf{R}_j\right)d\mathbf{R}_j = 2\pi\delta\left(\mathbf{K}',0\right)=0$ [39] since $\mathbf{K}'\neq 0$ always; this effect mirrors in all the first order terms, killing them off. Adequately equating and relabeling indices to eliminate double sums and keeping only those terms of the form $\sum\frac{1}{(\varepsilon-\varepsilon')^2}$, our matrix element now reads

$$
\begin{aligned}
V_{\sigma\sigma} = & -\frac{|N_n|^2|N_{n'}|^2}{\Omega}V\times \\
& \int d\mathbf{r}\left\{\left|\phi^{\sigma}_{\mathbf{k}'}(\mathbf{r})\right|^2\left|\phi^{\sigma}_{\mathbf{k}}(\mathbf{r})\right|^2 + \right. \\
& \left. N^{imp}\left(V_o^{imp}\right)^2\left[\left|\phi^{\sigma}_{\mathbf{k}}(\mathbf{r})\right|^2\left(\sum_{\mathbf{K}}\frac{\left|\phi^{\sigma}_{\mathbf{k}+\mathbf{K}}(\mathbf{r})\right|^2}{\left(\varepsilon^{\sigma}_{\mathbf{k}}-\varepsilon^{\sigma}_{\mathbf{k}+\mathbf{K}}\right)^2}+\sum_{\mathbf{q}}\frac{\left|\phi^{\pi}_{\mathbf{q}}(\mathbf{r})\right|^2}{\left(\varepsilon^{\sigma}_{\mathbf{k}'}-\varepsilon^{\pi}_{\mathbf{q}}\right)^2}\right)+\left|\phi^{\sigma}_{\mathbf{k}'}(\mathbf{r})\right|^2\left(\sum_{\mathbf{K}'}\frac{\left|\phi^{\sigma}_{\mathbf{k}+\mathbf{K}'}(\mathbf{r})\right|^2}{\left(\varepsilon^{\sigma}_{\mathbf{k}}-\varepsilon^{\sigma}_{\mathbf{k}+\mathbf{K}'}\right)^2}+\sum_{\mathbf{q}'}\frac{\left|\phi^{\pi}_{\mathbf{q}'}(\mathbf{r})\right|^2}{\left(\varepsilon^{\sigma}_{\mathbf{k}}-\varepsilon^{\pi}_{\mathbf{q}'}\right)^2}\right)\right]\right\},
\end{aligned}
$$

(2.76)

where $\Omega\equiv\int d\mathbf{r}\equiv 1$. Explicitly normalizing **Eqs. (2.72-73)** one draws

$$
\left|N_n\right|^2\left|N_{n'}\right|^2 \approx 1-N^{imp}\left(V_o^{imp}\right)^2\left\{\sum_{\mathbf{K}'}\frac{1}{\left(\varepsilon^{\sigma}_{\mathbf{k}'}-\varepsilon^{\sigma}_{\mathbf{k}'+\mathbf{K}'}\right)^2}+\sum_{\mathbf{q}'}\frac{1}{\left(\varepsilon^{\sigma}_{\mathbf{k}'}-\varepsilon^{\pi}_{\mathbf{q}'}\right)^2}+\sum_{\mathbf{K}}\frac{1}{\left(\varepsilon^{\sigma}_{\mathbf{k}}-\varepsilon^{\sigma}_{\mathbf{k}+\mathbf{K}}\right)^2}+\sum_{\mathbf{q}}\frac{1}{\left(\varepsilon^{\sigma}_{\mathbf{k}}-\varepsilon^{\pi}_{\mathbf{q}}\right)^2}\right\}.
$$

Substituting into **Eq. (2.76)** a cancelation between several terms occur, leaving

$$
\begin{aligned}
& V_{\sigma\sigma} = \\
& \left[-V\int d\mathbf{r}\left|\phi^{\sigma}_{\mathbf{k}'}(\mathbf{r})\right|^2\left|\phi^{\sigma}_{\mathbf{k}}(\mathbf{r})\right|^2\right] \\
& +N^{imp}\left(V_o^{imp}\right)^2\left\{\sum_{\mathbf{q}}\frac{1}{\left(\varepsilon^{\sigma}_{\mathbf{k}}-\varepsilon^{\pi}_{\mathbf{q}}\right)^2}\left[-V\int d\mathbf{r}\left|\phi^{\sigma}_{\mathbf{k}}(\mathbf{r})\right|^2\left|\phi^{\pi}_{\mathbf{q}}(\mathbf{r})\right|^2\right]+\sum_{\mathbf{q}'}\frac{1}{\left(\varepsilon^{\sigma}_{\mathbf{k}}-\varepsilon^{\pi}_{\mathbf{q}'}\right)^2}\left[-V\int d\mathbf{r}\left|\phi^{\sigma}_{\mathbf{k}'}(\mathbf{r})\right|^2\left|\phi^{\pi}_{\mathbf{q}'}(\mathbf{r})\right|^2\right]\right. \\
& \qquad\qquad + \\
& \left.\sum_{\mathbf{q}'}\frac{1}{\left(\varepsilon^{\sigma}_{\mathbf{k}}-\varepsilon^{\pi}_{\mathbf{q}'}\right)^2}\left[-V\int d\mathbf{r}\left|\phi^{\sigma}_{\mathbf{k}'}(\mathbf{r})\right|^2\left|\phi^{\sigma}_{\mathbf{k}}(\mathbf{r})\right|^2\right]+\sum_{\mathbf{q}}\frac{1}{\left(\varepsilon^{\sigma}_{\mathbf{k}}-\varepsilon^{\pi}_{\mathbf{q}}\right)^2}\left[-V\int d\mathbf{r}\left|\phi^{\sigma}_{\mathbf{k}'}(\mathbf{r})\right|^2\left|\phi^{\sigma}_{\mathbf{k}}(\mathbf{r})\right|^2\right]\right\}.
\end{aligned}
$$

(2.77)

The terms in square brackets imply a particular significance. Notice that, for example, the first addend at the right is the original $V_{\sigma\sigma}$ term evaluated in the ϕ- functions. This occurs with the other *V*- terms as well, whose structure corresponds to the *V*- terms evaluated via **Eq. (2.69)** but with the ϕ- functions as arguments. We denominate these new potential terms as the $\boldsymbol{V^0}$**- terms**, each of which is defined by

$$\begin{aligned} V^0_{\sigma\sigma} &= -V\int d\mathbf{r}\left|\phi^\sigma_{\mathbf{k}'}(\mathbf{r})\right|^2\left|\phi^\sigma_{\mathbf{k}}(\mathbf{r})\right|^2 \\ V^0_{\sigma\pi} &= -V\int d\mathbf{r}\left|\phi^\sigma_{\mathbf{k}}(\mathbf{r})\right|^2\left|\phi^\pi_{\mathbf{q}}(\mathbf{r})\right|^2 = V^0_{\pi\sigma} \\ V^0_{\pi\pi} &= -V\int d\mathbf{r}\left|\phi^\sigma_{\mathbf{q}'}(\mathbf{r})\right|^2\left|\phi^\pi_{\mathbf{q}}(\mathbf{r})\right|^2 . \end{aligned} \qquad \textbf{(2.78)}$$

Upon the result derived by Kim [32] [52] [53],

$$\sum \tfrac{1}{(\varepsilon-\varepsilon')^2} = \tfrac{N^0\pi}{2\Delta}\,, \qquad \textbf{(2.79)}$$

where labels were omitted, Δ stands for the energy gap associated with the corresponding sum and N^0 is the density of states at $\varepsilon' = 0$. By calling upon the formulas [4] [42]

$$\xi_o = \tfrac{\hbar v_F}{\pi\Delta}\quad , \qquad \textbf{(2.80)}$$

$$\tfrac{1}{\tau} = \tfrac{2\pi}{\hbar}\left(V^{imp}\right)^2 N^0 nc = \tfrac{2\pi}{\hbar} N^0 N^{imp}\left(V^{imp}\right)^2\ , \qquad \textbf{(2.81)}$$

and [31]

$$l = v_F\tau\,, \qquad \textbf{(2.82)}$$

where ξ_o is the coherence length, here interpreted as the size of the Cooper pair [4] [46], and *l* is the electron mean-free path, one can readily derive the simplifying result

$$N^{imp}\left(V^{imp}\right)^2 \sum \frac{1}{\left(\varepsilon-\varepsilon'\right)^2} = \frac{\pi\xi_o}{4l} \ , \qquad \textbf{(2.83)}$$

where, again, labels were omitted at both sides of the equation for simplicity. When the sub- and supra- scripts of ξ_o and *l* are particularized to each sum, the result finally yields [55]

$$V_{\sigma\sigma} = V_{\sigma\sigma}^0 + 2\left(V_{\sigma\pi}^0 - V_{\sigma\sigma}^0\right)\frac{\pi\xi_\sigma}{4l^{\sigma\pi}} .$$

Analogous calculations result in analogous expressions for the rest of the scattering *V*-terms. If listed, these terms read [55]:

$$\begin{aligned} V_{\sigma\sigma} &= V_{\sigma\sigma}^0 + 2\left(V_{\sigma\pi}^0 - V_{\sigma\sigma}^0\right)\frac{\pi\xi_\sigma}{4l^{\sigma\pi}} \\ V_{\pi\pi} &= V_{\pi\pi}^0 + 2\left(V_{\sigma\pi}^0 - V_{\pi\pi}^0\right)\frac{\pi\xi_\pi}{4l^{\pi\sigma}} \\ V_{\sigma\pi} &= V_{\sigma\pi}^0 + \left(V_{\sigma\sigma}^0 - V_{\sigma\pi}^0\right)\frac{\pi\xi_\pi}{4l^{\sigma\pi}} + \left(V_{\pi\pi}^0 - V_{\sigma\pi}^0\right)\frac{\pi\xi_\sigma}{4l^{\sigma\pi}} = V_{\pi\sigma}. \end{aligned} \qquad \textbf{(2.84)}$$

However, as Kim *et al.* estimate, the reach of Anderson's theorem is rather limited [42]. As impurity concentration increases, the set **(2.84)** rapidly loses validity because of the augmentation in disorder. **Weak localization** is a typical effect in disordered systems at low temperatures and occurs because of the diffusive nature of the electron at the quantum-mechanical level when repeatedly scattered by random impurities [56]. Because elastic scattering dominates at low temperatures [47], electrons may maintain phase coherence over large distances giving rise to coherence interference phenomena. For example, a random array of

impurity scatterers will not give rise to a uniform scattering of electrons in all directions but to a backscattering enhanced [56]. This happens because coherent interference of electrons between self-crossing paths can take place when two electrons are scattered around in loops in different directions, i.e., clockwise or counterclockwise; then, because the length of the optical path is the same, the phase coherence occurs [56]. Electrons are thus said to be localized. Weak localization in superconductors is caused by impurity doping or radiation damage [43]. The effects of weak localization evidently have an influence over conductivity, as demonstrated by Kim and Park [43] and as found experimentally [57]. In consequence, a weak localization correction has to be introduced in **Eq. (2.84)**. Such correction is also worked out by Kim *et al.* [42] [43] [57] [58], where a decrease in the phonon-mediated matrix elements is found as result [43].

The foundation of KO's assertion is related with the calculation of the matrix element **(2.69)**. When scattered states of **Eq. (2.67)** are expanded in plane waves,

$$\psi_n = \sum_{\mathbf{k}} \phi_{\mathbf{k}} \langle \mathbf{k} | n \rangle \tag{2.85}$$

and such unitary transformation is brought into **Eq. (2.69)**, the *V*-terms can be rewritten as

$$V_{nn'} = \sum_{\mathbf{k}\mathbf{k}'\mathbf{q}} V_{\mathbf{k}\mathbf{k}'\mathbf{q}} \langle -\mathbf{k}' | n \rangle \langle \mathbf{k} | n \rangle^* \langle \mathbf{k} - \mathbf{q} | n' \rangle \langle -\mathbf{k}' - \mathbf{q} | n' \rangle^* . \tag{2.86}$$

Anderson's theorem is achieved when Fröhlich's pairing interaction is considered within BCS cutoff and the sum in $\mathbf{k}'$ is omitted by making $\mathbf{k}' = -\mathbf{k}$ [42]. In other words, when not all the terms of the sum are taken into consideration and a portion of them are disregarded [47] [58];

however, these remaining "non-BCS" *V*-terms cannot always be ignored. KO state that in the weak localization regime such remaining term has a significant contribution [43].

In light of these considerations and counting in both BCS and non-BCS terms in the calculation, Kim rewrites **Eq. (2.86)** as [58]

$$V_{nn'} = -V\left(1+\sum_{\mathbf{k}\neq-\mathbf{k}'\mathbf{k}\mathbf{q}}\langle-\mathbf{k}'|n\rangle\langle\mathbf{k}|n\rangle^{*}\langle\mathbf{k}-\mathbf{q}|n'\rangle\langle-\mathbf{k}'-\mathbf{q}|n'\rangle^{*}\right), \qquad \textbf{(2.87)}$$

where the second addend in parentheses is the one neglectible in the dirty limit scheme. In order to calculate this correction term, Kim decides to work with the phenomenological power-law scattered-state wavefunctions derived by Kaveh and Mott [59], which read

$$\psi_{\mathbf{k}}(\mathbf{r}) = A\exp(i\mathbf{k}\cdot\mathbf{r}) + B\tfrac{1}{r^2}\exp(ikr), \qquad \textbf{(2.88)}$$

when the proper labels are omitted. In **Eq. (2.88)**

$$A^2 = 1-4\pi B^2\left(\tfrac{1}{l}-\tfrac{1}{L}\right) \qquad \textbf{(2.89)}$$

$$B^2 = \tfrac{3}{8\pi}\tfrac{1}{k_F l}, \qquad \textbf{(2.90)}$$

where *L* denotes the diffusion length [43]. Approximating the eigenstates by an incoherent superposition of plane wave states, as suggested by Thouless' approach [60], Kim determines

$$\psi_n(\mathbf{r}) = \sum_{\mathbf{k}} a_{\mathbf{k}}^{n}\left[A\exp(i\mathbf{k}\cdot\mathbf{r}) + B\tfrac{1}{r^2}\exp(ikr)\right],$$

and substituting back into **Eq. (2.69)**, for the 3-D case [43] [55] [57],

$$V_{nn'} = -V\left[1-\frac{3}{(k_F l)^2}\left(1-\frac{l}{L}\right)\right].$$

Carrying the expression above into our particular two-band case yields [55]

$$V_{\sigma\sigma} = V^0_{\sigma\sigma}\left(1-\frac{\pi\xi_\sigma}{2l^{\sigma\pi}}\right)\left[1-\frac{3}{\left(k_F^\sigma l^{\sigma\sigma}\right)^2}\right]+V^0_{\sigma\pi}\,\frac{\pi\xi_\sigma}{2l^{\sigma\pi}}\left[1-\frac{3}{2\left(k_F^\sigma l^{\sigma\sigma}\right)^2}-\frac{3}{2\left(k_F^\pi l^{\pi\pi}\right)^2}\right]$$

$$V_{\pi\pi} = V^0_{\pi\pi}\left(1-\frac{\pi\xi_\pi}{2l^{\pi\sigma}}\right)\left[1-\frac{3}{\left(k_F^\pi l^{\pi\pi}\right)^2}\right]+V^0_{\sigma\pi}\,\frac{\pi\xi_\sigma}{2l^{\sigma\pi}}\left[1-\frac{3}{2\left(k_F^\sigma l^{\sigma\sigma}\right)^2}-\frac{3}{2\left(k_F^\pi l^{\pi\pi}\right)^2}\right]$$

$$V_{\sigma\pi} = V^0_{\sigma\pi}\left(1-\frac{\pi\xi_\sigma}{4l^{\sigma\pi}}-\frac{\pi\xi_\pi}{4l^{\pi\sigma}}\right)\left[1-\frac{3}{\left(k_F^\sigma l^{\sigma\sigma}\right)^2}-\frac{3}{\left(k_F^\pi l^{\pi\pi}\right)^2}\right]+V^0_{\sigma\sigma}\,\frac{\pi\xi_\pi}{4l^{\pi\sigma}}\left[1-\frac{3}{\left(k_F^\sigma l^{\sigma\sigma}\right)^2}\right]+V^0_{\pi\pi}\,\frac{\pi\xi_\sigma}{4l^{\sigma\pi}}\left[1-\frac{3}{\left(k_F^\pi l^{\pi\pi}\right)^2}\right]=V_{\pi\sigma}.$$

(2.91)

Matrix elements of **Eq. (2.91)** therefore correspond to the matrix elements of **Eq. (2.84)** within the weak localization limit. The formalism adopted for tracing the behavior of the energy gaps in **Eqs. (2.56-57)**, adapted to the two-band gap model, will read as

$$\Delta_\sigma\left[1-N^0_\sigma V_{\sigma\sigma}F\left(\Delta_\sigma\right)\right]=\Delta_\pi N^0_\pi V_{\sigma\pi}F\left(\Delta_\pi\right) \qquad \textbf{(2.92)}$$

$$\Delta_\pi\left[1-N^0_\pi V_{\pi\pi}F\left(\Delta_\pi\right)\right]=\Delta_\sigma N^0_\sigma V_{\sigma\pi}F\left(\Delta_\sigma\right), \qquad \textbf{(2.93)}$$

where formulas will have to account for the shift in the values of the *V*- terms by weak localization when impurity concentration grows big enough. Because of the decrease of T_c (see **Eq. (2.58)**) implied when such tracing is to be performed, the mean-free path spacing parameter *l*

becomes the perfect quantity to model the impurity concentration and hence the magnitude of the weak localization effect. The way in which this will be done and also the manner in which the calculations will be performed are the subject of the next Chapter.

III. NUMERICAL CALCULATIONS, RESULTS AND DISCUSSION

1. INTRODUCTION

The numerical modeling of the problem is performed by the numerical adaptation of **Eqs. (2.92-93)**. In the following, corresponding computations based in the single-gap and double-gap model (in absence and presence of impurities) will be performed. Such numerical calculations will play the role of both a background to compare the calculations performed including the corrections in the *V*-terms due to the presence of impurities and to test the computing algorithms. All the numerical computations were performed with the computer software `MATLAB 7.4.0 (R2007a).`

It has to be observed that it's an obvious fact that no computer program can calculate the integral **(2.55)** accurately. Any software will approximate the infinite sum by a finite sum of representative, yet appropriate geometric figures to estimate the area under the curve, in our case, that curve described by the argument of **(2.55)**; `MATLAB` contains several functions to perform this. I chose `quad`, a function that approximates the integral of a function with a tolerance of 10^{-6} using a recursive adaptive Simpson cuadrature [61]. For all mathematical purposes (excluding certain syntax implied) `quad` and *F* in **(2.55)** are the same.

Finally, a few statements applicable to all our calculations have to be kept in mind:

- In all the *n*-iterating integral equations (of the type of **Eqs. (2.92-93)**, for example), $\hbar = 1$, $k_B = 1$ and $k_F = 1$ were adopted.

- In all the *n*-iterating integral equations *n* stands for the number of iterations.

The numerical method employed in all the calculations is the standard for solving integral equations by a successive approximation method [62].

2. TRACING OF THE ENERGY GAP FOR A PURE SINGLE ENERGY GAP SUPERCONDUCTOR AT $T \neq 0$.

2.1 NUMERICAL FITTING

According with **(2.40)** and **(2.54)**, each Δ at the left hand side depends of the Δ- terms in the sum(s) at the right hand side. This suggests that the ultimate value of a given Δ- term will be the result of a repeated iteration for a fixed T. For the single band case, where only one Δ - term appears, the numerical fitting inspired in **(2.40)** is remarkably simple and dictated by

$$\Delta^{n+1} = N^0 V \Delta^n F\left(\Delta^n\right), \qquad \textbf{(3.1)}$$

where the product N^0V and the initial value Δ^0 are properly chosen from the experimental data [49].

Units are also accommodated. Henceforth the upper limit of **(2.54)** is taken in temperature units by the known equivalency $\hbar\omega_D = k_B\theta_D$, with θ_D standing for the Debye temperature. For the next results, the values for T_c are calculated via **Eq. (2.41)**. Experimental values for N^0V and θ_D are excerpted from [49]. For the single band the results shown for the size of Δ are normalized to the size of the energy gap at zero temperature (**Eq. (2.42)**). This is done to match the results available in literature [4] [13].

2.2. RESULTS

The computations implemented here produced the following results for the single band case, impurities absent:

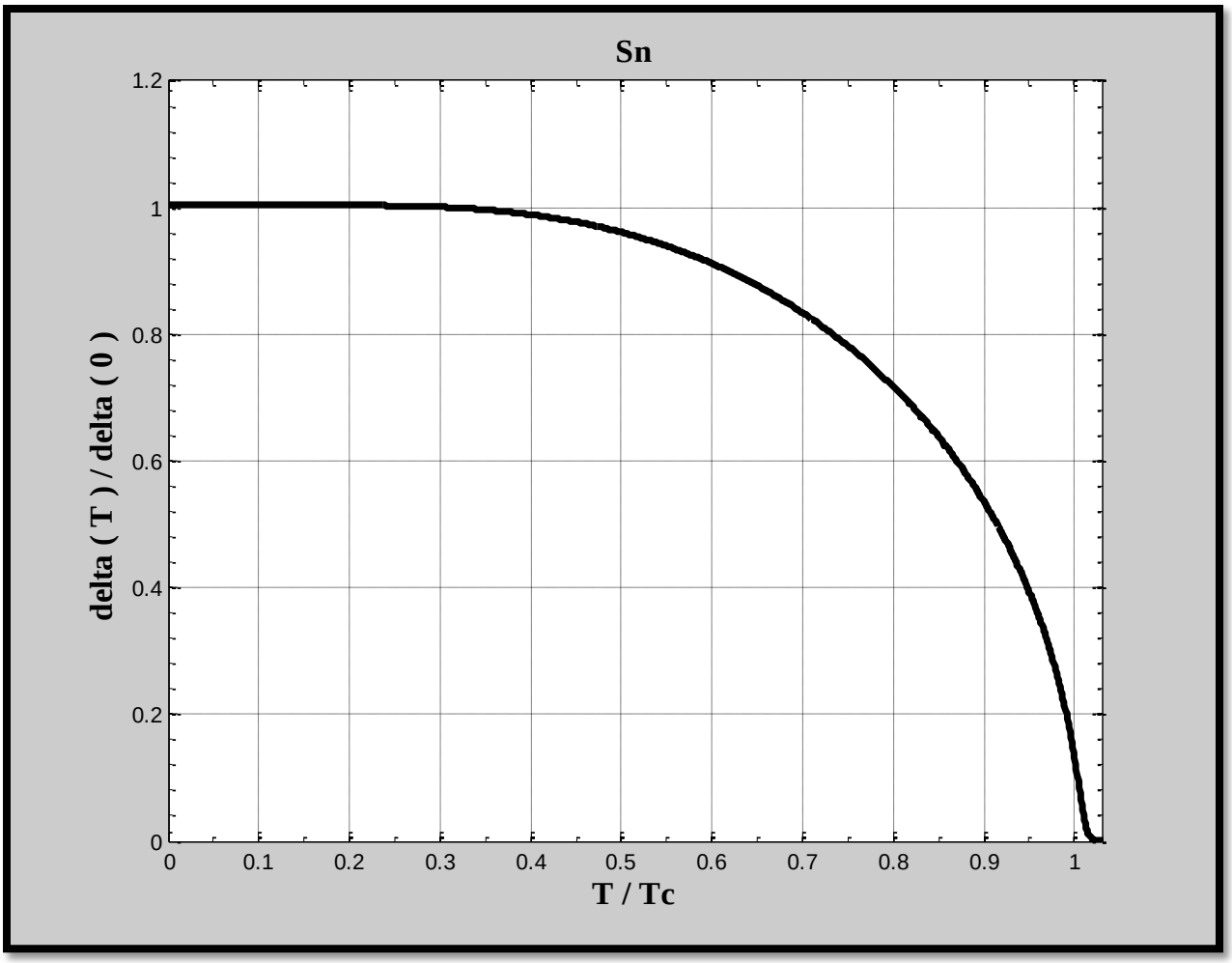

Plot 1. Parameters: $N^0V = 0.25,\ T_c = 4.0359\text{K},\ \theta_D = 195\text{K},\ n = 100.$

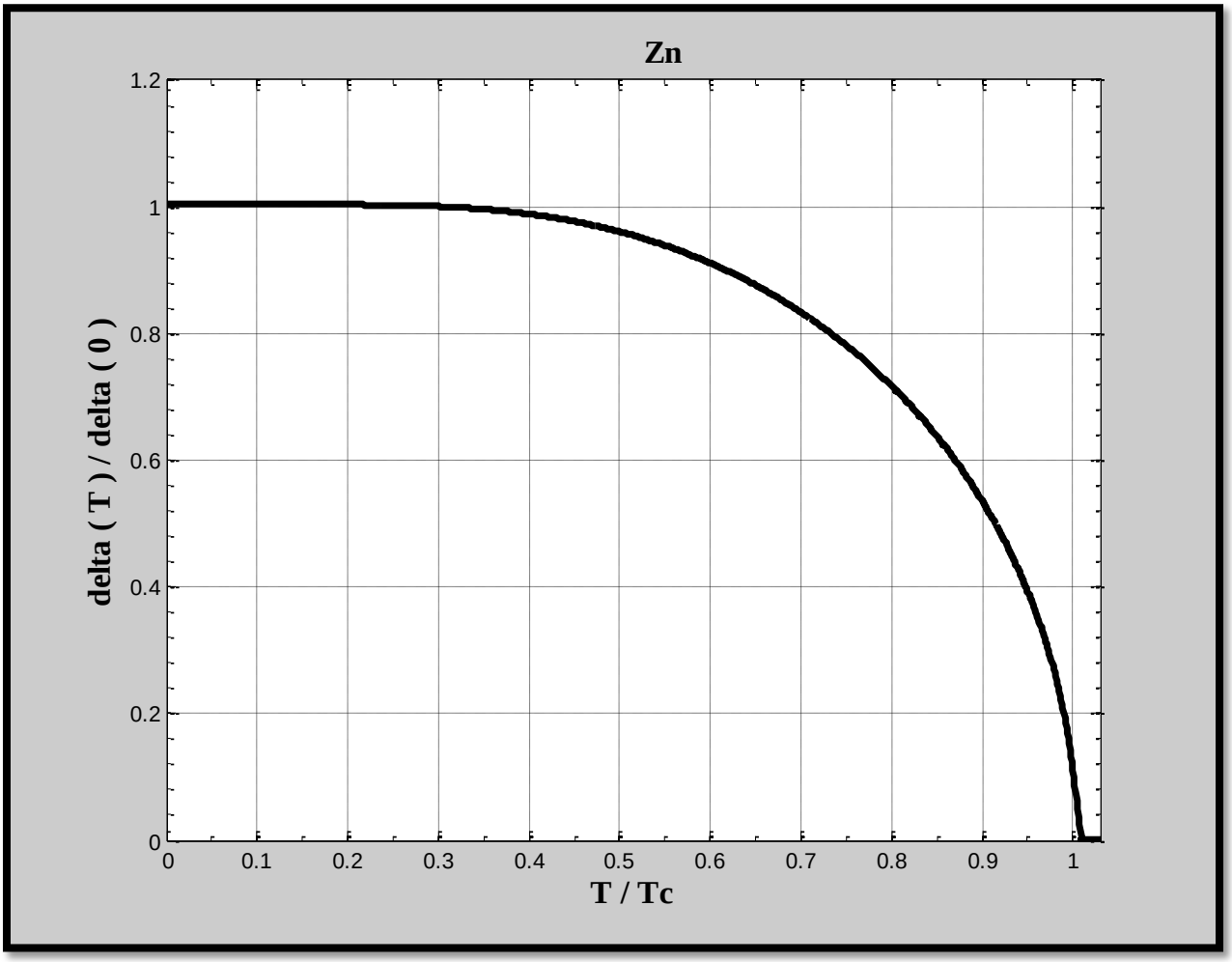

Plot 2. Parameters: $N^0V = 0.18$, $T_c = 1.0266\text{K}$, $\theta_D = 235\text{K}$, $n = 500$.

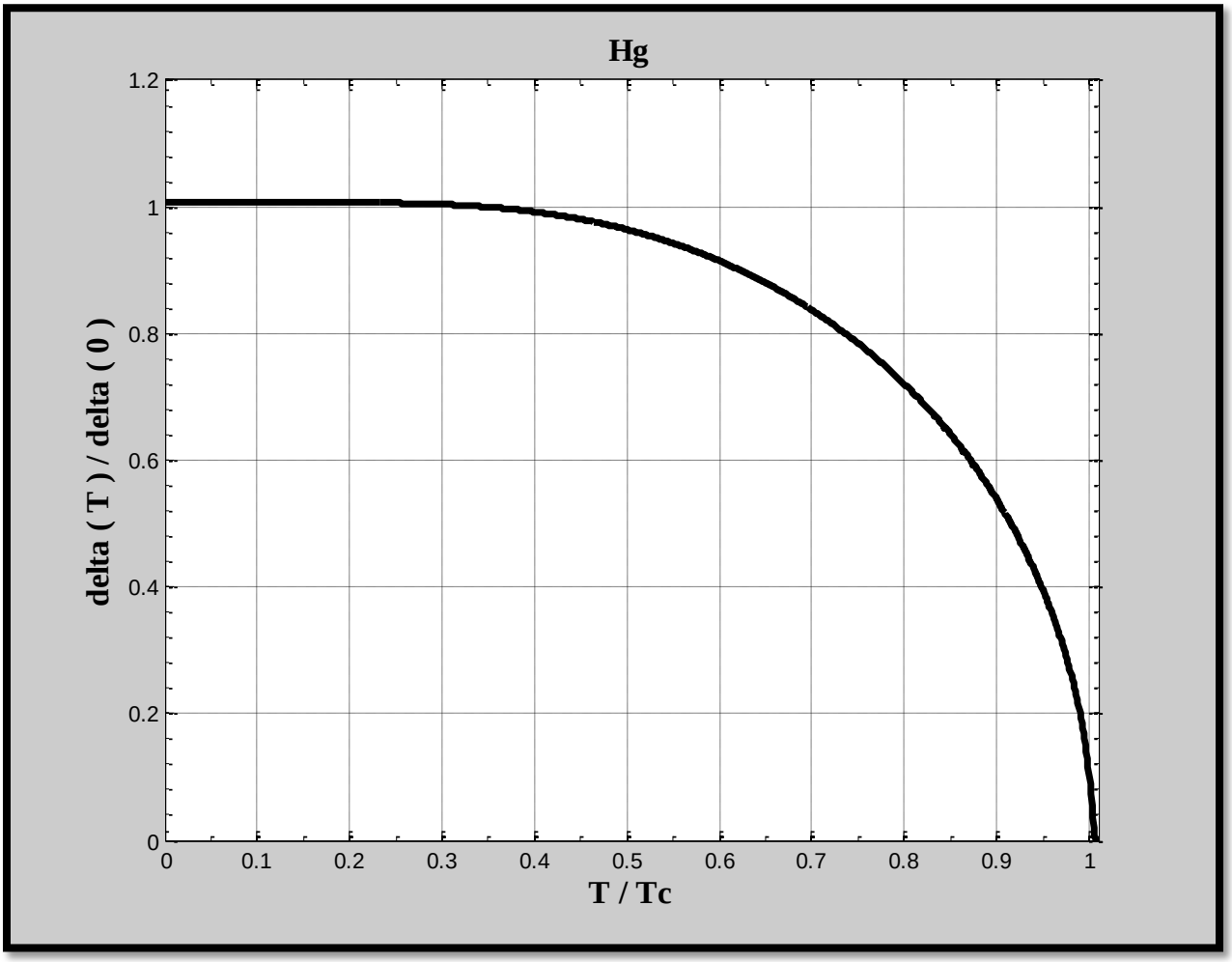

Plot 3. Parameters: $N^0V = 0.35$, $T_c = 4.5429\text{K}$, $\theta_D = 70\text{K}$, $n = 1000$.

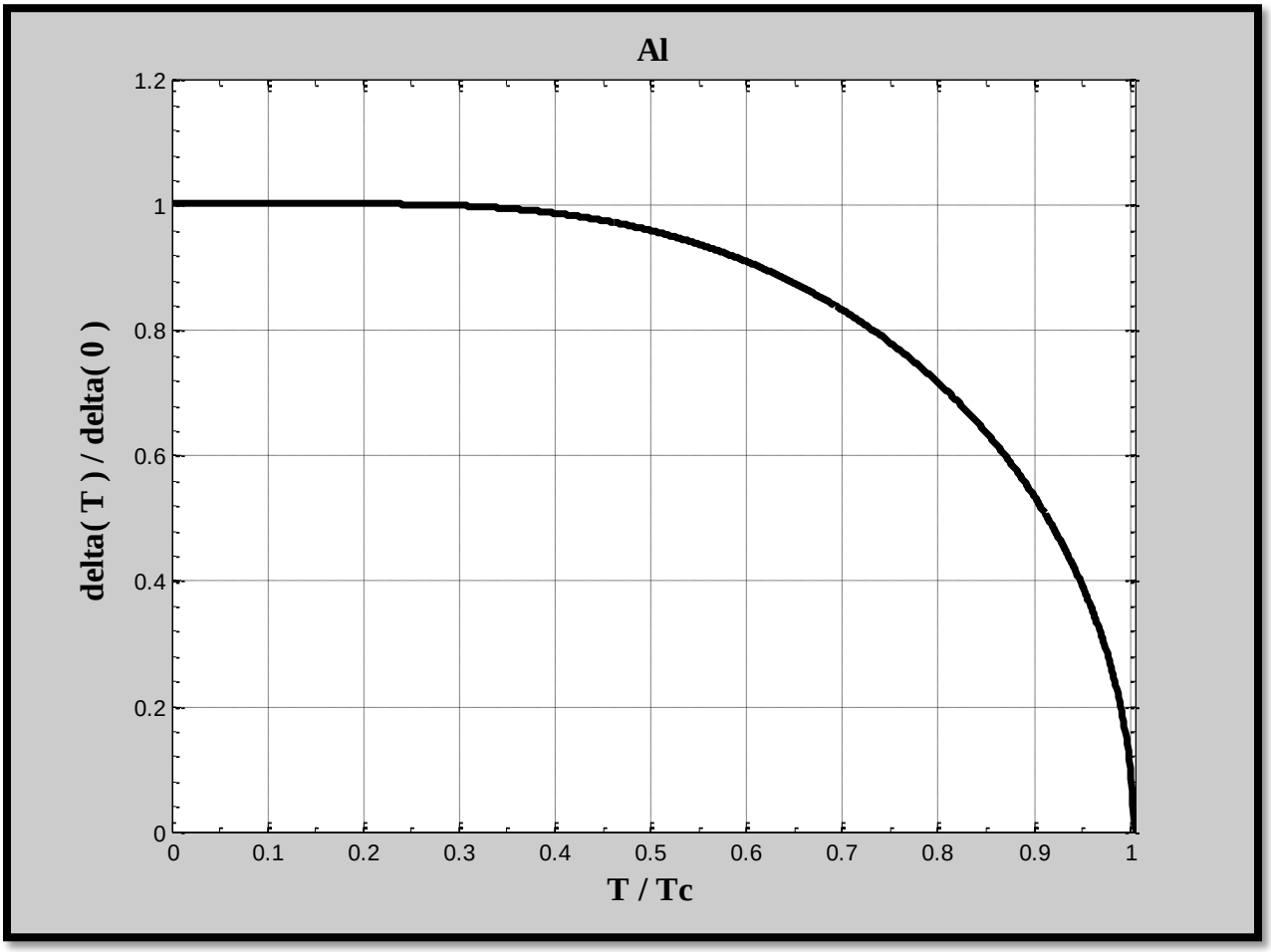

Plot 4. Parameters: $N^0V = 0.18$, $T_c = 1.6382\text{K}$, $\theta_D = 375\text{K}$, $n = 5000$.

2.2. DISCUSSION

The plots for the single-band case show to be in perfect concordance with those portrayed in most of the common superconductivity references in literature, as below, where the tracing of the energy gap performed by Bardeen *et al.* in their fundamental paper [4] is displayed.

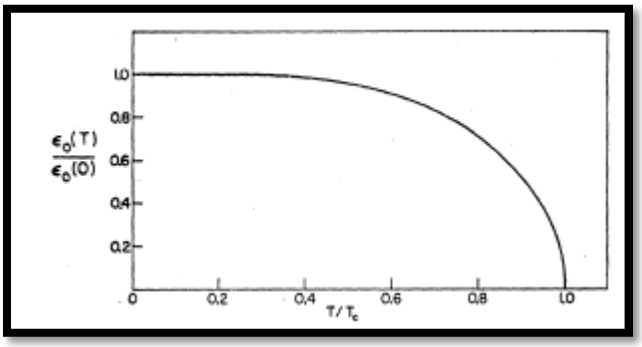

Figure 4.1. Ratio of the energy gap performed by Bardeen *et al.* [4]

In the plots obtained the behavior of the curve is in discussion when $\frac{T}{T_c} \approx 0$ and 1. In the first case, the plot behaves as expected from literature, where an expansion in **Eq. (2.40)** and an approximation for $T \ll T_c$ produces the relation $\Delta(T) \propto \left\{\Delta^0 - (const)\exp\left[-\frac{\Delta(0)}{k_B T}\right]\right\}$ [13] which leaves an almost constant energy gap size near $T = 0$ as evidenced in **Fig. 4.1**. Also as observed above, the convergence improves naturally with increasing number of cycles. It's to be noticed that the integral **(2.55)** converges rather fast in a fashion considerably insensitive to the initial value Δ^0 (except, obviously $\Delta^0 = 0$). In the second case, it's well known the approximation relation $\Delta(T) \propto \Delta(0)\sqrt{1-\frac{T}{T_c}} = \Delta(0)\sqrt{1-x}$ when $T \approx T_c$ [4] [63], where $x = \frac{T}{T_c}$; by evaluating

$\left.\frac{d\Delta}{dx}\right|_{x=1}$ the asymptotic behavior of the slope of the curve at $T = T_c$ turns very evident as achieved in the plots above. As suggested by Bardeen *et al.*, this is a behavior predicted for all conventional superconductors [4].

3. TRACING OF THE ENERGY GAPS FOR A PURE DOUBLE ENERGY GAP SUPERCONDUCTOR AT $T \neq 0$.

3.1 NUMERICAL FITTING

The double band case, however, is more complicated. Since the Δ- terms in **Eqs. (2.56-57)** are mutually coupled, an appropriate numerical fitting of **Eqs. (2.92-93)** inspired in **(2.54)** will stand as

$$\begin{aligned} \Delta_\sigma^{n+1} &= N_\sigma^0 V_{\sigma\sigma} \Delta_\sigma^n F\left(\Delta_\sigma^n\right) + N_\pi^0 V_{\sigma\pi} \Delta_\pi^n F\left(\Delta_\pi^n\right) \\ \Delta_\pi^{n+1} &= N_\pi^0 V_{\pi\pi} \Delta_\pi^n F\left(\Delta_\pi^n\right) + N_\sigma^0 V_{\sigma\pi} \Delta_\sigma^n F\left(\Delta_\sigma^n\right). \end{aligned} \tag{3.2}$$

Most of the results are replications of the calculations done in [41]. Here, computations were made in absence and/or presence of either the inter- or the intra- scattering matrix element.

Normalization of the energy gaps for this case is done with respect to the quantity $k_B T_c$; the parameters used are the same implemented in [41]. The values of T_c were calculated using **Eq. (2.58)**; the Debye temperature θ_D is estimated to fit results. Results are shown with and without normalization to the units. At the end, some calculations were performed considering parameters from MgB_2.

3.2 RESULTS

The computations implemented here produced the following results for the double band case, impurities absent, no intra-band scattering allowed:

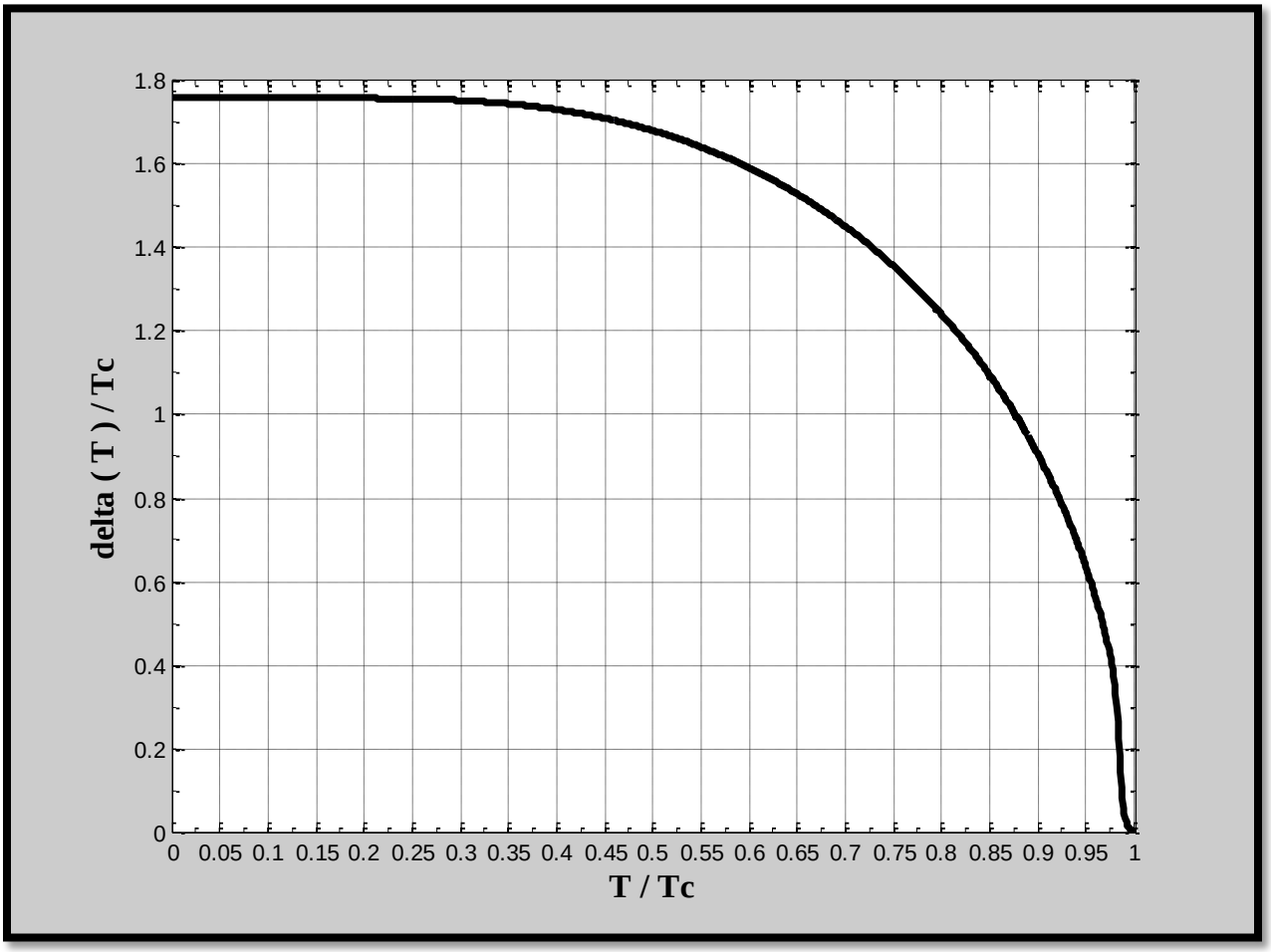

Plot 5. Parameters:

$$V_{\sigma\sigma} = V_{\pi\pi} = 0, V_{\sigma\pi}\sqrt{N_\sigma N_\pi} = \tfrac{1}{3},\ T_c = 11.0677\text{K},\ \theta_D = 195\text{K},\ \tfrac{N_\sigma}{N_\pi} = 1,\quad n = 1000.$$

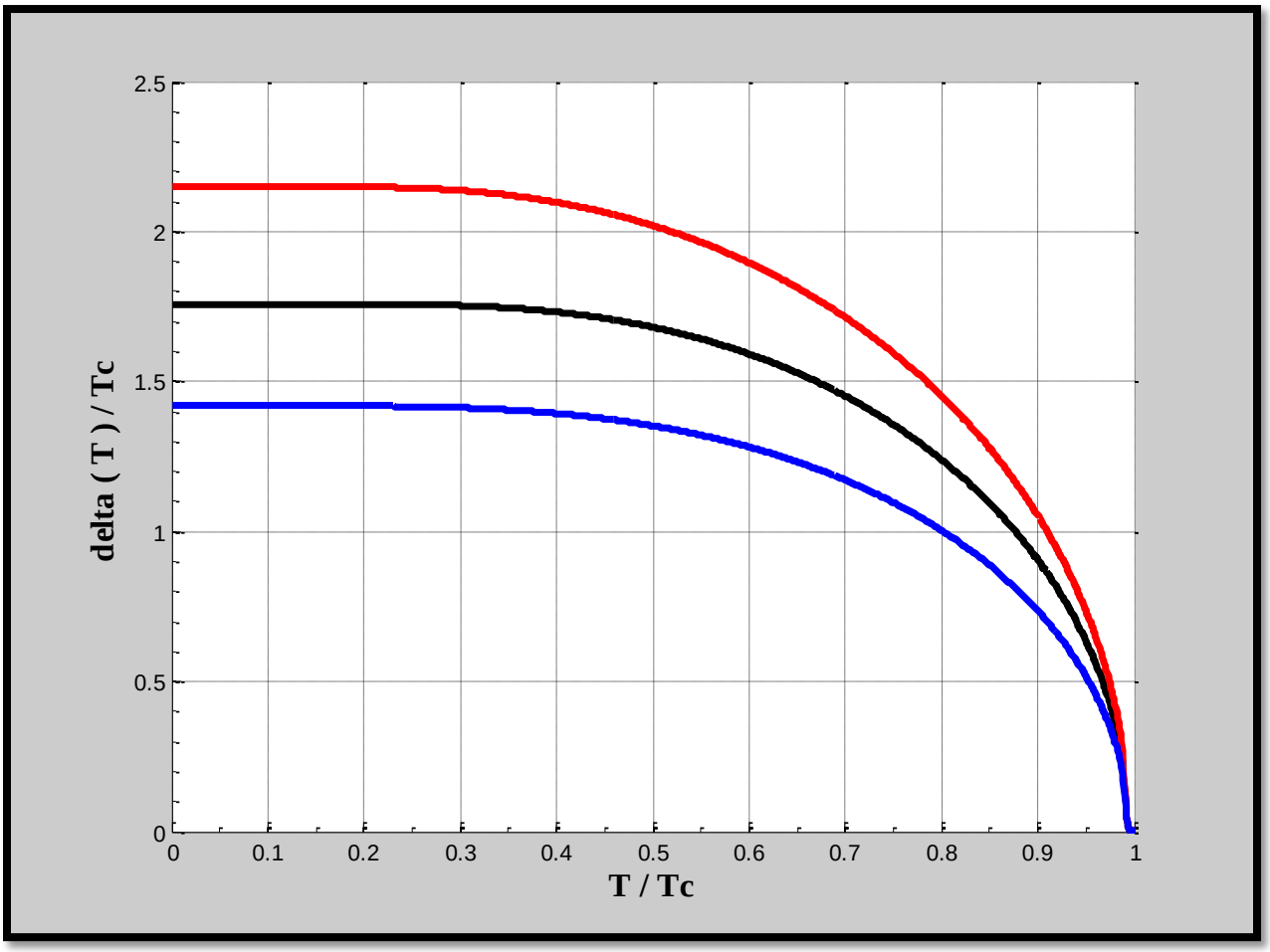

Plot 6. Parameters:

$$V_{\sigma\sigma} = V_{\pi\pi} = 0,\ V_{\sigma\pi}\sqrt{N_\sigma N_\pi} = \tfrac{1}{3},\quad T_c = 11.0677\text{K},\ \theta_D = 195\text{K},\ n = 2000.$$

$\frac{N_\pi}{N_\sigma}$	Color
1	Black
2	Red and blue

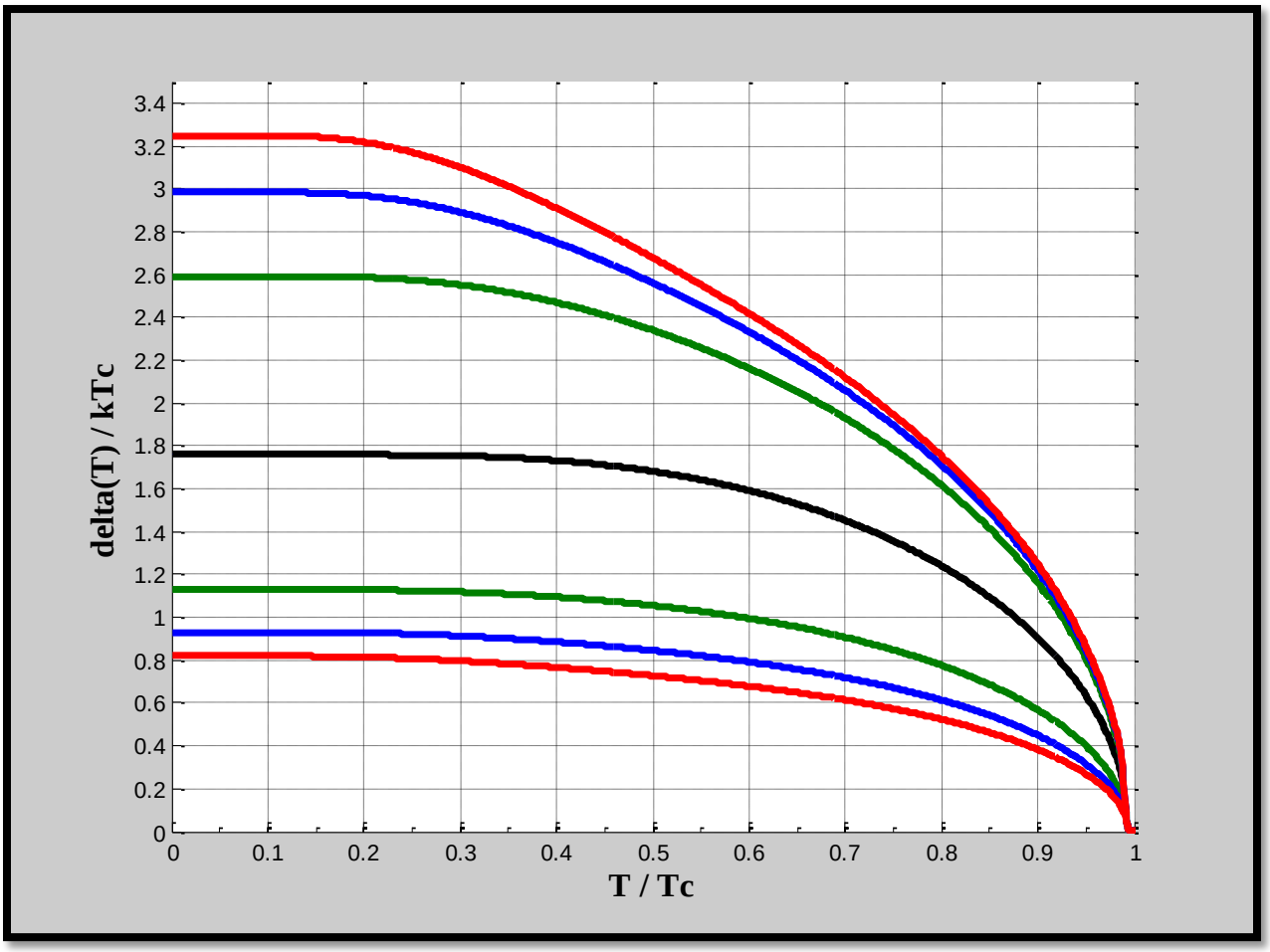

Plot 7. Parameters:

$$V_{\sigma\sigma} = V_{\pi\pi} = 0,\ V_{\sigma\pi}\sqrt{N_\sigma N_\pi} = \tfrac{1}{3},\quad T_c = 11.0677\text{K},\ \theta_D = 195\text{K},\ n = 2000.$$

$\frac{N_\pi}{N_\sigma}$	Color
1	Black
4	Green
7	Blue
10	Red

The computations implemented here produced the following results for the double band case, impurities absent, no inter-band scattering allowed:

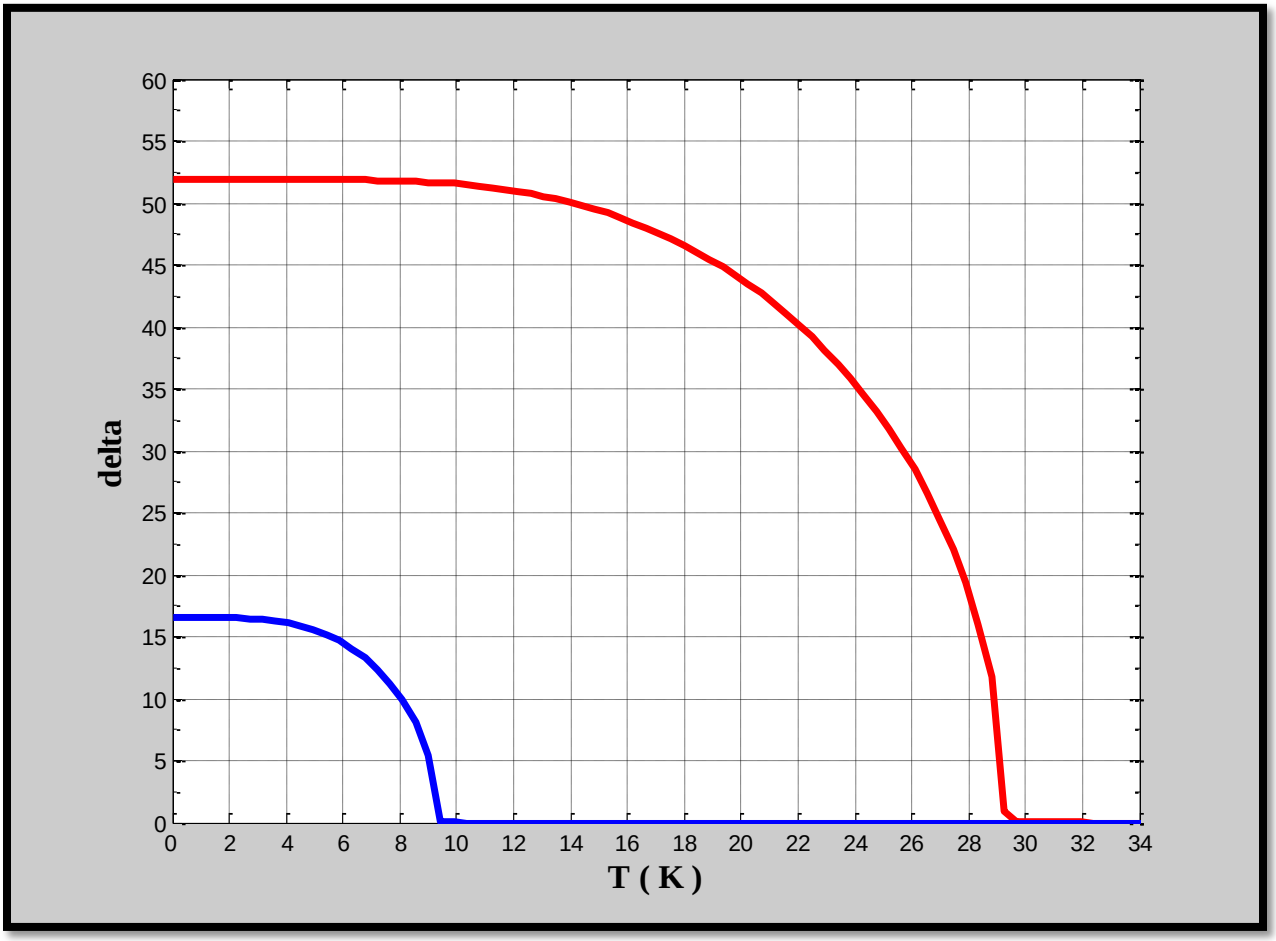

Plot 8. The energy gap size is not normalized

Parameters:

$$V_{\sigma\pi} = 0,\ T_c^{(1)} = 9.3959\text{K},\ T_c^{(2)} = 29.4649\text{K},\ \theta_D = 450\text{K},\ n = 1000.$$

$$N_\pi V_{\pi\pi} = 0.25,\ N_\sigma V_{\sigma\sigma} = 0.35.$$

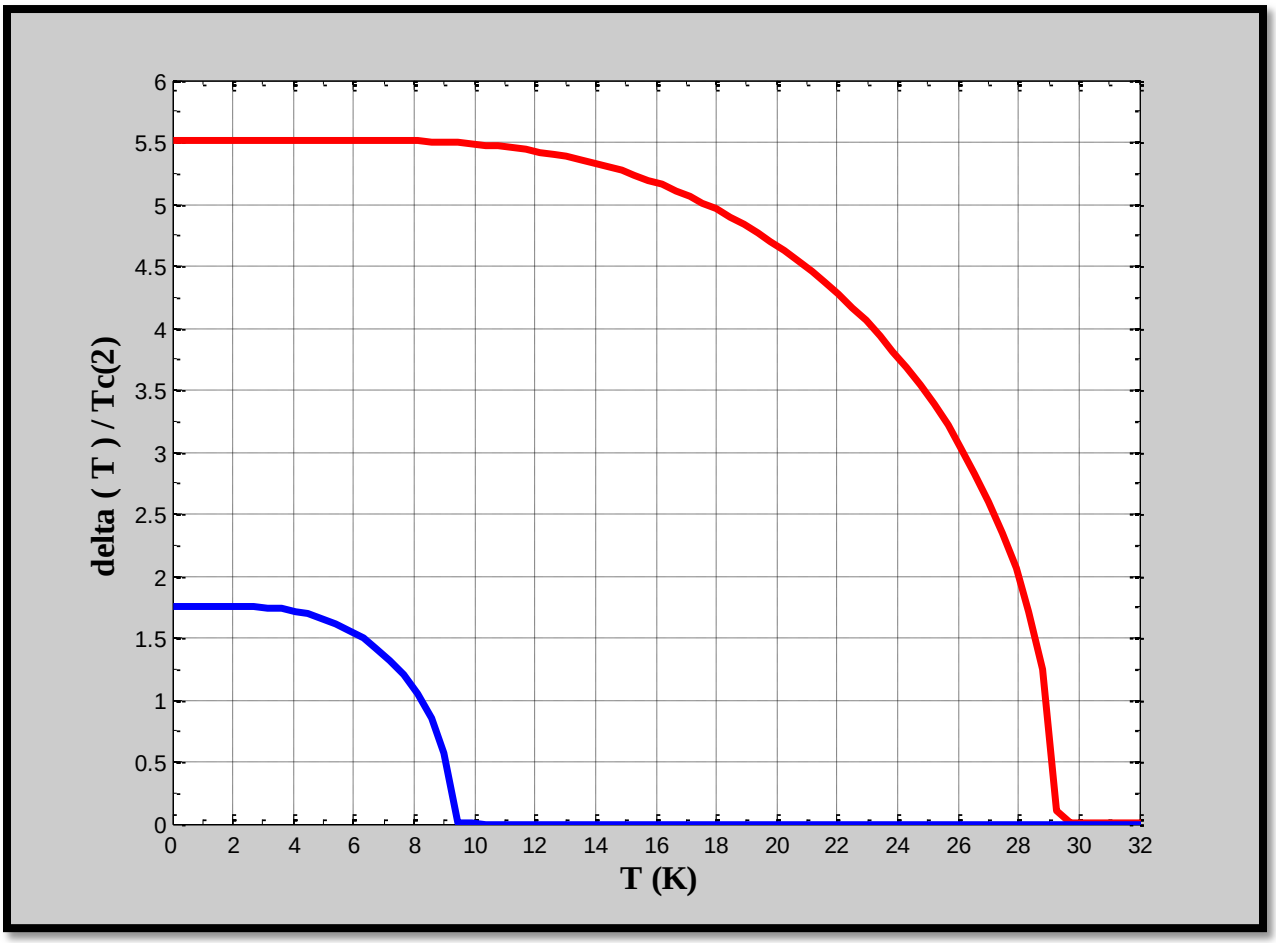

Plot 9. The energy gap size is normalized.

Parameters:

$$V_{\sigma\pi} = 0,\ T_c^{(1)} = 9.3959\text{K},\ \ T_c^{(2)} = 29.4649\text{K},\ \ \theta_D = 450\text{K},\ \ n = 1000.$$

$$N_\pi V_{\pi\pi} = 0.25,\ N_\sigma V_{\sigma\sigma} = 0.35.$$

The computations implemented here produced the following results for the double band case, impurities absent, with inter- and intra- band scattering allowed:

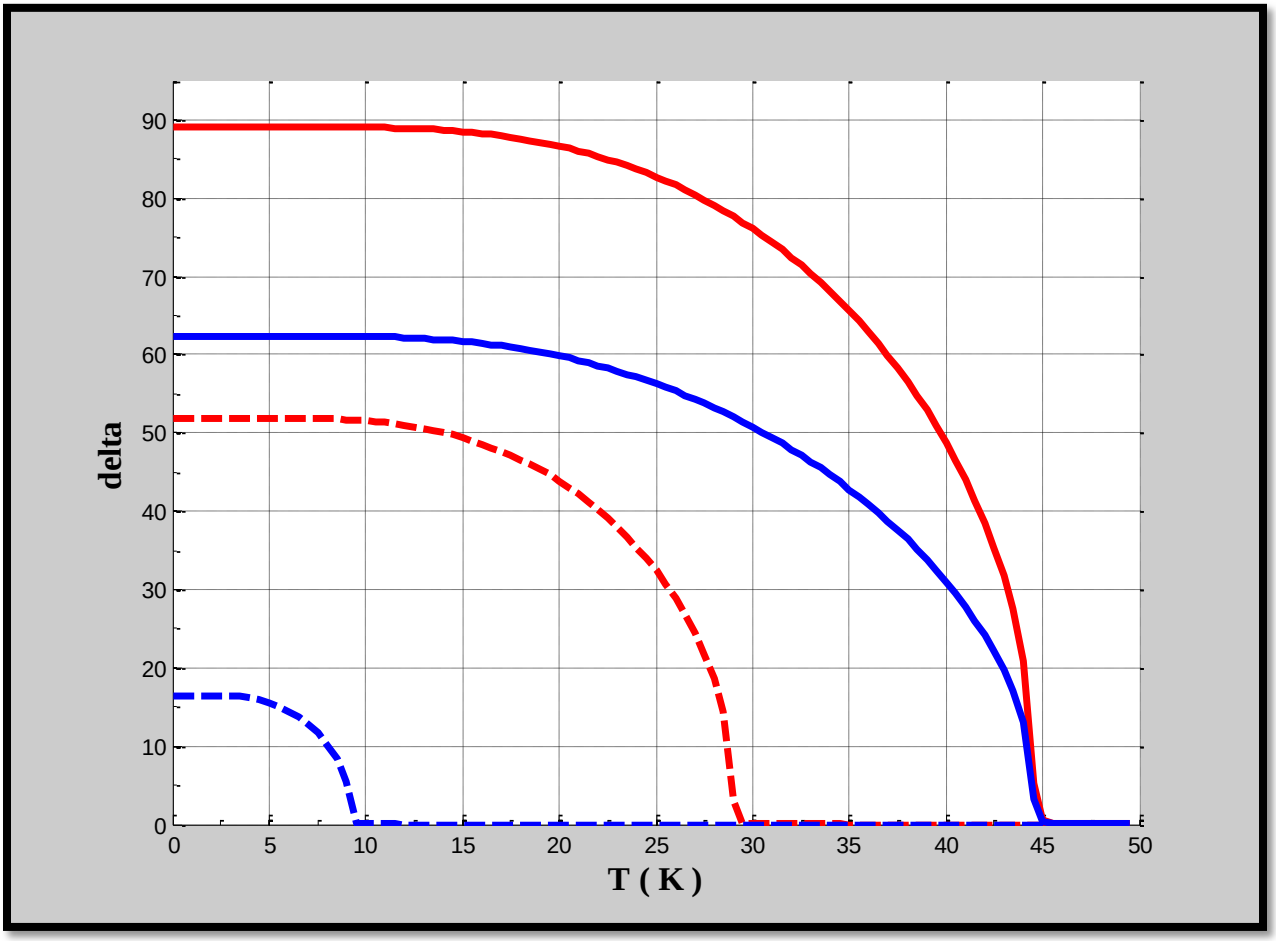

Plot 10. The energy gap size is not normalized.

Parameters:

$$N_\pi V_{\pi\pi} = 0.25,\ N_\sigma V_{\sigma\sigma} = 0.35,\ \theta_D = 450\text{K},\ n = 500.$$

$N_\sigma V_{\pi\sigma}$	Feature
0.0	Dotted-lines
0.1	Solid lines

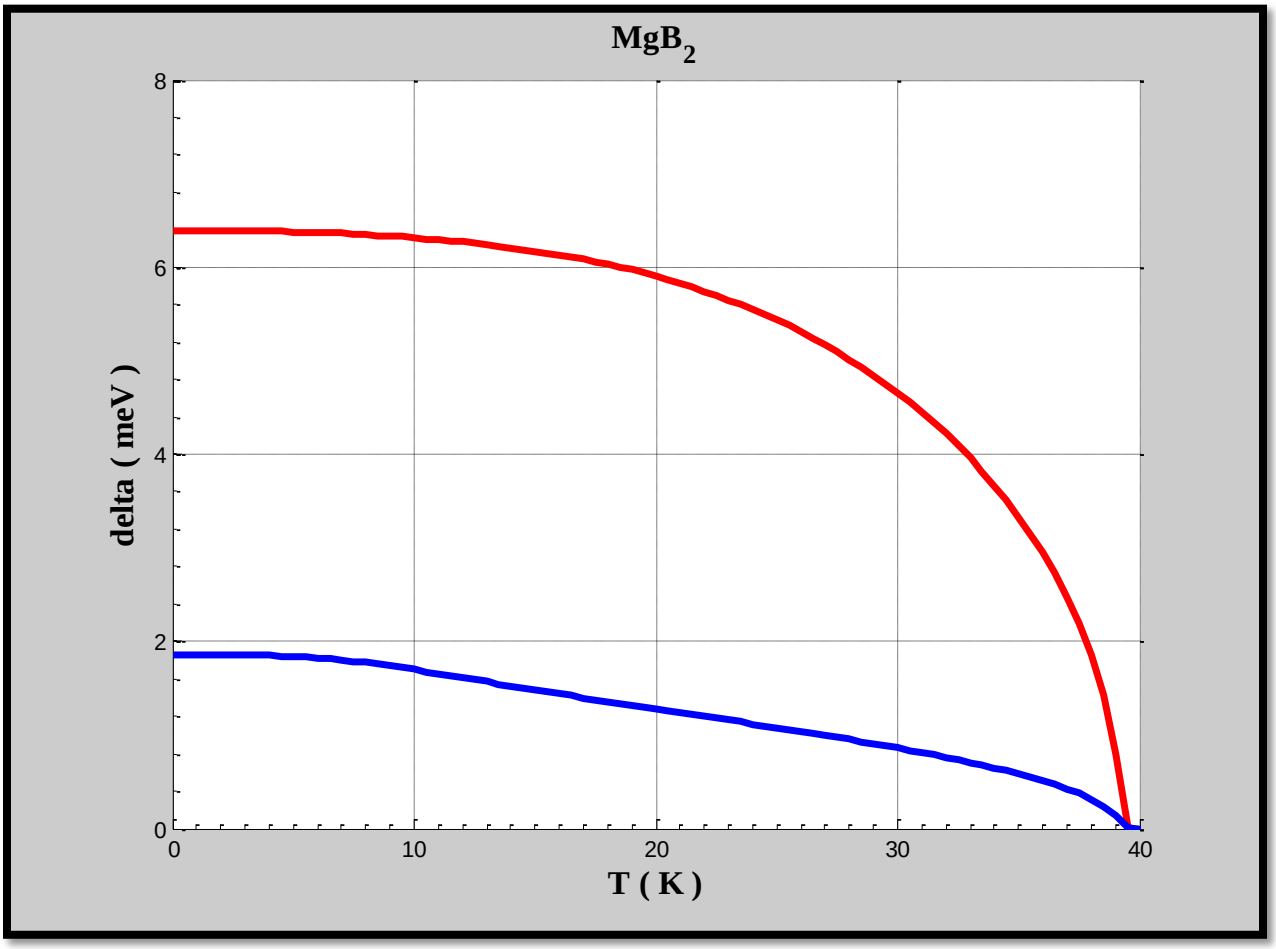

Plot 11. Energy gaps in pure MgB_2 compound normalized to meV units. The red plot corresponds to the tracing of Δ_σ; The blue plot corresponds to the tracing of Δ_π.

Parameters:

$$N_\pi V_{\pi\pi} = 0.2000,\ N_\sigma V_{\sigma\sigma} = 0.4255,\ N_\pi V_{\sigma\pi} = N_\sigma V_{\sigma\pi} = 0.039,$$
$$\Delta_\sigma^0 = 6.38\,meV,\ \Delta_\pi^0 = 1.86 meV, \theta_D = 350\text{K},\ T_c \approx 39.43\text{K},\ n = 5000.$$

3.3. DISCUSSION

As observed, the general behavior of the energy gaps follow that of the single band case in terms of the shape of the plot. However, the absence or presence of inter- or intra- band scattering becomes a determinant factor for the critical temperature.

It turns easy to note that in absence of the intra-band scattering ($V_{\sigma\sigma} = V_{\pi\pi} = 0$) but in presence of inter-band scattering ($V_{\sigma\pi} \neq 0$) only one sign of **Eq. (2.58)** prevails whereas the other is devoid of physical significance; by a simple substitution, **Eq. (2.58)** becomes

$$k_B T_c \approx 1.14 \exp\left[-F_{\text{inter}}(0)\right], \qquad \textbf{(3.3)}$$

where $F_{\text{inter}}(0) = \frac{1}{N_\sigma N_\pi}$. In these cases, normalization was possible to this one temperature (**Plot 5** to **Plot 7**). The other determinant factor is the ratio $\frac{N_\sigma}{N_\pi}$, which leaves a single band when equal to one (**Plot 5**; see also **Eqs. (2.92-93)**) but splits plots in pairs of symmetrical curves around the curve $\frac{N_\sigma}{N_\pi} = 1$ for increasing values of this ratio (**Plot 7**).

This situation changes in the presence of intra-band scattering ($V_{\sigma\sigma} \neq V_{\pi\pi} \neq 0$) and absence of inter-band scattering ($V_{\sigma\pi} = 0$). In such cases the two signs of *F* are evidently differentiated. A substitution in **Eq. (2.58)** yields:

$$k_B T_c^{(2,1)} \approx 1.14 \exp\left[-F_{\text{intra}}^{\pm}(0)\right], \qquad \textbf{(3.4)}$$

where $F_{\text{intra}}^{+}(0) = \frac{1}{N_\sigma V_{\sigma\sigma}}$ and $F_{\text{intra}}^{-}(0) = \frac{1}{N_\pi V_{\pi\pi}}$, which justifies the presence of two transition temperatures. This observation allows us to understand the behavior of the gaps when both intra-

and inter- scattering are permitted (**Plot 10**). As seen, in proportion to the increase in the magnitude of the inter-band scattering matrix element, the curve for the lesser T_c shows the initial tendency to a lower temperature to finally merge with the curve for the higher T_c as T continues increasing. These results are in concordance with those derived by Suhl *et al.* [41], as displayed below.

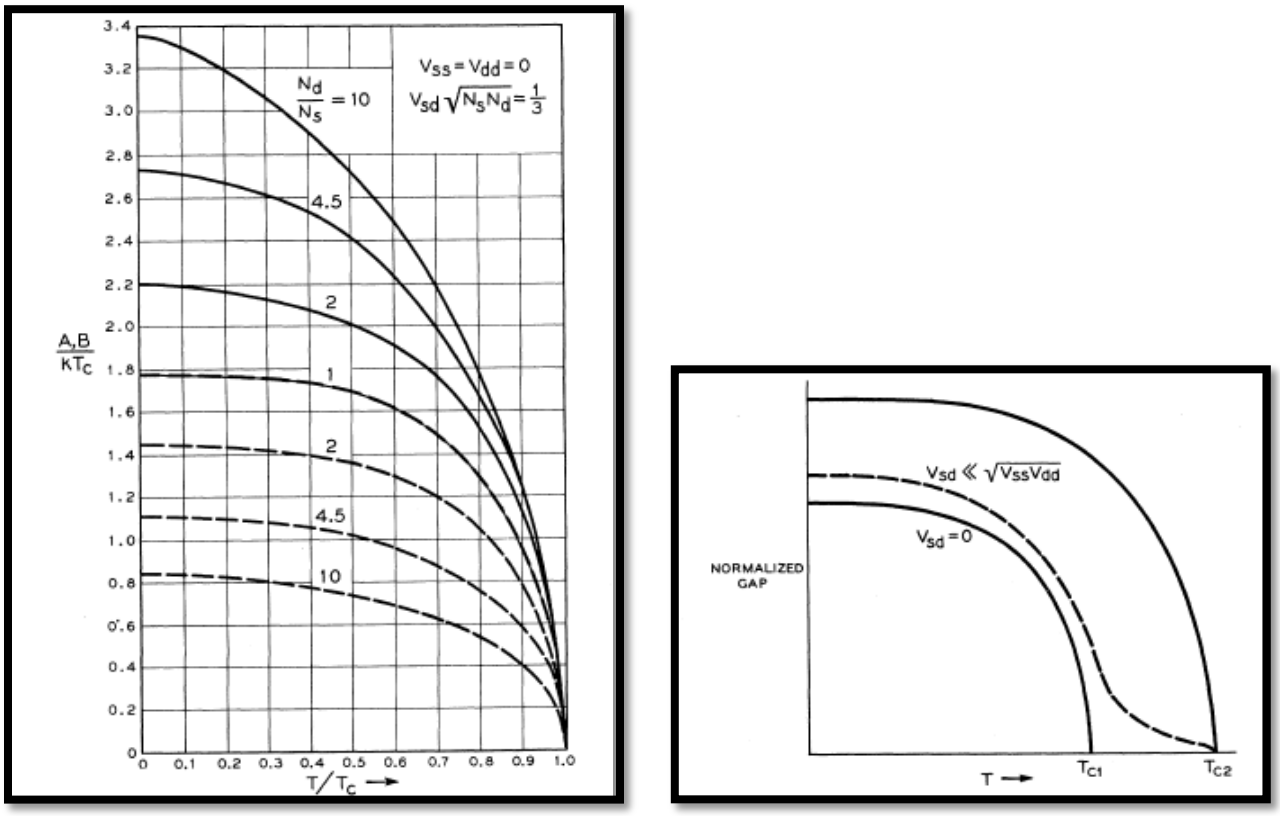

Figure 4.2. Results of the energy gap tracing for the double band case performed by Suhl *et al.* [41].

Finally, the results obtained using parameters of the MgB_2 compound (**Plot 11**) are in concordance with the numerical trace performed by Choi *et al.* [27], shown below. The values of N^0V and θ_D were conveniently chosen to fit the experimental data.

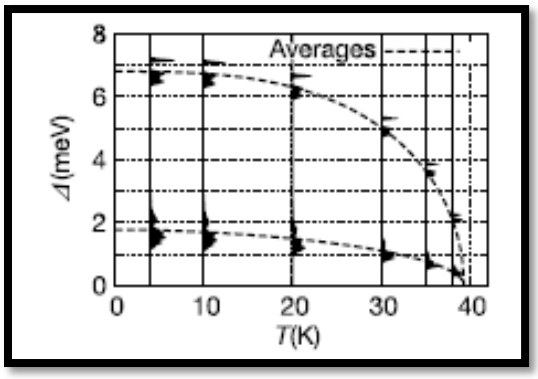

Figure 4.3. Numerical trace of then energy gaps in MgB_2 performed by Choi *et al.* [27] using the iterative technique of Marsiglio *et al.*[64]

4. TRACING OF THE ENERGY GAPS FOR A DOUBLE ENERGY GAP SUPERCONDUCTOR AT $T \neq 0$ IN THE PRESENCE OF NON-MAGNETIC IMPURITIES

4.1 NUMERICAL FITTING

As depicted before, numerical tracing is done by **Eq. (3.2)** but the the variations in the matrix elements because of the influence of the scattering due to impurities in the dirty limit and within the weak localization correction (**Eqs. (2.84)** and **(2.91)**) have to be accounted for. In order to contrast results, the experimental tracing on the superconducting energy gaps of MgB_2 done by Y. Wang *et al.* [65], F. Bouquet *et al.* [66] and several studies of M. Putti *et al.* [67]-[69] and Z. Hoîanová *et al.* [70] are considered. Specifically, Wang *et al.* present a study where the evolution of the energy gaps is followed by bulk specific-heat measurements while disorder is introduced [66]. This is exactly what our theoretical model allows us to do.

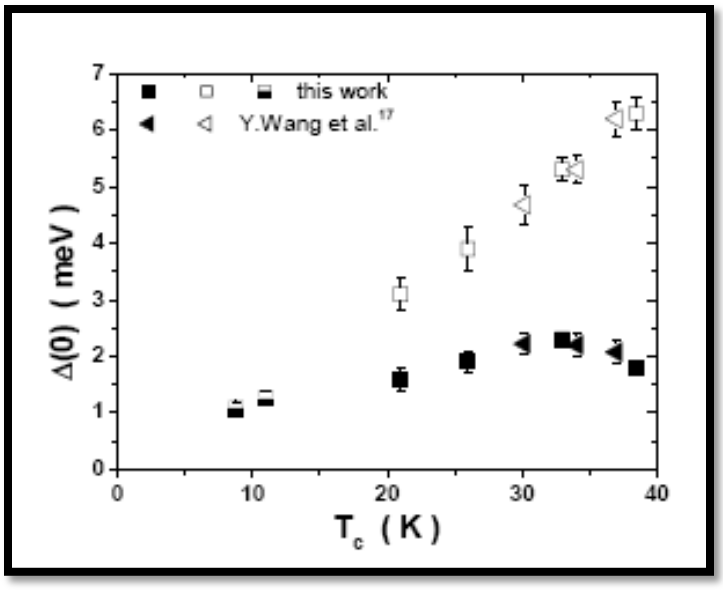

Figure 4.4. Experimental tracing of the energy gaps in MgB_2 by Putti *et al.* [67].

As observed above, because the quantities whose change is to be followed are Δ^0 and T_c (and not Δ and T, like in the former Sections) an important simplification occurs because F in **Eqs. (2.92-93)** is now evaluated at $\Delta^0 = \Delta(T=0)$; hence, by the definition of F in **Eq. (2.55)**, $\beta^0 = \infty$, yielding $\tanh(\infty) = 1$ and thus the integral loses its hyperbolic trigonometric part becoming the simple nice analytic integral of **page 39**. This will save an enormous quantity of calculations, at least compared with those performed in **S. 2** and **S. 3**. Furthermore, because $l^{\sigma\pi} \gg l$, where l stands for $l^{\sigma\sigma}$ or $l^{\pi\pi}$ henceforth, the assumption $\frac{1}{l^{\sigma\pi}} \approx 0$ will be reasonable and the matrix elements **(2.91)** are dramatically reduced to [55]:

$$V_{\sigma\sigma} = V_{\sigma\sigma}^{0}\left[1-\frac{3}{\left(k_F^{\sigma} l^{\sigma\sigma}\right)^2}\right]$$

$$V_{\pi\pi} = V_{\pi\pi}^{0}\left[1-\frac{3}{\left(k_F^{\pi} l^{\pi\pi}\right)^2}\right] \qquad \textbf{(3.3)}$$

$$V_{\sigma\pi} = V_{\sigma\pi}^{0}\left[1-\frac{3}{\left(k_F^{\sigma} l^{\sigma\sigma}\right)^2}-\frac{3}{\left(k_F^{\pi} l^{\pi\pi}\right)^2}\right] = V_{\pi\sigma}.$$

Upon observations from Kim *et al.* [57] [71] [72] and experimental results [22] [25], the dirty limit is conditioned by $\frac{1}{k_F l^{\sigma\pi}} \leq 0.1$, while the weak localization correction becomes important for $\frac{1}{k_F l} > 0.1$. Besides, in the calculations implemented here $10000\text{Å} \geq l^{\sigma\pi} \geq 700\text{Å}$ is assumed, where $l^{\sigma\pi}$ diminishes as $T_c \to 0$ because of the increasing in disorder. Notice that this variation directly affects the Cooper pair sizes, as defined in **Eq. (2.80)**. Once outside the dirty limit, weak localization correction turns important and $l^{\sigma\pi} = 700\,\text{Å}$ is left fixed; then the *V*-terms calculated up to this point from **Eq.(2.84)** enter as V^0- terms in **Eq. (3.3)** with $75\text{Å} \geq l \geq 3\text{Å}$. Initial values for the Cooper pair sizes were calculated from **Eq. (2.80)** as $\xi_{\sigma}^{0} = 83\,\text{Å}$ and $\xi_{\pi}^{0} = 262.5\,\text{Å}$ by using $\Delta_{\pi}^{0} = 2\text{meV}$ and $\Delta_{\sigma}^{0} = 6.3\text{meV}$ as very rough approximations from experimental data [27]. These values are fixed at the entry of the weak localization correction limit as well.

4.2 RESULTS

With these implementations in mind, the computations implemented here produced the following results for the double band superconductor MgB_2, impurities present:

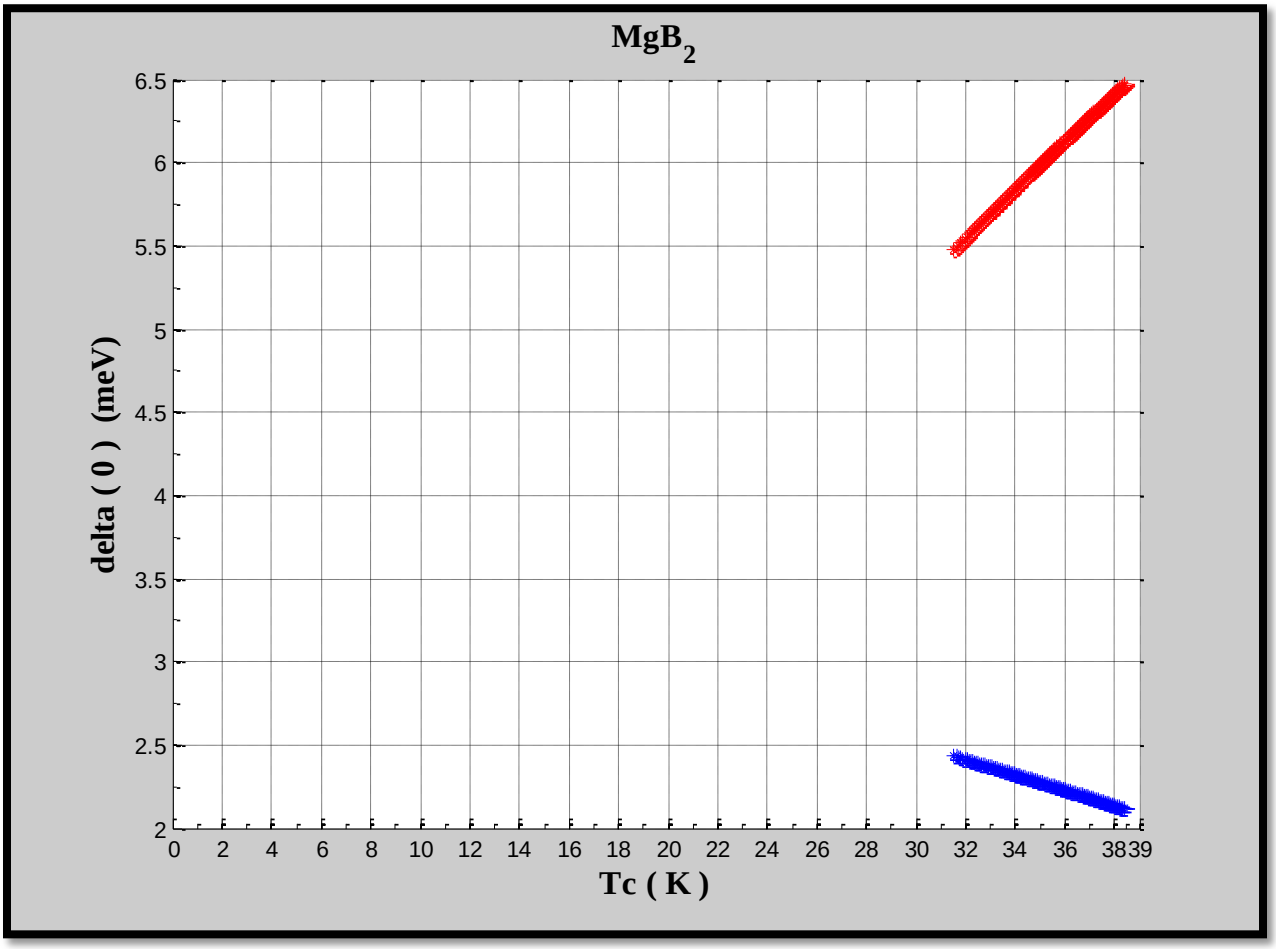

Plot 12a. Tracing of MgB_2's zero-temperature energy gaps within the dirty limit with increasing disorder ($0 < T_c < 38.5\text{K}$) (red line corresponds to Δ_σ^0, blue line corresponds to Δ_π^0).

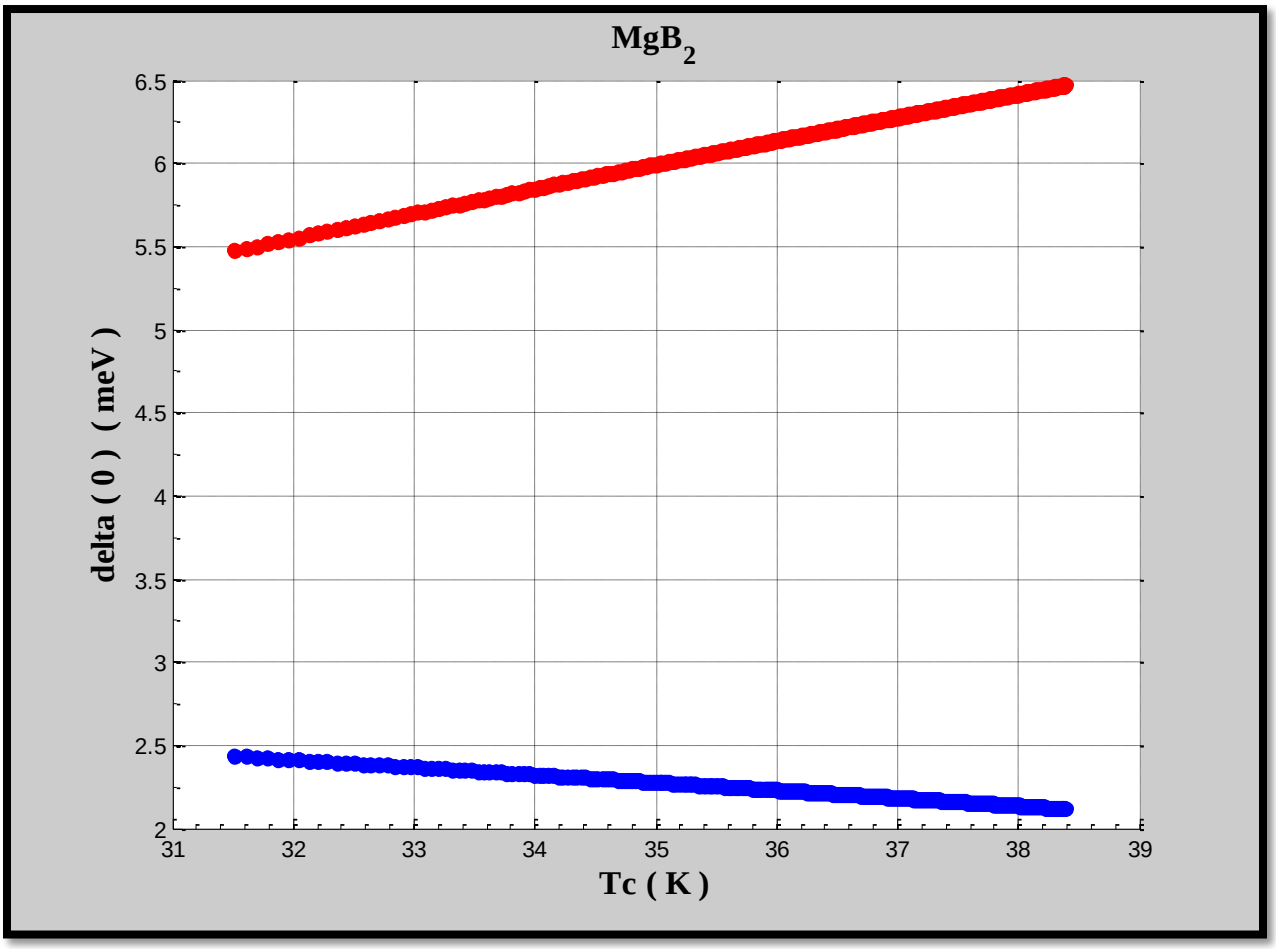

Plot 12b. Tracing of MgB_2's zero-temperature energy gaps within the dirty limit with increasing disorder ($31.5\text{K} < T_c < 38.5\text{K}$) (red line corresponds to Δ_σ^0 , blue line corresponds to Δ_π^0).

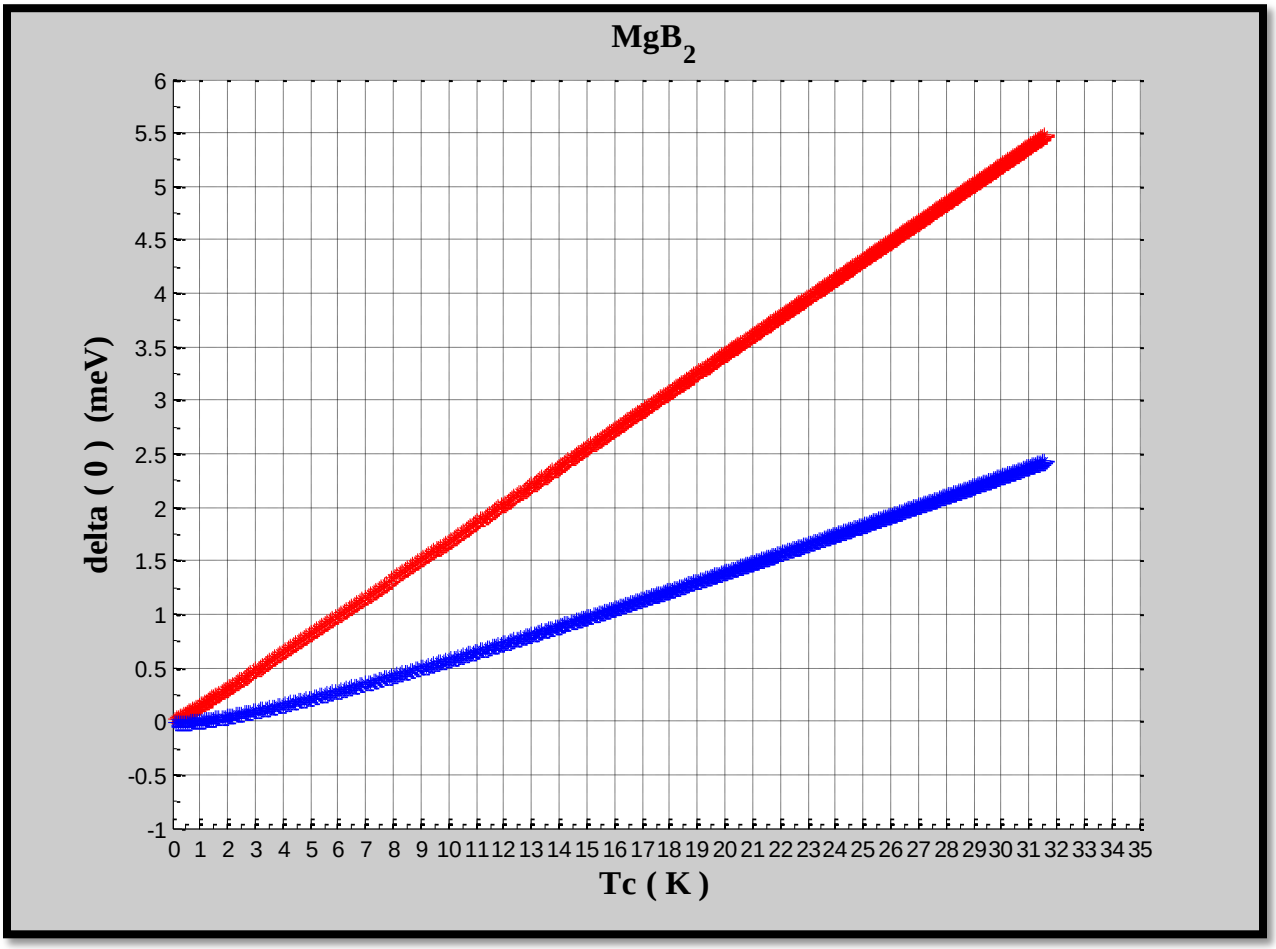

Plot 13. Tracing of MgB_2's zero-temperature energy gaps with increasing disorder including the weak localization correction (red line corresponds to Δ_σ^0, blue line corresponds to Δ_π^0).

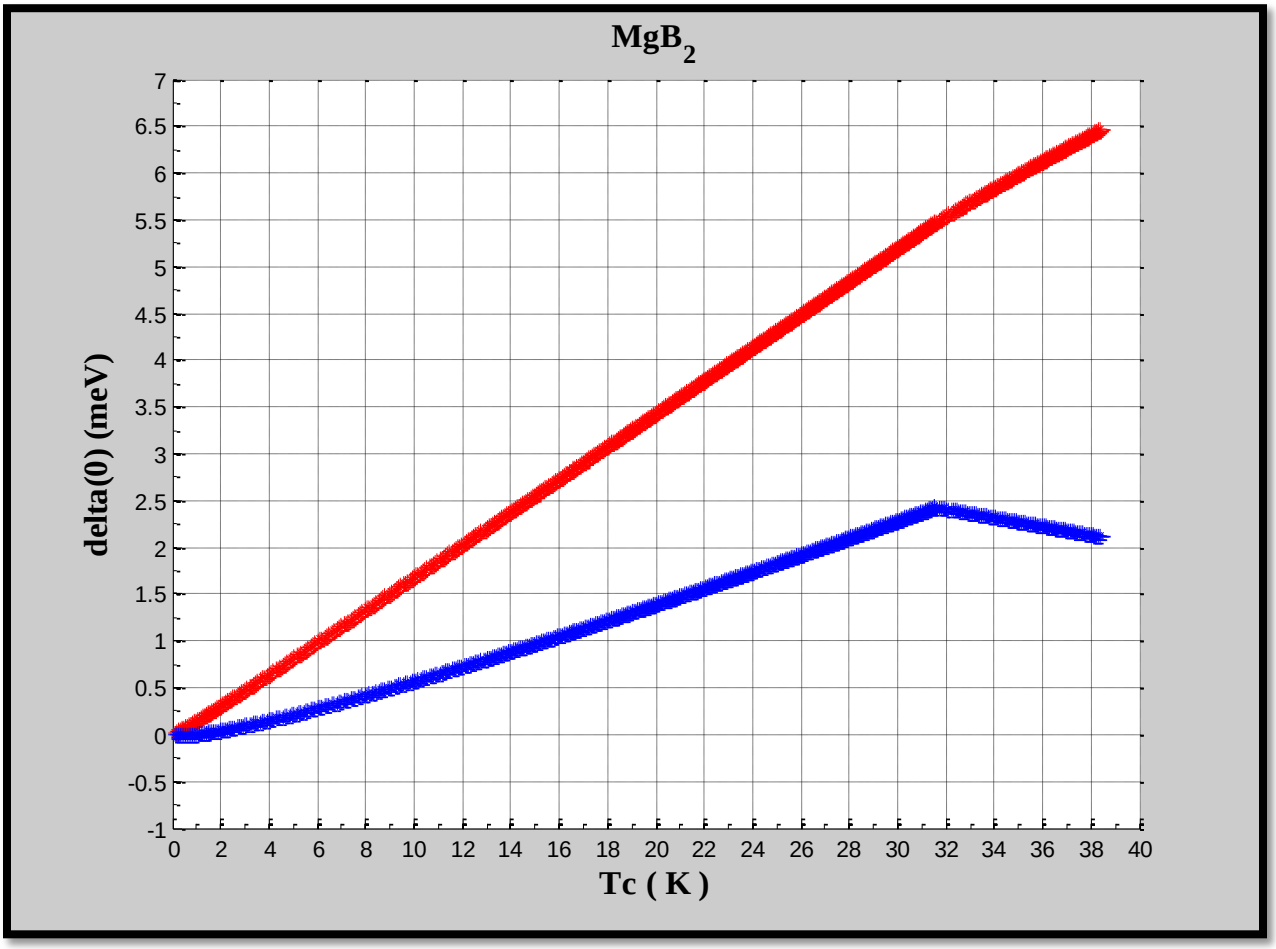

Plot 14. Tracing of MgB_2's zero-temperature energy gaps with increasing disorder (red line corresponds to Δ_σ^0, blue line corresponds to Δ_π^0).

4.3 DISCUSSION

The shapes of the curves obtained are quite distinct from those of the former Sub-sections, mainly due to the change in the parameters plotted. In theory, with the older parameters one should expect a behavior as that portrayed in **Fig. 4.3**. An experimental trace on MgB_2's energy gaps of the kind performed using our theoretical model is conducted by Hoîanová *et al*. [70] on Carbon substituted $Mg(B_{1-x}C_x)_2$ samples (**Fig. 4.6**). The values of T_c change slowly within the dirty limit ($31.5\text{K} < T_c \leq 38.5\text{K}$) but they experience a quite significant decrease when weak localization ($T_c \leq 31.5\text{K}$) is taken into account. This is observed and explained by KO [42] and Kim [55] [57]. As well the remarkably different behavior displayed by the zero-temperature energy gaps in different regimes is also significant. Within the dirty limit, where scattering matrix elements of **Eq. (2.84)** are valid, a decrease in Δ_σ^0 (red) is observed (although not at a constant slope, as one can conclude from **Plot 14**), while a minor increase in Δ_π^0 (blue) occurs; it is considerably important to observe that some experiments report no change of Δ_π^0 at all (with $\Delta_\pi^0 \sim 2$ meV) in this interval [73]. A slight increase is reported by Daghero *et al.* [74] and Gonnelli *et al.* [75] [76]. On the other hand, once the weak localization correction of **Eq. (2.84)** becomes important both gaps are seen to diminish down to zero in a rather linear fashion; a linear trend of the energy gaps can also be compared with the point-contact spectroscopy (PCS) experimental results of Hoîanová *et al*. [70] on C-substituted MgB_2 (see **Fig. (4.5)**). Other research groups as Putti *et al.* [67], Hoîanová *et al*. [70] and Gonelli *et al.* [75] also attract attention on this linear behavior with different slopes.

Also observed by Putti *et al.* [67] in their experimental trace (**Fig. 4.4**) is that the saddle point in the π- gap curve occurs at 30K. For the plots obtained here it occurs at 31.5K. For these researchers, however, both gaps merge from approximately 21K and continue as a single gap down to zero [67]. As said a few lines above such merging is also observed experimentally by Gonelli *et al*. [75]. For the plots derived here the merge occurs at 0K. Such observation is suggested by the results of Hoîanová *et al.* [70].

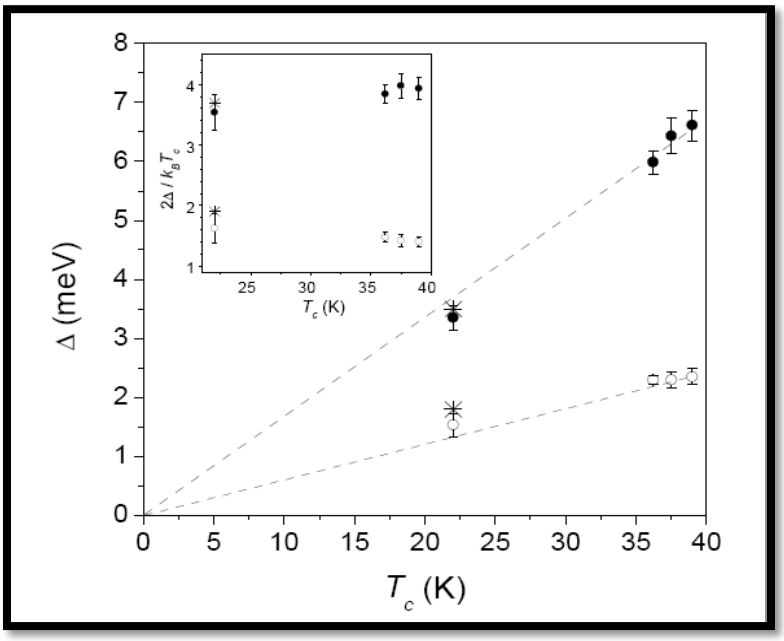

Figure 4.5. Superconducting energy gaps from PCS experiments as a function of T_c from Hoîanová *et al.* [70]

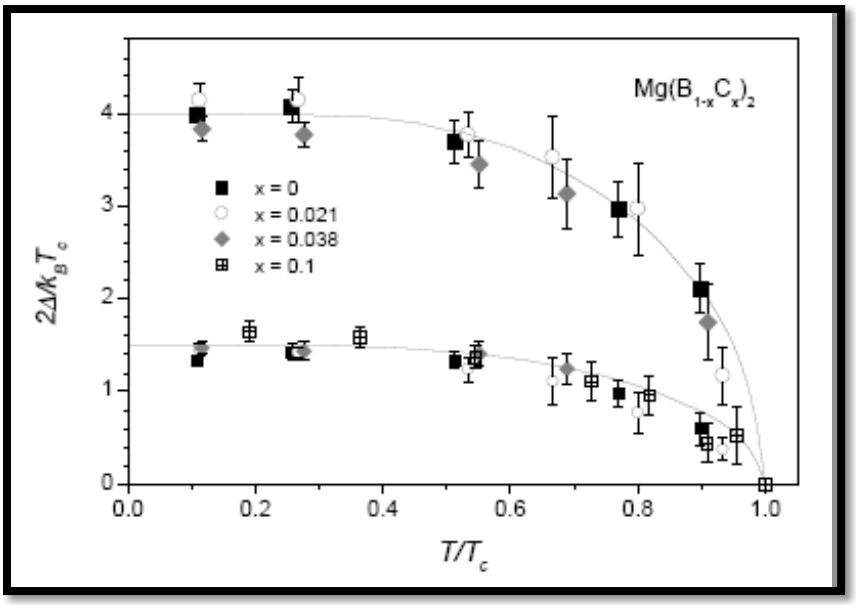

Figure 4.6. Experimental trace of the energy gaps in MgB_2 in presence of impurities conducted by Hoîanová *et al.* [70]

IV. CONCLUSIONS AND FUTURE WORK

1. CONCLUSIONS

A qualitative theoretical model for the tracing of the energy gaps in a two band superconductor was elaborated and an outline of such energy gaps within the BCS theory was performed considering several regimes. The effect of weak localization on a two band superconductor was studied. It is found that within the "clean regime", i.e. impurities absent, T_c is rather sensitive to the inter- and intra- band scattering, the first one being clearly responsible for the merging of the energy gaps at a single T_c, as seen in **Plots 10** and **11** [77]. Despite the BCS crude approximation of the phonon-mediated interaction (See **Eqn. (2.25)**), the results are in qualitative good agreement with experimental results (See **Fig. 1.5**). Blatt [3] (p. 244-245) shows a numerical tabulation of Δ; values are comparable with those derived here. In the double band case, the results are sensitive to the fraction $\frac{N_\pi}{N_\sigma}$ in the absence of intra-band scattering; in absence of inter-band scattering, an ideal situation of two superconducting transition temperatures was obtained; in the case of no impositions on the values of these scattering elements we derive results applicable to MgB_2 and comparable with experiments (**Plot 11**).

Within the "dirty regime", i.e. impurities present, the inter- and intra- band scattering matrix elements play different roles in proportion to the range of validity of Anderson's theorem, i.e. the dirty limit, and the weak-localization correction from Kim [55]. It is easily seen from **Eq.**

(2.91) that *inter-band scattering is predominant within the dirty limit* (because of the absence of l in the equations). As pointed by Putti *et al.* [67], as well as Kim [55], the decrease of Δ_σ^0 and the slight rise of Δ_π^0 is apparently a direct consequence of the inter-band scattering. Kortus *et al.* [73] claim that this behavior of the π- gap is the result of a compensation effect between band filling (in the case of doped samples) and inter-band scattering. Kortus also predicts a shift in the merging point for higher doping concentrations at lower T_c; Daghero *et al.* [74], however, attributes this to the moderate increase of the inter-band scattering whereas for Gonnelli *et al.* [75] [76] such change and the subsequent merge of the gaps is dependent on the kind of doping [76]. Different experimental groups predict different critical temperatures for the merging of the gaps to occur. Merging at 0K is justified by theory (see **Eq. (3.2)**). Daghero *et al.* [74] predicts an extremely high inter-band scattering matrix element to produce a significant suppression of T_c and the subsequent gap merge for neutron-irradiated MgB_2 samples; this group obtains better results for a merging in the gaps by manipulating other parameters like the magnitude of the density of states and disregarding the effect of disorder [74]. Impurity concentration is being increased by decreasing of $l^{\sigma\pi}$ (and later decreasing l), as described back in **S.S. 4.1** in **Ch. III**.

As seen in **Eq. (3.3)**, *intra-band scattering becomes predominant when weak localization is considered* [55] (because of the absence of $l^{\sigma\pi}$ of the equations). It is easy to observe that even without the assumption $\frac{1}{l^{\sigma\pi}} \approx 0$, the dependence remains since this parameter is left fixed (see **S.S. 4.1** in **Ch. III**). The descent in the values of the gaps outside the dirty limit is quite linear (although observe that Δ_π^0 is not completely linear at $T_c \approx 0$) which suggests some sort of

relation between Δ^0 and T_c of the type of **Eq. (2.42)**; such expression, however, doesn't seem to be easy to deduce analytically since being $N^0 V_{\sigma\pi} \neq 0$ there isn't a simple equation relating $F(0)$ and $F(\Delta^0)$ (which is simply $\frac{1}{\lambda}$ in the single band model) and, in consequence, a straightforward comparison is not possible. This was precisely what one was enabled to do to derive **Eq. (2.42)** [13] and this is why an equivalent expression for the two band model is absent. Kim [71] shows that the BCS T_c equation within the dirty regimen is

$$k_B T_c \approx 1.14 \hbar \omega_D \exp\left(-\frac{1}{\lambda_{\text{eff}}}\right), \qquad \textbf{(4.1)}$$

where $\lambda_{\text{eff}} = \lambda A^4$ is the coupling constant and A is defined as in **Eq. (2.89)**, clearly predicting decrease in T_c due to the presence of impurities. However, the desired equation is still unattained because (again) a simple equation of the type of **Eq. (2.27)** is missing in the two band model. The question remains open.

2. FUTURE WORK AND RECOMMENDATIONS

Further numerical work is still in order. The calculations implemented here are extremely rough. For example, they didn't take into account a trace of the energy gaps without the extremely uneven constraint $\frac{1}{l^{\sigma\pi}} \approx 0$, although such assumption is still in the range of acceptance [57] if one just looks for a qualitative description. The implementation of the more precise matrix elements of **Eq. (2.91)** can clarify more of the quantitative behavior of the energy gaps. However, a considerable number of variables were ignored; a finer model to implement the

calculations would have to account for changes in the density of states of the electronic bands, the influence of the phonon frequencies and the cell volume. Daghero *et al.* [74] worked out a model with these features. As well, a more sophisticated theoretical approach can be implemented; such theoretical approach is available via the Eliashberg theory formalism. Choi *et al.* [27] uses it to trace the energy gaps as in **Fig. 4.3**. The Green's function formalism of superconductivity [79], which is commonly used in literature, was not adopted here. These implementations might considerably improve the theoretical predictions.

Other improvements of the work done here can consist in more elaborate manners of changing the parameters used. This can be done via use of more powerful software tools. In this case there is not an easy way to predict the shape of the plots. As well, a trace Δ vs. T as that performed in **S. 2** and **S. 3** in **Ch. III** with impurities present is left pendant. The experimental data of such trace is provided in **Fig. 4.6** [70].

The character of the impurities implemented in the model totally discarded their magnetic properties. A more sophisticated model that includes such magnetic behavior is in order. Wide literature concerning the effect of magnetic impurities in superconductivity is available [42] [53] [78] [80] as well as scientific evidence to contrast results [67]-[70] [74]-[77]. As well, the model implemented here considered the positioning of the impurities in a rather vague manner by assuming them randomly and uniformly distributed and its contribution being neglectible except when point-interacting with Cooper pairs. A more sophisticated model would probably

implement the specific localization of the impurity elements in relation with the lattice as well as other parameters pertaining to them.

It is also important to point out that the weak localization corrections suggested by Kim *et al.* extend in a very similar manner to several other quantities [43] [71] [81], such as the conductivity, correlation function and transition temperature (see **Eq. (4.1)**), which also can be adopted for further calculations in future computations.

Several inconsistencies between theory and experiment remain still unexplained [73]. Further experimental studies on this phenomenon are suggested.

V. REFERENCES

[1] H.K. Onnes, *Comm. Phys. Lab. Univ. Leiden*, Nos. 119, 120, 122 (1911).

[2] W. Meissner and R. Oschsenfeld, *Naturwiss*. **21** 787 (1933).

[3] A. Mourachkine, "Room-Temperature Superconductivity", Cambridge International Science Publishing, 2004.

[4] J. Bardeen, L.N. Cooper and J.R. Schrieffer, *Phys. Rev*. **108**, 1175 (1957).

[5] E. Cornell, *J. Res. Natl. Stand. Technol*. **101**, 419 (1996).

[6] J. M. Blatt, "Theory of Superconductivity", Academic Press, Inc., 1964.

[7] P. Townsend and J. Sutton, *Phys. Rev.* **128**, 591 (1962).

[8] R. Eisberg and R. Resnick, "Quantum Physics of Atoms, Molecules, Solids, Nuclei and Particles", 1974, John Wiley & Sons, Inc., p. 413.

[9] H. Fröhlich, *Phys. Rev*. **79**, 845 (1950).

[10] E. Maxwell, *Phys. Rev*. **78**, 477 (1950).

[11] C. A. Reynolds, *et al.*, *Phys. Rev*. **78**, 487 (1950).

[12] L. N. Cooper, *Phys. Rev*. **104**, 1189 (1956).

[13] M. Tinkham, "Introduction to Superconductivity", McGraw-Hill, Inc., 1975.

[14] J. Bardeen, *et al.*, *Phys. Rev*. **99**, 1140 (1937).

[15] J. R. Schrieffer, "Theory of Superconductivity", W. A. Benjamin, Inc., 1964.

[16] R. A. Ogg, *Phys. Rev*., **69**, 243, 544 (1946).

[17] N. N. Bogoliubov, *Soviet Physics JETP*, **7**, 41-55 (1958).

[18] A. Griffin, *et al.*, "Bose-Einstein Condensation", Cambridge University Press, 1995.

[19] http://www.magnet.fsu.edu/education/tutorials/magnetacademy/superconductivity101/images/superconductivity-periodictable.jpg

[20] P. Charles, *et al*., "Superconductivity", Academic Press, Inc., 1995, p.60-61.

[21] J. Nagamatsu, *et al.*, *Nature,* **410**, 63.

[22] C. Buzea and T. Yamashita, *Supercond. Sci. Technol.* **14** (2001) R115-R146.

[23] N. W. Ashcroft, *Phys. Rev. Lett.*, **174**, 1748 (1968).

[24] J. Kortus, *et al.*, *Phys. Rev. Lett.*, **86**, 4656 (2001).

[25] A. Y. Liu, *et al.*, *Phys. Rev. Lett.*, **87**, 087005 (2001).

[26] K. Vinod, *et al.*, *Supercond. Sci. Technol.* **20** (2007) R-31-R-45.

[27] H. J. Choi, *et al.*, *Nature*, **418**, 758 (2002).

[28] I. I. Mazin and V. P. Antropov, *Physica C* 385(2003), 49-65.

[29] H. J. Choi, *et al.*, *Physica C* 385 (2003), 66-74.

[30] Y. Kong, *et al.*, *Phys. Rev. B*, **64** 020501 (2001).

[31] M. P. Marder, "Condensed Matter Physics", John Wiley & Sons, Inc., 2000.

[32] C. Kittel, "Quantum Theory of Solids", John Wiley & Sons, Inc., 1963.

[33] D. Pines, *Phys. Rev.*, **109**, 280 (1957).

[34] J. Bardeen and D. Pines, *Phys. Rev.*, **99**, 1140 (1955).

[35] J. Bardeen, *Phys. Rev.* **80**, 567 (1950).

[36] R. D. Parks, "Superconductivity", V. 1, Marcel Dekker, Inc., New York, 1969, p.51-76.

[37] J. G. Valatin, *Il Nuovo Cimento*, Vol VII., N. 6 (1958).

[38] K. Yoshida, *Phys. Rev.* **111**, 1255 (1958).

[39] M. R. Spiegel, *et al.*, "Mathematical Handbook of Formulas and Tables", 2nd edition, Schaum's Outline Series, McGraw-Hill, 1999.

[40] R.D. Parks, "Superconductivity", R.D. Parks, V. 2., Marcel Dekker, Inc., New York, 1969.

[41] H. Suhl, *et al.*, *Phys. Rev. Lett.* **3**, 552 (1959).

[42] Y. J. Kim and A. W. Overhauser, *Phys. Rev. B* **47**, 8025 (1993).

[43] Mi-Ae Park and Y. J. Kim, http://arxiv.org/abs/cond-mat/9909358v1.

[44] G. Rickayzen, "Theory of Superconductivity", John Wiley & Sons, Inc., 1965, p.282-285.

[45] R. J. Radtke, http://arxiv.org/abs/cond-mat/9306037v1.

[46] A. A. Abrikosov and L. P. Gor'kov, *Sov. Phys. JETP* **12**, 1243 (1961).

[47] P. W. Anderson, *J. Phys. Chem. Solids* **11**, 26 (1959).

[48] M. Ma and P. A. Lee, *Phys. Rev. B* **32**, 5658 (1985).

[49] P. G. De Gennes, "Superconductivity of Metals and Alloys", Ch. 5, Perseus Books Publishing, 1999.

[50] Y. J. Kim, http://arxiv.org/abs/cond-mat/9701102v1.

[51] J. J. Sakurai, "Modern Quantum Dynamics", Addison-Wesley Publishing Company, Inc., 1994, Chapters 5 and 7.

[52] Y. J. Kim, *J. App. Phys.* **103**, 103902, Sec. **IIB**, (2008).

[53] Y. J. Kim and A. W. Overhauser, *Phys. Rev. B* **49**, 15799 (1994).

[54] P. W. Anderson, *Phys. Rev.* **109**, 1492 (1958).

[55] Y. J. Kim, http://meetings.aps.org/link/BAPS.2007.MAR.A8.9.

[56] E. D. Black, "Weak Localization", http://www.pma.caltech.edu/~ph77/labs/exp20.pdf

[57] Y. J. Kim and K. J. Chang, http://arxiv.org/abs/cond-mat/9706032v1.

[58] Y. J. Kim and K. J. Chang, *Journal of the Korean Physical Society*, Vol.31, S298-S301.

[59] M. Kaveh and N. F. Mott, *J. Phys. C* **14**, L177 (1981).

[60] D. J. Thouless, *Phil. Mag.* **32**, 877 (1974).

[61] `MATLAB 7.4.0 (R2007a)` built-in Help file.

[62] A. Polyanin and A. Manzhinov, "Handbook of Integral Equations", CRC Press LLC, 1998, Eq. 19, p.395 with $g(x)=0$. For solution and convergence, see p. 408 and 672.

[63] M. J. Buckingham, *Phys. Rev.* **101**, 1431 (1956).

[64] F. Marsiglio, *et al.*, *Phys. Rev. B* **37**, 4965-4969 (1988).

[65] Y. Wang, *et al.*, *J. Phys: Condes. Matter* **15**, 883-893 (2003).

[66] F. Bouquet, *et al. Europhys. Lett.* **56**, 856 (2001).

[67] M. Putti *et al.*, http://arxiv.org/abs/cond-mat/0508582.

[68] M. Ortolani, *et al.*, http://arxiv.org/abs/cond-mat/0411616v1.

[69] P. Brotto, *et al.*, http://arxiv.org/abs/0807.1263.

[70] Z. Hoîanová, *et al.*, http://arxiv.org/abs/cond-mat/0404096v1

[71] Y. J. Kim and M. A. Park, *Phys. Rev. B* **61**, 14733 (2000)

[72] M. A. Park, *et al.*, *Supercond. Sci. Technol.* **14** L31-L35 (2001).

[73] J. Kortus, *et al.*, *Phys. Rev. B* **94**, 027002 (2005).

[74] D. Daghero, *et al.*, http://arxiv.org/abs/cond-mat/0607515v2.

[75] R. S. Gonnelli, *et al.*, http://arxiv.org/abs/cond-mat/0407267v1.

[76] R. S. Gonnelli, *et al.*, http://arxiv.org/abs/cond-mat/0510329v2.

[77] P. Szabó, *et al.*, *Phys. Rev. Lett.* **87**, 137005 (2001).

[78] A. Abrikosov and L. Gor'kov, *Sov. Phys. JETP* **12**, 6 (1961).

[79] A. Abrikosov, *et al.*, "Quantum Field Theoretical Methods in Statistical Physics", Pergamon Press Ltd., Second Edition, 1965.

[80] H. Suhl and B. Mathias, *Phys. Rev.* **114**, 4 (1959).

[81] M. Park, *et al.*, http://arxiv.org/abs/cond-mat/0105090v1.